

CHARACTERIZATION OF THE ROLES OF THE NCK INTERACTING KINASE  
MIG-15 AND THE RAC GTPASES IN NEURONAL MIGRATION IN  
*CAENORHABDITIS ELEGANS*.

BY

Copyright 2010  
Jamie Olivia Dyer

Submitted to the graduate degree program in Molecular Biosciences  
and the Graduate Faculty of University of Kansas  
in partial fulfillment of the requirements for the degree of  
Doctor of Philosophy.

\_\_\_\_\_  
Chairperson – Erik Lundquist

Committee members

\_\_\_\_\_  
Brian Ackley

\_\_\_\_\_  
Robert Cohen

\_\_\_\_\_  
John Kelly

\_\_\_\_\_  
Kristi Neufeld

\_\_\_\_\_  
Lisa Timmons

Date defended: April 23, 2010

The Dissertation Committee for Jamie Olivia Dyer certifies  
that this is the approved version of the following dissertation:

CHARACTERIZATION OF THE ROLES OF THE NCK INTERACTING KINASE  
MIG-15 AND THE RAC GTPASES IN NEURONAL MIGRATION IN  
*CAENORHABDITIS ELEGANS*.

Committee:

\_\_\_\_\_  
Chairperson – Erik Lundquist

\_\_\_\_\_  
Brian Ackley

\_\_\_\_\_  
Robert Cohen

\_\_\_\_\_  
John Kelly

\_\_\_\_\_  
Kristi Neufeld

\_\_\_\_\_  
Lisa Timmons

Date approved: April 26, 2010

## Abstract

Neuronal migration is essential to the formation of the central nervous system in vertebrates. In *Caenorhabditis elegans*, a screen was performed previously to identify mutations that affected the migration of the Q neuroblast descendants. One of the mutants isolated from this screen was *mig-15*. MIG-15, a Nck Interacting Kinase (NIK), is homologous to proteins found in a wide variety of organisms, including *Drosophila*, mice, and humans, in which NIK kinases have been implicated in cell migration. Interestingly, multiple components of the canonical Wnt signaling pathway had already been found to control the Q cell descendant migrations. Additionally, the MIG-15 homolog in *Drosophila*, Misshapen had also been found to work with Wnt signaling components in the non-canonical planar cell polarity pathway.

To determine how MIG-15 was working to control the migrations of the Q cell descendants, a characterization of the Q neuroblast migration defects was performed. *mig-15* mutants were found to affect the Q neuroblasts, along with their descendants as previously described. I carried this work further and found that MIG-15 is required for extension of lamellipodial protrusions, maintenance of the initial polarization directing these initial protrusions, and migration of the Q neuroblasts. Since the Wnt signaling pathway had been implicated in Q cell descendant migration as well, several Wnt signaling mutants were also examined in the Q neuroblasts. This analysis determined that for the Wnt signaling mutants that were observed, there was no effect on early Q neuroblast protrusion

extension or migration. Therefore, MIG-15 does not appear to be acting with the Wnt signaling pathway to control Q neuroblast migration. Subsequently, the Q cell descendant migrations of the AQR and PQR neurons were also examined for both *mig-15* and Wnt signaling mutants. Double mutants of *mig-15* with Wnt signaling mutants resembled *mig-15* mutants alone, further suggesting that MIG-15 is not working with the Wnt signaling pathway to control the Q neuroblast lineage migrations.

In attempt to elucidate how MIG-15 is controlling the migrations of the Q neuroblasts and descendants, a candidate gene approach was taken to determine other possible proteins that are required for Q neuroblast migration. The C-terminal region of MIG-15 had previously been found to bind to PAT-3, the  $\beta$ -integrin homolog in *C. elegans*. Since available mutants in *pat-3* are not viable, INA-1/ $\alpha$ -integrin was examined for defects in Q neuroblast migration. This analysis found that, like MIG-15, INA-1 is required for the extension of polarized protrusions and migration of the Q neuroblasts. Though, INA-1 was not involved in maintenance of polarization as was MIG-15. Another molecule that was examined was ERM-1, the *C. elegans* homolog of the ezrin, radixin, and moesin (ERM) family of proteins. Previous studies have found that ERM proteins bind to and are phosphorylated by Nck interacting kinases in cell culture. These studies found that removal of ERM-1 from *mig-15* mutants suppressed the migration defects seen for the QL neuroblasts in the *mig-15* mutants alone. Together, these results suggest that MIG-15 could be acting with the integrins for proper

polarization and with both ERM-1 and the integrins to direct migration of the Q neuroblasts and descendants.

Previous studies had suggested that MIG-15 works upstream of the Rac GTPases MIG-2 and CED-10 in axon pathfinding. Additionally, these molecules had been found to act in parallel to control axon pathfinding. In order to determine if these Rac GTPases are also required for migration of the Q neuroblasts, single and double mutants of the Rac GTPases and several other molecules that are known to work with these molecules in other systems, including CDC-42 and UNC-73, were examined for their effects on the Q neuroblasts and their migrations. Singly, mutants of *mig-2*, *ced-10*, and *cdc-42* did not cause strong defects in the ability to extend protrusions or the migrations of the Q neuroblasts. When double mutants were analyzed, strong defects in the polarization and migration of the Q neuroblasts were observed for the *mig-2;ced-10* double mutants. Previous data has suggested that UNC-73 acts as a guanine nucleotide exchange factor (GEF) for MIG-2 and CED-10. *unc-73* mutants displayed polarization and migration defects like the *mig-2; ced-10* double mutant, but the defects were less severe in the *unc-73* mutants, suggesting that there is another GEF that facilitates GTP exchange for MIG-2 and CED-10. Observations of a second GEF, PIX-1, suggest that PIX-1 is involved in the protrusion extension and migration of the Q neuroblasts, suggesting that PIX-1 might act as the other GEF for MIG-2 and CED-10. Further studies found that PIX-1 might be functioning in a linear pathway with CED-10 and in parallel to the UNC-73/MIG-2 signaling pathway.

In summary, my work reveals the roles of the Rac GTPases and MIG-15/NIK kinase in the migrations of the Q neuroblasts in *Caenorhabditis elegans*, which provides insight into the mechanisms that drive neuronal migration during nervous system development.

## Acknowledgements

Acquiring a Ph.D. from the Department of Molecular Biosciences is one of the most difficult and rewarding accomplishments that I have achieved. Though much effort was required on my part in order to fulfill the requirements for the Ph.D. degree, many other people played key roles in helping me to reach my goals. I would like to recognize and extend my deepest gratitude to those that have encouraged and provided support for me along the way. Without them, this accomplishment would not have been possible.

I would like to sincerely thank my Ph.D. mentor, Dr. Erik Lundquist for providing me with the knowledge and skills to be able to complete my research, teaching me how to approach scientific questions, and inspiring me as a scientist. He has invested much time and effort to provide me with the tools that I will continue to require for the rest of my career as a scientist, and for that, I am grateful.

My graduate career would not have been the same without the other members of the Lundquist laboratory. I appreciate the many helpful discussions and suggestions for my research project and technical support that they have provided me throughout my time in the laboratory.

I would also like to express my gratitude to my graduate committee, consisting of Dr. Brian Ackley, Dr. Robert Cohen, Dr. Erik Floor, Dr. John Kelly, Dr. Kristi Neufeld, and Dr. Lisa Timmons, who have provided me with guidance,

encouragement, and helpful suggestions for my research project and scientific career.

Additionally, I would also like to thank the Graduate Program Assistant for the Department of Molecular Biosciences, John Connolly, for all of his help during my graduate career. He provided me with guidance for all of the administrative requirements while attending the University of Kansas.

Finally, I would like to acknowledge my family, my father Joe Chapman, mother Sondra Gann, sister Marla Chapman, and husband Aaron Dyer, who have provided me with endless love and support throughout my graduate studies and in each step my life.



## Table of Contents

	<b>Page</b>
<b>Abstract</b>	<b>iii</b>
<b>Acknowledgements</b>	<b>vii</b>
<b>List of Figures</b>	<b>xi</b>
<b>List of Tables</b>	<b>xv</b>
<b>Chapter I: Introduction</b>	<b>1</b>
<b>Chapter II: The MIG-15 NIK kinase acts cell-autonomously in neuroblast polarization and migration in <i>C. elegans</i></b>	<b>14</b>
2.1. Abstract	<b>15</b>
2.2. Introduction	<b>16</b>
2.3. Materials and Methods	<b>19</b>
2.4. Results	<b>24</b>
2.5. Discussion	<b>35</b>
<b>Chapter III: The mechanism of action of MIG-15 NIK kinase in neuroblast protrusion extension and migration in <i>C. elegans</i></b>	<b>69</b>
3.1. Abstract	<b>70</b>
3.2. Introduction	<b>71</b>
3.3. Materials and Methods	<b>78</b>
3.4. Results	<b>83</b>
3.5. Discussion	<b>101</b>
<b>Chapter IV: Rac GTPases and the UNC-73/Trio and PIX-1/<math>\beta</math>PIX Rac GTP exchange factors mediate neuroblast protrusion and</b>	

<b>migration in <i>C. elegans</i></b>	<b>137</b>
4.1. Abstract	<b>138</b>
4.2. Introduction	<b>139</b>
4.3. Materials and Methods	<b>143</b>
4.4. Results	<b>146</b>
4.5. Discussion	<b>165</b>
<b>References</b>	<b>194</b>

## List of Figures

<b>Figure</b>	<b>Page</b>
1.1. Schematic diagram of the Q neuroblast and descendant migrations.	12
2.1. The MIG-15 NIK kinase.	40
2.2. Q neuroblast polarization and migration.	42
2.3. Schematic diagram of Q neuroblast polarization and migration.	44
2.4. <i>mig-15</i> NIK kinase hypomorphic mutation affects the polarizations and migrations of the Q neuroblasts.	46
2.5. <i>mig-15</i> NIK kinase strong loss-of-function mutation affects the polarizations and migrations of the Q neuroblasts.	49
2.6. Canonical Wnt signaling does not affect the migrations of the Q neuroblasts.	51
2.7. The Q neuroblast descendants AQR and PQR have direction of migration defects and fail to migrate in <i>mig-15</i> NIK kinase hypomorphic mutants.	53
2.8. The PQR neuron has direction of migration defects and fails to migrate in canonical Wnt signaling mutants.	55
2.9. The AQR/PQR direction of migration defects seen in <i>mig-15</i> NIK kinase hypomorphic mutants are dependent on MAB-5, whereas the failure to migrate defects are independent of MAB-5.	57
2.10. <i>mig-15</i> is expressed in the Q neuroblasts.	59
2.11. MIG-15 NIK kinase acts cell autonomously in AQR and PQR migration.	61

<b>3.1.</b> NCK-1/Nck is not required for the migrations of the Q neuroblast descendants AQR and PQR.	<b>109</b>
<b>3.2.</b> Mutations in <i>dpy-19</i> and <i>unc-40</i> increase the AQR and PQR migration defects seen in <i>mig-15(rh148)</i> mutants.	<b>111</b>
<b>3.3.</b> The planar cell polarity pathway does not control the migrations of AQR and PQR.	<b>113</b>
<b>3.4.</b> <i>ina-1</i> $\alpha$ -integrin null mutations affect the extension of protrusions and migrations of the Q neuroblasts.	<b>115</b>
<b>3.5.</b> Loss of function of INA-1 and overexpression of INA-1::GFP increase the AQR and PQR migration defects in a <i>mig-15(rh148)</i> mutant background.	<b>117</b>
<b>3.6.</b> Mutations in the Rac GTPases MIG-2 and CED-10 and in CDC-42 cause an increase in migration defects in a <i>mig-15(rh148)</i> mutant background.	<b>119</b>
<b>3.7.</b> The <i>erm-1(tm677M+)</i> mutation does not cause strong defects in Q neuroblast extension of protrusions or migrations.	<b>121</b>
<b>3.8.</b> Loss of function <i>erm-1</i> mutation suppresses the QL migration defects observed in <i>mig-15</i> mutants.	<b>123</b>
<b>3.9.</b> <i>erm-1</i> ERM mutant suppresses the PQR migration defects observed in <i>mig-15(rh148)</i> mutants.	<b>125</b>
<b>3.10.</b> Localization of ERM-1 in the Q neuroblasts is not disrupted in <i>mig-15(rh148)</i> mutants.	<b>127</b>
<b>3.11.</b> Lack of phosphorylation of ERM-1 does not cause AQR and PQR	

neuron migration defects.	<b>129</b>
<b>3.12</b> Schematic diagram of the MIG-15 structure function constructs.	<b>131</b>
<b>3.13.</b> Removal of the citron/NIK homology domain from the <i>mig-15</i> coding region causes PQR migration defects in <i>wild type</i> animals and increases the PQR migration defects observed in <i>mig-15(rh148)</i> mutants.	<b>133</b>
<b>4.1.</b> Polarizations and migrations of the Q neuroblasts and migrations of the AQR and PQR neurons in <i>wild type</i> animals.	<b>173</b>
<b>4.2.</b> Polarizations of the Q neuroblasts at 1-1.5h after hatching.	<b>176</b>
<b>4.3.</b> Failure of the Q neuroblasts to extend <i>wild type</i> protrusions.	<b>178</b>
<b>4.4.</b> Migrations of the Q neuroblasts.	<b>180</b>
<b>4.5.</b> Failure of the Q neuroblasts to migrate before dividing.	<b>182</b>
<b>4.6.</b> Final migratory positions of the Q neuroblast descendants, AQR and PQR.	<b>184</b>
<b>4.7.</b> UNC-73/Trio is required for the proper polarizations and migrations of the Q neuroblasts and migrations of the Q cell descendants.	<b>186</b>
<b>4.8.</b> PIX-1/ $\beta$ PIX is required for the proper migrations of the QL neuroblast and the Q neuroblast descendants.	<b>188</b>
<b>4.9.</b> Double mutants of <i>pix-1</i> and <i>unc-73</i> display a synergistic increase in defects in the polarization and migration of the Q neuroblasts and the migrations of the Q neuroblast descendants.	<b>190</b>
<b>4.10.</b> Double mutants of <i>pix-1</i> with <i>mig-2</i> exhibit a synergistic increase in defects in Q neuroblast protrusion extension and migration and Q	

neuroblast descendant migration, whereas *pix-1;ced-10* double mutants do not display a large increase in defects in the protrusions or migrations of the Q neuroblasts or the Q neuroblast descendants. **192**

## List of Tables

<b>Table</b>	<b>Page</b>
<b>2.1.</b> <i>mig-15</i> polarity maintenance defects (~3-3.5 hours after hatching).	<b>63</b>
<b>2.2.</b> The locations of AQR and PQR with the loss of the <i>mig-15(+)</i> transgene in AQR and PQR, but maintained in other tissues.	<b>65</b>
<b>2.3.</b> The locations of AQR and PQR with the loss of the <i>mig-15(+)</i> transgene in other tissues, but maintained in AQR and PQR.	<b>67</b>
<b>3.1.</b> <i>ina-1</i> Q cell migration defects (~3-3.5 hours after hatching).	<b>135</b>

**Chapter I**  
**Introduction**



Neuronal migration is essential for the development of the central nervous system. Neurons are often born in one location and have to migrate over long distances in order to form various portions of the central nervous system and to make synapses with the proper targets. In order for neurons to migrate, these cells must be able to modulate their actin cytoskeletons to allow for the steps of migration. Migration can be broken down into several simplified steps; cells must be able to receive a signal that tells the cell in which direction to migrate, interpret that cue, send out protrusions in the direction of migration, and finally, exert the pulling force that moves the cell in the proper direction (Lauffenburger DA, 1996; Ridley et al., 2003).

One of the key components in sending out the protrusive structures that then allow for the physical movement of the cell is modulation of the actin cytoskeleton (Pollard and Borisy, 2003). These protrusive structures, lamellipodia and filopodia, are formed by reorganization of the actin cytoskeleton (Welch and Mullins, 2002). Elongation of the actin cytoskeleton under the plasma membrane allows for the lamellipodia and filopodia to extend in the direction of migration. Without these protrusive structures, the migration of the cell could not occur.

Numerous molecules have been determined to be involved extension of lamellipodia and filopodia, and therefore, the modulation of the actin cytoskeleton. Though many molecules have been identified, it is not yet understood how these molecules work together in a variety of pathways to form the protrusive structures necessary to allow for migration. In order to further

elucidate how several of the molecules known to be involved in neuronal migration work together to drive migration, *in vivo* genetic studies were performed to determine the roles of each of these molecules in migrating neurons in the model organism *Caenorhabditis elegans*.

Using the nematode *C. elegans* provides many advantages to the other approaches used to study neuronal migration (Brenner, 1974). *C. elegans* has a relatively simple nervous system, with only 302 neurons present in the adult hermaphrodite (White et al., 1986). Additionally, the cell lineage map has been determined for these animals, detailing the location and time of birth of each neuroblast, which cells will come from those neuroblasts, and where the resulting neurons should migrate (Sulston, 1988). An additional important feature that facilitates neurological studies in *C. elegans* is that they are transparent, allowing for the observation of migrating neurons *in vivo*. With all of these features and full genomic sequencing, *C. elegans* allows for *in vivo* studies that would not be available in many other organisms.

In *C. elegans*, the Q neuroblasts and their descendants provide a useful, yet simple system in which to study migrations of neurons. The Q neuroblasts are born bilaterally in the posterior of the animal (Chalfie and Sulston, 1981; White et al., 1986). The QL neuroblast originates from the division of a precursor cell, ABplapapaa, which gives rise to both QL and the V5L seam cell on the left side of the animal. Likewise, the QR neuroblast originates from the division of a precursor cell, ABprapapaa, which gives rise to both QR and the V5R seam cell on the right side of the animal. Both QL and QR undergo identical division

patterns to each produce 3 neurons (Fig. 1.1). The QL neuroblast undergoes three rounds of postembryonic division and two apoptotic events to produce the PQR, SDQL, and PVM neurons. Of the three QL descendants, PQR migrates the farthest, migrating posteriorly into the phasmid ganglion in the tail of the animal. The QR neuroblast also undergoes three rounds of postembryonic division and two apoptotic events to produce AQR, SDQR, and AVM. Of these three QR descendants, AQR migrates the farthest, migrating anteriorly into the anterior deirid ganglion in the head of the animal.

At hatching, the unpolarized QL and QR neuroblasts are located between the V4 and V5 seam cells on their respective sides of the animal (Sulston and Horvitz, 1977). The QL neuroblast receives a signal to polarize posteriorly, causing QL to send protrusions posteriorly over the V5L seam cell. The QR neuroblast receives a signal to polarize anteriorly, causing the QR neuroblast to send protrusions anteriorly over the V4R seam cell. The Q cells then follow these protrusions, migrating over their respective seam cells, QL over V5L and QR over V4R. The QL and QR neuroblasts then divide, giving rise to daughter cells that continue to migrate in the same direction as the precursor.

In a screen to identify molecules involved in neuronal migration, Hedgecock and Guo isolated a mutant, named *mig-15*, in which there were migration defects in the descendants of the Q neuroblast lineages. Cloning of the *mig-15* locus determined that MIG-15 is homologous to other proteins belonging to the group of Nck interacting kinases (NIK) (Poinat et al., 2002; Su et al., 1997; Su et al., 2000; Su et al., 1998). Therefore, MIG-15 is a member of the

Ste20 kinase family of proteins and is classified as part of the Group I type of Germinal Center Kinases. This group of proteins contains an N-terminal kinase domain and a C-terminal regulatory domain.

NIK kinases were originally identified in a yeast two-hybrid screen for molecules that interact with the SH3 domains found in the small adaptor molecule Nck (Su et al., 1997). Nck is a signaling molecule containing 1 SH2 domain and 3 SH3 domains (Lehmann et al., 1990). Though Nck does not contain any catalytic activity on its own, Nck molecules are thought to perpetuate signals through their ability to bind phosphotyrosine through their SH2 domain and proline-rich domains through their SH3 domains, allowing for the localization of effector proteins upon activation of growth factor receptor activation. Nck molecules have been found to bind the Wiskott-Aldrich syndrome protein (WASP), a molecule that modulates the actin cytoskeleton through its interactions with the Rac GTPases and CDC-42 (Aspenstrom et al., 1996). Additionally, the *Drosophila* homolog of Nck, Dreadlocks (Dock), was determined to play a role in axon guidance, suggesting that Nck molecules might have a role in modulation of the actin cytoskeleton through its interactions with effector molecules (Garrity PA, 1996).

Amino acid sequence comparisons of the mammalian NIK with other NIK homologs found that the *C. elegans* MIG-15 shared the most homology with NIK (Su et al., 1997). Alignments of the entire coding regions of NIK and MIG-15 found that these genes are 52% identical and 68% similar. The N-terminal S/T kinase domain and the C-terminal CNH domain of these proteins were more

highly conserved, with 72% identical and 86% similarity between these domains of MIG-15 and NIK. The strong conservation seen for NIK kinases between divergent species suggests that NIK kinases play an important role in these organisms. Additionally, the degree of conservation would also suggest that *C. elegans* MIG-15 and mammalian NIK are likely to perform the same functions. Thus, examination of the role of MIG-15 in neuronal migration in *C. elegans* will likely have implications that can explain the functions of NIK kinases in human cell migrations.

Studies focused on the mechanisms of action of NIK kinases have determined a variety of functions for these proteins. Numerous studies have determined that NIK kinases are acting in the mitogen-activated protein kinase (MAPK) signaling pathway that leads to activation of the c-Jun N-terminal kinase (JNK), including studies in mammalian cell culture and for the *Drosophila* Misshapen (Msn) (Fu et al., 1999; Liu et al., 1999; Su et al., 2000; Su et al., 1998; Wright et al., 2003). Additionally, experiments in yeast determined that the serine/threonine kinase STE20 also activates the MAPK signaling pathway (Herskowitz, 1995). As such, NIK kinases have also been named MAP4K4. In addition to the role of NIK kinases upstream of JNK activation, the *Drosophila* NIK homolog Msn has been found interact with Bicaudal-D and dynein in nuclear translocation during cell migration of photoreceptor cells of the developing eye (Houalla et al., 2005). Other studies found contrasting functions for NIK kinases in their role of regulating integrin function, with studies done in mouse cell lines finding that NIK acts downstream of Eph receptors to activate integrin adhesion

whereas examination of the human NIK kinase HGK (hepatocyte progenitor kinase-like/GCK-like kinase) found that a kinase-inactive form of HGK caused increased cell spreading and cell adhesion that could be blocked by anti-integrin antibodies, suggesting that wild type HGK acts to decrease cell spreading and adhesion via integrins (Becker et al., 2000; Wright et al., 2003). NIK kinases were also shown to directly interact with the cytoplasmic tail of  $\beta$ -integrin, for both murine NIK and *C. elegans* MIG-15 (Poinat et al., 2002). Additional cell culture experiments have found that NIK binds to moesin, a member of the ERM family of proteins (for ezrin, radixin, and moesin), and also phosphorylates these three ERM-1 proteins *in vitro* (Baumgartner et al., 2006).

As illustrated by the several examples stated above, it appears that NIK kinases work in multiple pathways to control various developmental events. Additionally, it seems that NIK kinases can function in a cell specific manner. In *Drosophila*, Msn appears to be working in multiple pathways in the developing compound eye, with Msn working downstream of the Frizzled receptor and Dishevelled through the JNK protein to control planar cell polarity in the eye whereas proper targeting of the axonal projections of the photoreceptors appears to require Msn function, though Msn was found to be working with Dreadlocks (Dock) and not through JNK signaling to control these pathfinding events (Paricio et al., 1999; Su et al., 2000). Further studies also found cell specific roles for NIK in the development of mouse embryos. NIK knockout mice had defects in the migrations of the mesodermal cells away from the primitive streak, resulting in a failure of somites to form, though it appears that this defect in migration is due to

a nonautonomous affect of NIK (Xue et al., 2001). Additionally, it appears that NIK is required autonomously for the differentiation of mesoderm into dermamyotome (Xue et al., 2001). As mesodermal and somite formation are not dependent on JNK signaling, the NIK knockout studies suggest a role for NIK independent of JNK. Taken together, these results suggest the NIK kinases act in multiple tissues and in multiple pathways to control migration and differentiation of cells during development.

Another class of molecules that have been implicated in cell migration, including the migration of the Q neuroblast descendants, is the Rac GTPases (Hall, 1998; Raftopoulou and Hall, 2004; Ridley et al., 2003; Shakir et al., 2006). The Rac GTPases belong to the Rho family of small GTPases, a group of proteins that have been implicated in a variety of cellular processes, including cell proliferation, gene expression, and actin cytoskeleton dynamics (Hall, 1998; Mackay and Hall, 1998). These small GTPases cycle between an active state when bound to GTP and an inactive state when bound to GDP, allowing these molecules to act as molecular switches. The exchange of GDP for GTP to activate these small GTPases is facilitated by guanine nucleotide exchange factors (GEFs), whereas the inactivation of Rho GTPases is expedited by the activity of GTPase-activating proteins (GAPs). Since Rho GTPases have a role in modulation of the actin cytoskeleton, these small GTPases play an essential role in the ability for cells to undergo morphological changes, like the extension of lamellipodia and filopodia, and for migration (Hall, 1998, 2005; Heasman and Ridley, 2008; Raftopoulou and Hall, 2004; Ridley, 1992).

There are three classes of Rho GTPases, Rac, Rho, and CDC42 (Mackay and Hall, 1998). Of these three, CDC42 has been found to play a role in the establishment of cellular polarity through regulation of the actin cytoskeleton (Heasman and Ridley, 2008). This role of CDC42 in cell polarity also has implications in cell migration, as CDC42 had been shown to be required for directional migration. In addition to its role in polarity, CDC42 has also been shown to be involved in the formation of filopodia (Nobes and Hall, 1995). Lamellipodial formation was found to be regulated by another member of the Rho GTPase family, Rac (Heasman and Ridley, 2008; Ridley, 1992). Rac GTPases are thought to regulate the extension of lamellipodia through their interactions with effector proteins that modulate the actin cytoskeleton, such as the ARP2/3 complex, WAVE complex (WASP-family verprolin homologous proteins), cofilin and gelsolin (Heasman and Ridley, 2008). Through the activities of these effectors, the actin cytoskeleton can form an extending meshwork beneath the plasma membrane that allows for lamellipodial protrusions. Though much has been done to determine the individual roles of these Rho GTPases in the process of cell migration, most of these studies have been performed in cell culture using dominant-negative and constitutively active forms of these Rho GTPases (Heasman and Ridley, 2008). Additionally, these experiments have produced confounding results, though these differences could be due to varying cell specific roles of these molecules.

To further elucidate the roles of the NIK kinases and Rho GTPases in the migration of neurons, *in vivo* studies were performed in *Caenorhabditis elegans*



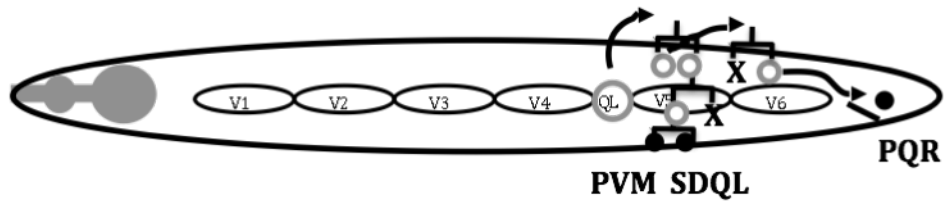
to study the functions of the MIG-15/NIK kinase, CDC-42, CED-10/Rac, and MIG-2/RhoG. Characterization of *mig-15* mutants in the Q neuroblasts found that MIG-15 is required for the extension of protrusions, maintenance of the initial protrusions, and migration of the Q neuroblasts. Further studies to determine how MIG-15 might be functioning in the Q neuroblasts found that MIG-15 appears to interact genetically with INA-1/ $\alpha$ -integrin and ERM-1/ERM to drive the migrations of these neuroblasts. Examination of the Rho GTPases found that MIG-2/RhoG and CDC-42 are required for the ability of the Q neuroblasts to migrate. Conversely, it appears that CED-10/Rac is normally involved in the inhibition of the Q neuroblasts from migrating past their normal stopping point. Studies examining the potential Rac GEFs found that UNC-73/Trio, which has previously been shown to act as a GEF for MIG-2 and CED-10, does not act alone as the GEF for MIG-2 and CED-10, but rather PIX-1, PAK (p21-activated kinase) Interacting Exchange Factor, also functions as a GEF for CED-10. Investigations into the relationship of MIG-15 with the Rho GTPases found that MIG-15 appears to be interacting with both MIG-2/RhoG and CDC-42 to give the Q neuroblasts the ability to migrate.

Overall, the experiments presented here provide insight into how molecules that are required for cell migration interact to allow for directed neuronal migration. The Rho GTPases have previously been shown to modulate the actin cytoskeleton to extend protrusions necessary for cell migration (Ridley et al., 2003). Studies shown here suggest that MIG-15 is also allowing for cell migration through the modulation of the actin cytoskeleton, as both INA-1 and

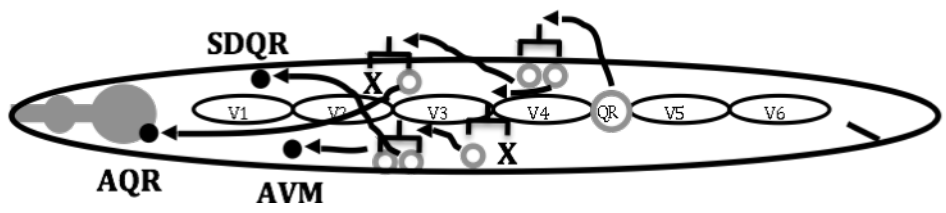
ERM-1 which were found to interact with MIG-15 have also been implicated in actin cytoskeleton regulation. Both the Rho GTPases and NIK kinases have been shown to be involved in cell migrations, but these molecules have additionally been implicated in determining the invasiveness of tumor cells (Collins et al., 2006; Sanz-Moreno et al., 2008). Thus, these studies provide insight not only into how neuronal migration occurs during development, but they also examine molecules and mechanisms that control metastasis of cancer cells.

Figure 1.1

A



B



**Figure. 1.1. Schematic diagram of the Q neuroblast and descendant migrations.** (A) The migration and division pattern of the QL lineage. Black circles represent the final locations of the PVM, SDQL, and PQR neurons. (B) The migration and division pattern of the QR lineage. Black circles represent the final locations of the AQR, SDQR, and AVM neurons.

## **Chapter II**

### **The MIG-15 NIK kinase acts cell-autonomously in neuroblast polarization and migration in *C. elegans***

## 2.1. Abstract

Cell migration is a fundamental process in animal development, including development of the nervous system. In *C. elegans*, the bilateral QR and QL neuroblasts undergo initial anterior and posterior polarizations and migrations before they divide to produce neurons. A subsequent Wnt signal from the posterior instructs QL descendants to continue their posterior migration. Nck-interacting kinases (NIK kinases) have been implicated in cell and nuclear migration as well as lamellipodia formation. Studies here show that the *C. elegans* MIG-15 NIK kinase controls multiple aspects of initial Q cell polarization, including the ability of the cells to polarize, to maintain polarity, and to migrate. These data suggest that MIG-15 acts independently of the Wnt signal that controls QL descendant posterior migration. Furthermore, MIG-15 affects the later migrations of neurons generated from Q cell division. Finally, a mosaic analysis indicates that MIG-15 acts cell autonomously in Q descendant migration.

## 2.2. Introduction

Cell migration is a key morphogenetic process in animal development. Migration of neurons and their precursors are important in forming distinct cortical layers and functional nuclei of neurons in the developing vertebrate central nervous system. In *C. elegans*, the bilateral Q neuroblasts, born in the posterior-lateral region of the animal, and their neuronal descendants execute long-range anterior and posterior migrations in the first larval stage (Chalfie and Sulston, 1981; Sulston and Horvitz, 1977). After hatching, QL and QR undergo initial, short-distance posterior and anterior migrations, respectively, after which they divide. QL and descendants encounter a Wnt signal in the posterior which, via canonical Wnt signaling, drives expression of the *mab-5 Hox* gene in QL descendants (Chalfie et al., 1983; Eisenmann and Kim, 2000; Harris et al., 1996; Herman, 2001; Kenyon, 1986a; Korswagen et al., 2000; Salser and Kenyon, 1992; Whangbo and Kenyon, 1999). *mab-5* expression in QL descendants causes them to continue posterior migration. QL generates three neurons: SDQL and PVM reside near the site of Q cell birth in the left postdeirid ganglion, and PQR migrates posteriorly into the phasmid ganglion in the tail (Sulston and Horvitz, 1977; White et al., 1986). In mutants affecting Wnt signaling and in *mab-5* mutants, QL descendants reverse their direction of migration and migrate anteriorly instead of posteriorly (Chalfie et al., 1983; Eisenmann, 2005; Kenyon, 1986a; Salser and Kenyon, 1992). QR, which migrates a short distance anteriorly and divides, does not respond to the posterior Wnt signal and does not express *mab-5*. Consequently, the three neurons generated by QR (SDQR,

AVM, and AQR) migrate anteriorly. AQR migrates the longest distance into the head of the animal in the anterior deirid ganglion.

Mutations in *unc-40*, which encodes the netrin receptor (Keino-Masu, 1996), and *dpy-19*, which encodes a novel, conserved transmembrane protein (Honigberg and Kenyon, 2000), randomize initial Q cell polarization, and mutations in *unc-73*, which encodes the Rac GEF Trio (Steven et al., 1998), affect the ability of Q cells to polarize and migrate (Honigberg and Kenyon, 2000). The transmembrane molecule MIG-13 might be involved in establishing an anterior-posterior guidance system that is required for anterior migration of QR descendants (Sym et al., 1999). These studies have identified potential guidance ligands, guidance receptors, and cellular effectors that mediate Q cell migration. While much has been learned about Q cell migration, many of the mechanisms that control Q cell polarity and Q cell migration remain to be elucidated.

Previous studies have implicated the Nck-interacting kinases, NIK kinases, as regulators of a variety of morphogenetic events involving cytoskeletal regulation and cell shape. In *Drosophila*, the NIK molecule Misshapen is involved in cell and nuclear migration, interacts with a JNK/MAPK kinase pathway, and controls axon pathfinding (Houalla et al., 2005; Su et al., 2000; Su et al., 1998). Vertebrate studies have also implicated NIK kinases in cell migration and as acting with JNK signaling and integrins (Becker et al., 2000; Xue et al., 2001). In cultured cells, treatment with EGF and PDGF leads NIK



kinase-dependent phosphorylation of ERM proteins responsible for actin organization and lamellipodium formation (Baumgartner et al., 2006).

*mig-15* encodes a *C. elegans* Nck-interacting kinase (NIK) (Poinat et al., 2002; Su et al., 1997). MIG-15 contains an N-terminal pak/ste20-type serine/threonine kinase domain followed by a proline-rich region. The C-terminus of MIG-15 contains a citron-NIK homology domain (CNH), a conserved domain thought to interact with Rac GTPases and  $\beta$ 1 integrin (Figure 2.1). Mutations in *mig-15* cause defects in axon pathfinding as well as Q descendant migration (Poinat et al., 2002; Shakir et al., 2006). *mig-15* acts upstream of *mab-5*, as the constitutively-active *mab-5(e1751)* allele, which causes constitutive *mab-5* expression in both QL and QR descendants, rescues the anterior QL descendant migration defects in *mig-15* mutants (i.e. in *mig-15; mab-5(e1751)* doubles, QL descendants always migrate to the posterior) (Shakir et al., 2006).

Previous work showed that MIG-15 was required for initial Q cell migration (Williams, 2002), but it is not clear if *mig-15* also affects Q cell polarization or if *mig-15* might also affect later Wnt-related events. Furthermore, it is not clear if MIG-15 acts in the Q cells and descendants or in another tissue such as a substrate for Q descendant migration. Described here are studies showing that MIG-15 controls initial Q cell polarization and maintenance of polarity in addition to affecting Q cell and Q descendant migration. Furthermore, analysis of *mig-15* genetic mosaics was consistent with a cell-autonomous role of MIG-15 in AQR and PQR migration.

## 2.3. Materials and Methods

### Genetic Methods

All experiments were performed at 20°C using standard techniques (Brenner, 1974; Sulston and Hodgkin, 1988). The following mutations and transgenic constructs were used: X: *bar-1(ga80)*, *qid-7(mu327)*, *qid-8(mu342)*, *mig-15(rh148)* and *rh80*; I: *lin-17(e1456)*, *lqls40[Pgcy-32::gfp]*; II: *mul516[mab-5::gfp]*; III: *gmls5[ina-1::gfp]*, *mab-5(e1239)* and *e1751*; IV: *lqls3[osm-6::gfp]*. The chromosomal locations of *lqls80[scm promoter::gfp::caax]* and *lqls58[Pgcy-32::cfp]* were not determined. *Pmig-15::gfp*, *Pgcy-32::yfp*, and *mig-15(+)* were extrachromosomal arrays. Extrachromosomal arrays were generated by germ line microinjection and integrated into the genome by standard techniques (Mello and Fire, 1995).

**Synchronization of L1 larvae to visualize Q cell polarization.** Methods described previously to synchronize larval development were used (Honigberg and Kenyon, 2000). Adults and larvae were washed from a plate with M9 buffer. Eggs adhered to the agarose and were not removed. Newly-hatched L1 larvae were washed from the plate at 30 minute intervals, placed on a fresh NGM plate with a bacterial lawn, and allowed to develop for given times: imaged immediately (0-0.5h), 1-2.5h, 3-3.5h, 4-4.5h, and 5.5-6h (for *mig-15(rh80)*). In the case of egg-laying-defective genotypes, eggs were isolated from gravid adults by bleach treatment (Sulston and Hodgkin, 1988).

**Epifluorescence microscopy and visualization of Q cell polarization and migration.** Animals were analyzed by epifluorescence microscopy for GFP, YFP, or CFP using a Leica DMR compound microscope. Images were captured using Openlab software and a Qimaging Retiga EXi camera. For Q cell imaging, a z-series of images of the Q cells was captured, and images were subjected to nearest-neighbor deconvolution (Openlab).

**Scoring and analysis of AQR and PQR migration defects.** The final positions of AQR and PQR were scored in L4 larvae and young adult worms. The position of each neuron was given a value of 1-5, depending on the anterior-posterior position of the neuron: a value of 1 was the normal position of AQR in the anterior deirid ganglion; 2 was posterior to the anterior deirid to approximately half the distance to the vulva; 3 was around the vulva (half the distance from the vulva to the anterior deirid and from the vulva to the post-deirid); 4 was the post-deirid to the anus; and 5 was posterior to the anus, the normal position of PQR in the phasmid ganglion. A position of 4, around the post-deirid, is the position of Q cell birth. Thus, some cells with a score of 4 had not migrated from the Q cell birthplaces. PQR neurons with scores of 1 to 3 had reversed direction and migrated anteriorly instead of posteriorly. AQR neurons with a score of 5 had reversed direction of migration and migrated posteriorly instead of anteriorly. These coordinates correspond to the following landmarks in the L1 larva: 1 = anterior to the V1.a/p cells; 2 = near the V1.a/p and V2.a/p cells; 3 = near the

V3.a/p and V4.a/p cells; 4 = near the V4.a/p, V5.a/p, and V6.a/p cells (Q cells are born between V4 and V5); and 5 = posterior to the anus.

***mig-15*, *gcy-32*, and *scm::gfp::caax* transgenes.** The sequences of all plasmids used in this work are available upon request. All coding regions amplified by polymerase chain reaction (PCR) were sequenced to ensure that no mutations had been introduced by PCR. All regions were amplified from N2 genomic DNA unless otherwise noted. The entire *mig-15(+)* gene included the entire *mig-15* coding region plus 4-kb of upstream promoter sequence and was amplified using primers: 5'-CTCCAATAGTTTGCTCCCGG and 5'-CCAATTTGTCAACCCTGGCTT. The *mig-15* promoter included 4-kb of DNA upstream of the *mig-15* coding region and was amplified using primers: 5'-CTCCAATAGTTTGCTCCCGGT and 5'-GGTTTTGGGTGCTGTGAGCG. The *mig-15* promoter fragment was then placed upstream of the *gfp* coding region in vector pPD95.77 (kindly provided by A. Fire). The *scm::gfp::caax* transgene was constructed using the seam cell marker (*scm*) plasmid pRT1 (Terns et al., 1997). The *lacZ* coding region of pRT1 was replaced by *gfp* coding region with the C-terminal CAAX prenylation domain coding region from *ced-10 Rac* at the 3' end (Reddien and Horvitz, 2000). *scm::gfp::caax* drove expression of membrane-associated, prenylated GFP in the lateral seam cells and in the Q neuroblasts. A similar construct was used previously to image Q cell development (Williams, 2002). The *gcy::32::gfp* transgene *adEx1295* (Yu et al., 1997) was integrated into the genome to generate *lqls40*. For the *Pgcy-32::yfp* and *Pgcy-32::cfp*

constructs, the *gcy-32* promoter was generated by PCR using primers: 5'-TGTATAGTGGGAAATACTGAAAT AND 5'-TATATTTTCCTTTCCGCTTTTCG. This *gcy-32* promoter fragment was then placed upstream of the *yfp* and *cfp* coding regions (courtesy of A. Fire).

***qid-7* and *qid-8* complementation tests and sequencing.** *mig-15(rh148)* and *mig-15(rh80)* males harboring the rescuing *mig-15(+)* transgene were mated to *qid-7* and *qid-8* hermaphrodites, and some *trans*-heterozygous cross progeny displayed the Unc Dpy phenotype indicating failure to complement. The *mig-15* coding regions from *qid-7(mu327)* and *qid-8(mu342)* animals were amplified by PCR and sequenced. Nucleotide lesions were found associated with both as described in Figure 2.1 and were confirmed with second-strand sequencing.

**Mosaic Analysis.** An extrachromosomal array containing the wild-type *mig-15(+)* coding region rescued the gross morphological phenotype (Unc Dpy) as well as AQR and PQR migration defects of *mig-15(rh80)* (Figures 2.11C and D). Included in this extrachromosomal array was a *gcy-32::yfp* transgene, which drove the expression of yellow fluorescent protein (YFP) in AQR, PQR, and the two bilateral URX neurons. This extrachromosomal array was spontaneously lost during mitotic divisions, resulting in mosaic animals in which some cells harbored the *mig-15(+)* transgene and other did not. AQR, PQR, and URX neurons with the transgene expressed YFP whereas those that lost the transgene did not. In these studies, approximately 10% of animals harboring this

extrachromosomal array displayed mosaicism in AQR, PQR and the URX neurons, and animals with multiple losses were observed and analyzed.

A strain was constructed including *mig-15(rh80)*, the rescuing *mig-15(+)* *gcy-32::yfp* extrachromosomal array, and a stable, integrated *gcy-32::cfp* transgene, which drove expression of cyan fluorescent protein (CFP) in AQR, PQR, and the two URX neurons and which was used to report AQR and PQR position (see Figure 2.11B).

To identify mosaics with losses in AQR and PQR, animals with a wild-type gross morphological phenotype (non-Dpy non-Unc) were screened for those that lacked YFP expression in AQR and/or PQR. These animals retained *mig-15(+)* function in tissues underlying the Dpy and Unc defects of *mig-15* mutants, and many of these mosaics also maintained *mig-15(+)* in AQR, PQR, or the URX L/R neurons as judged by YFP fluorescence (Table 2.2).

To identify mosaics that retained *mig-15(+)* in AQR or PQR, animals with the *mig-15* gross morphological phenotype (Unc and Dpy) were screened for those with YFP expression in AQR and/or PQR. These animals had lost *mig-15(+)* in tissues underlying the Dpy Unc phenotype but retained *mig-15(+)* in AQR and PQR. In 44/70 of these animals, no loss could be detected in the AQR, PQR and URX L/R neurons, suggesting that the cellular focus of the Dpy Unc phenotype of *mig-15* was in the P lineage and not the AB lineage. Many of these also retained *mig-15(+)* in AQR or PQR and the URX neurons (Table 2.3).

## 2.4. Results

**The MIG-15 NIK kinase.** Previous studies showed that mutations in the *mig-15* gene, which encodes a molecule similar to vertebrate Nck-interacting kinase (NIK) (Poinat et al., 2002) (Figure 2.1), perturbed the migrations of Q cell descendants (Shakir et al., 2006). As shown in Figure 2.1, the *qid-7(mu327)* and *qid-8(mu342)* mutations previously found to perturb Q descendant migration (Ch'ng et al., 2003) were new alleles of *mig-15* (see Materials and Methods). The hypomorphic *rh148* mutation is a missense mutation in the ATP-binding-pocket of the kinase domain, and the stronger allele *rh80* is a premature stop codon after the kinase domain (Figure 2.1) (Shakir et al., 2006). While *rh80* causes a premature stop, it might have residual *mig-15* activity and might not represent a null. However, *rh80* causes a more severe phenotype than *rh148* and represents a strong loss-of-function of the *mig-15* gene.

**Imaging initial QL and QR migrations.** Initial Q cell migrations were visualized in wild-type and *mig-15* mutants. In the wild-type L1 larva, QL and QR undergo initial posterior and anterior migrations, respectively, followed by cell division (Sulston and Horvitz, 1977). QL descendants then receive a Wnt signal from posterior cells that directs further posterior migrations of the QL descendants by activating the *mab-5 Hox* gene (Maloof et al., 1999; Salser and Kenyon, 1992; Whangbo and Kenyon, 1999). QR descendants do not respond to this Wnt signal, do not express *mab-5*, and migrate anteriorly (Salser and Kenyon, 1992).

The initial, Wnt-independent migrations of the Q neuroblasts were imaged using an *scm promoter::gfp::caax* transgene. L1 larvae were synchronized by hatching (see Materials and methods), and Q neuroblasts were observed at different timepoints after hatching. Results presented here were consistent with other observations of initial Q cell migration (Honigberg and Kenyon, 2000).

At hatching, the Q cells were unpolarized and were located between the V4 and V5 seam cells (Figures 2.2A and B). At 1-2.5h after hatching, QL sent a process posteriorly over the left V5 seam cell (V5L) and QR sent a process anteriorly over the right V4 seam cell (V4R) (Figures 2.2C and D). In most cases, the processes extended greater than half the distance over the respective V cells. The Q cell processes resembled the leading edges of migrating cells in other systems and displayed lamellipodia-like protrusions with filopodia-like extensions (Figures 2.2C and D). These anterior and posterior protrusions persisted, and at 3-3.5h, the cell bodies of QL and QR followed the protrusions and migrated over their respective seam cells such that QL was located over V5L and QR was located over V4R (Figures 2.2E and F). At 4-4.5h after hatching, QL and QR underwent mitosis, producing anterior and posterior daughters (QL.a/QL.p and QR.a/QR.p) located above V5L and V4R, respectively (Figures 2.2G and H). A schematic diagram of wild-type initial Q cell migration is shown in Figure 2.3. To summarize, the Q cells underwent an initial polarization (QL posteriorly and QR anteriorly); the cell bodies of QL and QR migrated posteriorly and anteriorly over V5L and V4R, following the initial protrusions; and QL and QR underwent mitosis above V5L and V4R.



### **MIG-15 is required for Q cell polarization and maintenance of Q cell**

**polarity.** *mig-15(rh80)* causes a premature stop codon and is a strong loss-of-function allele, and *mig-15(rh148)* is a missense mutation affecting the ATP-binding pocket of the kinase domain (Figure 2.1) (Shakir et al., 2006). Shown here and in Shakir et al., 2006, Q descendant migration defects of *mig-15(rh148)* are generally less severe than *mig-15(rh80)*. The Unc Pvl Dpy phenotype of *mig-15(rh148)* was also less severe than *mig-15(rh80)* (data not shown), suggesting that *mig-15(rh148)* might cause weaker loss of *mig-15* function than *mig-15(rh80)*.

Q cell polarization was assayed in *mig-15(rh148)* and *mig-15(rh80)*. At hatching, Q cell position and morphology in both mutants resembled wild-type (n = 35 for each) (data not shown). Initial QL and QR polarization in the hypomorphic *mig-15(rh148)* mutant occurred apparently normally at 1.5-2.5h after hatching (Figures 2.4A and B). The posterior and anterior protrusions extended distances over V5L and V4R similar to wild-type. Often, *mig-15(rh148)* protrusions displayed more filopodia-like extensions than did wild-type (Figures 2.4A and B).

In *mig-15(rh80)* mutants, the time required for polarization and division was increased compared to the *scm::gfp::caax* strain alone. This was likely due to a general developmental delay in *mig-15(rh80)*, as the time to complete larval development was increased in these mutants (data not shown). At 2-2.5h after hatching, the equivalent of 1-2.5h in wild-type, the QL and QR cells always

appeared to polarize in the correct direction. However, the polarizations were abnormal in that the protrusions did not extend as far toward the posterior or anterior over the V5L and V4R seam cells, usually less than half the length of the V cells (compare Figures 2.5A and B with Figures 2.2C and D). All *mig-15(rh80)* animals displayed reduced protrusion, and QL and QR were equally affected. While *mig-15(rh80)* Q cells failed to fully polarize, the direction of initial Q cell polarization was not affected.

When observed later at 3-3.5h after hatching, at a time when wild-type Q cells began their migrations over the V cells, some *mig-15* mutant Q cells had failed to remain properly polarized (Figure 2.4 and Table 2.1). Some cells remained polarized in the correct direction but sent branches in the other direction (Figure 2.4C and D and 2.5C), some were polarized to both the anterior and posterior (Figure 2.4E), and some were not polarized strongly in either the anterior or posterior direction (Figure 2.4F-H and 2.5D).

**MIG-15 is required for Q cell migration.** In wild-type, the QL and QR cell bodies follow the posterior and anterior protrusions and migrate over V5L and V4R. In *mig-15* mutants, Q cells often failed to fully migrate over the respective seam cells before division (4-4.5h after hatching). Some Q cells did not migrate at all and divided between V4 and V5 (Figure 2.4I and Figure 2.5E and F). Some Q cells had migrated partially and divided on the edges of the V cells (Figure 2.4J). The percentages of Q cells that failed to migrate properly are shown in Figure 2.4K and Figure 2.5G. While the proportions of QL and QR that

failed to migrate properly in *mig-15(rh148)* were similar, QRs always migrated some distance over V4R as shown in Figure 2.4J whereas QLs often failed to migrate any distance before division as shown in Figure 2.4I. QL and QR were equally affected in *mig-15(rh80)*.

Interestingly, some QL cells (5%) in *mig-15(rh148)* were observed that, instead of having migrated posteriorly over V5L, migrated anteriorly and divided over V4L (Figure 2.4K), suggesting that a failure to maintain polarity could result in a repolarization and migration in the opposite direction. This is consistent with the earlier observation that some QL cells were apparently polarized in both the anterior and posterior directions (Figure 2.4E). Anterior QL division was not observed in *mig-15(rh80)*, possibly because of the more severe general defects in polarization and migration in this mutant. MIG-15 was previously shown to affect Q migration (Williams, 2002). Data reported here indicate that *mig-15* is required for the ability of Q cells to polarize and to maintain polarity, in addition to being required for Q cell migration. Initial direction of Q cell polarization was not affected by *mig-15(rh148)* or *mig-15(rh80)*. While *mig-15(rh80)* causes a premature stop, it might not represent a complete loss of function. Therefore, it is possible that complete loss of *mig-15* function might also affect direction of Q cell polarization.

**Canonical Wnt signaling does not affect initial Q cell migration.** Mutations in canonical Wnt signaling cause reversal of QL descendant migration (Eisenmann, 2005). Canonical Wnt signaling is thought to act after QL cell polarization and

migration. To confirm that canonical Wnt signaling did not affect early Q cell polarization and migration, these cells were analyzed in canonical Wnt signaling mutants. The initial polarizations and migrations of QL and QR in *lin-17(e1456)/Frizzled* (Sawa et al., 1996) and *bar-1(ga80)/ $\beta$ -catenin* (Eisenmann et al., 1998) were similar to wild-type (data not shown). Furthermore, QL and QR divided atop V5L and V4R in these mutants, indicating that initial QL and QR migrations were not affected by *lin-17(e1456)* and *bar-1(ga80)* (Figure 2.6). *bar-1(ga80)* is thought to be a strong loss-of-function allele, and *bar-1* encodes the only  $\beta$ -catenin involved in canonical Wnt signaling in *mab-5* activation (Herman, 2003; Korswagen et al., 2000; Maloof et al., 1999; Natarajan et al., 2001). These data confirm that complete loss of canonical Wnt signaling does not affect initial Q cell polarization and migration and that *mig-15* acts in a canonical Wnt-independent manner in Q cell polarization and migration.

***mab-5* expression in QL is reduced in *mig-15* mutants.** A full-length *mab-5* coding region fused to *gfp* (*mab-5::gfp*), shown previously to report MAB-5 expression (Cowing and Kenyon, 1996; Forrester et al., 2004), was used to visualize MAB-5 protein expression in wild-type and *mig-15(rh148)*. In wild-type, MAB-5::GFP expression was observed in QL descendants in 37/51 animals (67%), whereas 33/75 *mig-15(rh148)* animals (44%) showed visible MAB-5::GFP in the QL descendants ( $p = 0.01$ ). This approximately 35% reduction in MAB-5 expression in *mig-15(rh148)* is in line with the previously-reported percentage of PQR direction of migration defects. Furthermore, *qid-7(mu327)* and *qid-*

*8(mu342)*, alleles of *mig-15* as described above, caused reduced MAB-5::GFP expression in QL descendants (Ch'ng et al., 2003).

**The Q descendants AQR and PQR reverse direction of migration in *mig-15* mutants in a *mab-5*-dependent manner.** The migrations of Q cell descendants AQR (QR.ap) and PQR (QL.ap) were analyzed in *mig-15* mutants. Previous studies utilized an *osm-6::gfp* transgene, expressed in all ciliated sensory neurons including AQR and PQR, to score AQR and PQR position (Shakir et al., 2006). In work described here, a transgene consisting of the *gcy-32* promoter driving *gfp* expression (*gcy-32::gfp*) was used to score AQR and PQR. *gcy-32::gfp* was expressed in AQR and PQR after completion of their anterior and posterior migrations (Figure 2.7A and D) (Yu et al., 1997). *gcy-32::gfp* was also expressed in the non-Q cell-derived URX neurons in the head, one on the left and one on the right (Figure 2.7A). The posterior migration of PQR was dependent upon Wnt signaling, as mutations in the canonical Wnt pathway (*egl-20(mu39)/Wnt*, *lin-17(e1456)/Frizzled*, and *bar-1(ga80)/ $\beta$ -catenin*) caused PQR to migrate anteriorly instead of posteriorly and had no effect on AQR migration (Figure 2.8). Previous studies indicated that in *egl-20* mutants, the QR descendants AVM and SDQR stopped short of their normal anterior positions (Harris et al., 1996; Zinovyeva et al., 2008). We saw no effect on AQR position in *egl-20(mu39)*. Wnt activity in the control of AVM/SDQR placement is complex, as multiple Wnts are required for AVM/SDQR migration and they can have opposing activities, as *lin-44* partially suppresses AVM/SDQR defects of *egl-20*

(Zinovyeva et al., 2008). AQR migrates further to the anterior than AVM/SDQR, and possibly AQR migration does not rely on these Wnt interactions in the same manner as AVM/SDQR for its final position.

In both *mig-15(rh148)* and *mig-15(rh80)*, PQR reversed direction of migration to migrate anteriorly (39% and 47%, respectively) (Figure 2.7E and F). A small but significant proportion of AQR neurons migrated posteriorly into the phasmid ganglion in *mig-15(rh80)* (6%) (Figure 2.7F and Figures 2.9A and B), a defect never observed in wild-type or in *mig-15(rh148)*. Thus, *mig-15* loss of function caused reversal of both AQR and PQR direction of migration. Reversal of AQR direction of migration was also not observed in Wnt signaling mutants *egl-20(mu39)*, *lin-17(e1456)*, or *bar-1(ga80)* (Figure 2.8).

Anterior migration of PQR in *mig-15* mutants was likely due to failure of *mab-5* expression in QL descendants as shown above. That AQR migrated posteriorly in some *mig-15(rh80)* animals suggested that *mab-5* might occasionally be expressed in QR descendants in *mig-15(rh80)*. Indeed, posterior migration of AQR was dependent upon functional MAB-5, as the *mig-15(rh80); mab-5(e1239)* loss-of-function double mutant displayed no posteriorly-directed AQR neurons seen in *mig-15(rh80)* alone (Figures 2.9C and D). As expected, PQR was directed to the anterior in *mab-5(e1239)* alone. These data suggest that MAB-5 function was required for the posterior migration of some AQR neurons in *mig-15(rh80)* and that *mab-5* might be active in some QR descendants in *mig-15(rh80)*.

**AQR and PQR fail in migration in *mig-15* mutants in a *mab-5*-independent**

**manner.** In addition to directional migration defects, AQR and PQR in *mig-15* mutants failed to migrate to their normal positions in the anterior and posterior (Figure 2.7). In *mig-15* mutants, posteriorly-directed PQRs often failed to reach the phasmid ganglion, and anteriorly-misdirected PQRs often failed to reach the left anterior deirid ganglion (the contralateral position of normal AQR migration), but stopped along the anterior migration route (Figures 2.7B, E and F).

Furthermore, AQR neurons of *mig-15* mutants often failed in their migrations and stopped before reaching the right-side anterior deirid ganglion (Figures 2.7C, E, and F). AQR and PQR migration defects described above for *mig-15* were not observed in *bar-1(ga80)/ $\beta$ -catenin*, the presumptive null state of canonical Wnt signaling in Q cell migration (Figure 2.8). *egl-20(mu39)/Wnt* and *lin-17(e1456)/Frizzled* displayed no AQR migration defects, but misdirected PQRs often failed to migrate completely (Figure 2.8). The nature of this defect in *egl-20* and *lin-17* is unclear, but *bar-1(ga80)* did not display PQR migration defects.

The failure of migration of AQR and PQR in *mig-15* mutants was not dependent upon *mab-5* activity, as *mig-15* doubles with *mab-5(e1239)* loss of function still showed AQR and misdirected PQR migration defects (Figure 2.9D). The constitutively-active *mab-5(e1751)* allele causes constitutive expression of *mab-5* in both QL and QR descendants (Salser and Kenyon, 1992). As expected, constitutively-active *mab-5(e1751)* caused both AQR and PQR to be directed to the posterior (Figure 2.9E) (Salser and Kenyon, 1992). In *mig-15(rh80); mab-5(e1751)* doubles, both AQR and PQR were posteriorly directed

but they often stopped along their posterior migration routes before reaching the phasmid ganglion, a defect rarely observed in *mab-5(e1751)* alone (Figure 2.9F). These results indicate that MIG-15 has a MAB-5-independent role in AQR and PQR migration.

***mig-15* is expressed in the Q neuroblasts.** To determine the expression pattern of *mig-15*, a transgene consisting of a 4-kb upstream promoter fragment of *mig-15* driving *gfp* was constructed (*mig-15::gfp*). This transcriptional *mig-15::gfp* transgene was expressed in hypodermis, muscle, pharynx, and neurons as previously described (data not shown) (Poinat et al., 2002). Additionally, *mig-15 promoter::gfp* expression was observed in both Q neuroblasts as well as in the lateral seam cells and P cells neighboring the Q cells (Figure 2.10).

***mig-15* acts cell-autonomously in AQR and PQR migration.** Mosaic analysis was used to determine if *mig-15* acts cell-autonomously (Herman, 1984; Yochem and Herman, 2005) (see Materials and Methods for details of the experimental design). Figure 2.11A shows the lineage relationships between marker cells used in this mosaic analysis (Sulston et al., 1983), and Tables 2.2 and 2.3 show the loss profiles of each mosaic analyzed.

Mosaics that had lost *mig-15(+)* in AQR and/or PQR but retained *mig-15(+)* in other tissues were analyzed (Table 2.2). Forty seven mosaics had losses in the PQR lineage and displayed PQR direction and migration defects similar to *mig-15(rh80)* alone (Figure 2.11B and D). Twenty-five PQR(-) mosaics



had detectable losses only in PQR as shown in Figure 2.11B, and 20/25 displayed PQR migration defects. Thirty three mosaics were identified that had lost *mig-15(+)* in AQR and displayed AQR migration defects similar to *mig-15(rh80)* alone (Figure 2.11C). Of mosaics that retained *mig-15(+)* in AQR or PQR, all but one had normal AQR or PQR migration (Table 2.2).

Next, mosaics that retained *mig-15(+)* in AQR and/or PQR but that had lost *mig-15(+)* in other tissues were analyzed (Table 2.3). Of 64 mosaics that retained *mig-15(+)* in PQR, 62 displayed normal PQR migration (Figure 2.11F). Of 61 mosaics that retained *mig-15(+)* in AQR, 60 showed normal AQR migration (Figure 2.11E).

In sum, this mosaic analysis is consistent with a cell autonomous role of *mig-15* in AQR and PQR migration. A caveat of this analysis is that V5L is a potential substrate cell of QL and is also the sister of QL. Non-autonomous function of *mig-15* in V5L could not be excluded by this mosaic analysis. However, QR and V4R, a potential substrate of QR migration, are derived from distant lineages (V4R is from AB.a whereas QR is from AB.p). Functions in these lineages were resolved by this mosaic analysis: 12 mosaics with losses in URXR, an AB.a derivative, but not AQR had normal AQR migration; and 22 mosaics with losses in AQR but not in URXR had defective AQR migration.

## 2.5. Discussion

Mutations in *mig-15* reduced the size of the initial Q cell protrusions during polarization but did not affect the direction of initial polarization. *mig-15* mutations also disrupted the later maintenance of Q cell polarity and migration of the cells in the anterior (QR) and posterior (QL) directions. Later, after the Q cells have divided, *mig-15* affected the ability of the Q descendants AQR and PQR to migrate along their routes. Thus, MIG-15 might be required for robust Q cell polarization, maintenance of Q cell polarity, Q cell migration, and migration of the Q cell descendant neurons.

### **MIG-15 affects Q cell polarization, maintenance of polarity, and migration.**

Strong loss-of-function of *mig-15* resulted in shortened and less-robust Q cell protrusions, with QL and QR equally affected. Interestingly, the hypomorphic *mig-15(rh148)* did not strongly affect initial polarization. Possibly, robust protrusion requires less *mig-15* activity than does maintenance of polarity and migration, and the hypomorphic *mig-15(rh148)* might provide enough activity for proper polarization. *mig-15(rh148)* is a missense mutation in a conserved residue of the ATP-binding pocket of the kinase domain (Shakir et al., 2006). An alternate explanation is that the kinase activity of MIG-15, which might be specifically disrupted in *mig-15(rh148)*, is not required for initial Q cell polarization.

Both *mig-15(rh80)* and *mig-15(rh148)* affected maintenance of Q cell polarity and Q cell migration. These might be distinct processes, as *mig-*

*15(rh148)* had little effect on initial Q cell polarization but had a later effect on maintenance of Q cell polarity and migration.

**Failure of QL migration in *mig-15* might perturb *mab-5* expression.** In *mig-15(rh148)* mutants, *mab-5* often failed to be expressed in QL descendants, an effect also seen with the *qid-7/qid-8* alleles of *mig-15* (Ch'ng et al., 2003). Furthermore, the QL descendant PQR often migrated anteriorly instead of posteriorly in *mig-15* mutants, an expected effect of failure to express *mab-5* in these cells. The penetrance of failure of *mab-5* expression in *mig-15(rh148)* (35%; see Results) is in line with PQR direction of migration defects in *mig-15(rh148)* (39%; Figure 2.7E). It is possible that MIG-15 acts in this Wnt signaling pathway in addition to affecting early Q cell polarization and migration. Alternatively, the failure of QL to migrate posteriorly might result in a failure of some QL descendants to receive this Wnt signal. The observations that some AQR (QR descendants) migrated posteriorly in *mig-15(rh80)* and that this posterior migration was dependent upon functional MAB-5 supports the latter model. If MIG-15 acts in Wnt signaling and MAB-5 expression, MAB-5-dependent posterior migration of AQR would not be expected. Possibly, due to a failure in initial anterior migration of QR in *mig-15(rh80)*, QR responds to the posterior Wnt signal and activates MAB-5. The lower penetrance of posterior migration of AQR (6%; Figure 2.7F) compared to QR migration defects (45%; Figure 2.5G) could be explained by the previous observation that QR is

inherently less responsive than QL to the Wnt signal that controls *mab-5* expression (Whangbo and Kenyon, 1999).

**MIG-15 is required for Q descendant migration.** In *mig-15* mutants, AQR and PQR often failed to migrate to their normal final positions. Q descendant migration defects were independent of MAB-5, as migration defects were observed in *mab-5* loss-of-function and gain-of-function doubles with *mig-15*. MIG-15 might be required for the ability of AQR and PQR neurons to migrate along their normal routes. MIG-15 might control the speed of AQR and PQR migration or might control migration decisions at specific choicepoints along their migration routes. Further studies of MIG-15 in AQR and PQR migration will address these hypotheses.

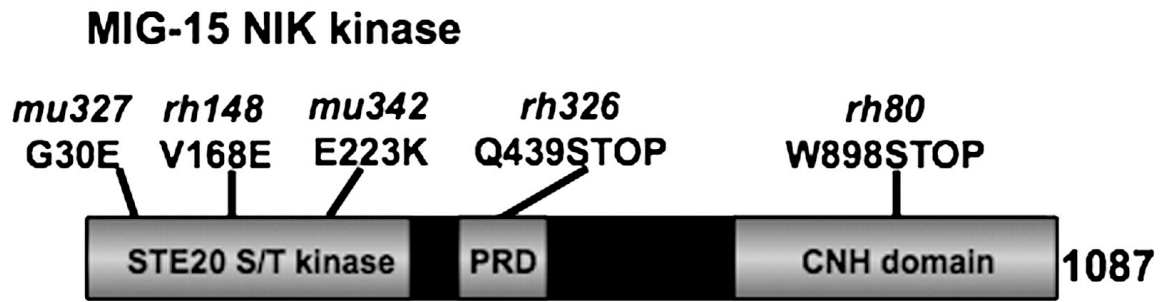
***mig-15* acts cell-autonomously in Q descendant migration.** Loss of *mig-15* in the PQR lineage resulted in both PQR direction and migration defects and loss in the AQR lineage results in AQR migration defects, despite retention of *mig-15(+)* in other tissues. Conversely, retention of *mig-15* activity in AQR or PQR lineages resulted in normal migration of these neurons despite loss in other tissues. The EGL-20 Wnt signal that controls *mab-5* expression emanates from the K, F, U, and B blast cells as well as from the anal muscle muAnal and the P9/P10 ectoblasts (Whangbo and Kenyon, 1999). QL, derived from AB.pla, is separated in lineage from these cells, derived from AB.pr and AB.plp. While EGL-20-secreting cells were not specifically assayed in this mosaic analysis, the

consistency of the data suggesting cell autonomy, the numbers of mosaics analyzed, and the wide lineage separation of QL and EGL-20-secreting cells suggests that MIG-15 is not required in these cells. A non-autonomous role of MIG-15 in V5L for QL migration could not be distinguished due to the fact that they are sister cells, but a non-autonomous role of V4R in QR migration could be excluded by this analysis (QR is an AB.p derivative and V4R is an AB.a derivative). While AQR and PQR migration was assayed in this mosaic analysis, it is likely that MIG-15 acts autonomously in initial Q cell polarization and migration, as anterior misdirection of PQR was cell-autonomous and likely dependent upon initial QL polarization and migration. In sum, this mosaic analysis is consistent with a cell-autonomous role of *mig-15* in initial Q cell polarization and migration and Q descendant migration.

**MIG-15 and cell polarization and migration.** These results indicate that MIG-15 is required for robust Q cell polarization, maintenance of Q cell polarity, and Q cell migration. The cellular mechanisms underlying these events could be the same, although *mig-15(rh148)* affects maintenance and migration without affecting polarity, suggesting the mechanisms might be distinct. In cultured cells, NIK kinase activity drives lamellipodial extension dependent upon the ERM class of actin modulatory molecules (Baumgartner et al., 2006), consistent with failure of *mig-15* mutants to extend robust lamellipodial protrusions during polarization. NIK kinases also physically and functionally interact with  $\beta$ 1 integrin (Becker et al., 2000; Poinat et al., 2002). Possibly, failure to maintain Q cell polarity in *mig-*

15 mutants is due to defects in adhesion mediated by integrin. NIK kinases are also involved in nuclear migration (Houalla et al., 2005), which could explain the failure of the Q cell bodies to migrate over the V cells, although this could also be due to a failure in initial polarization or maintenance of polarity. Further studies of MIG-15 in polarization and migration will be guided by these hypotheses.

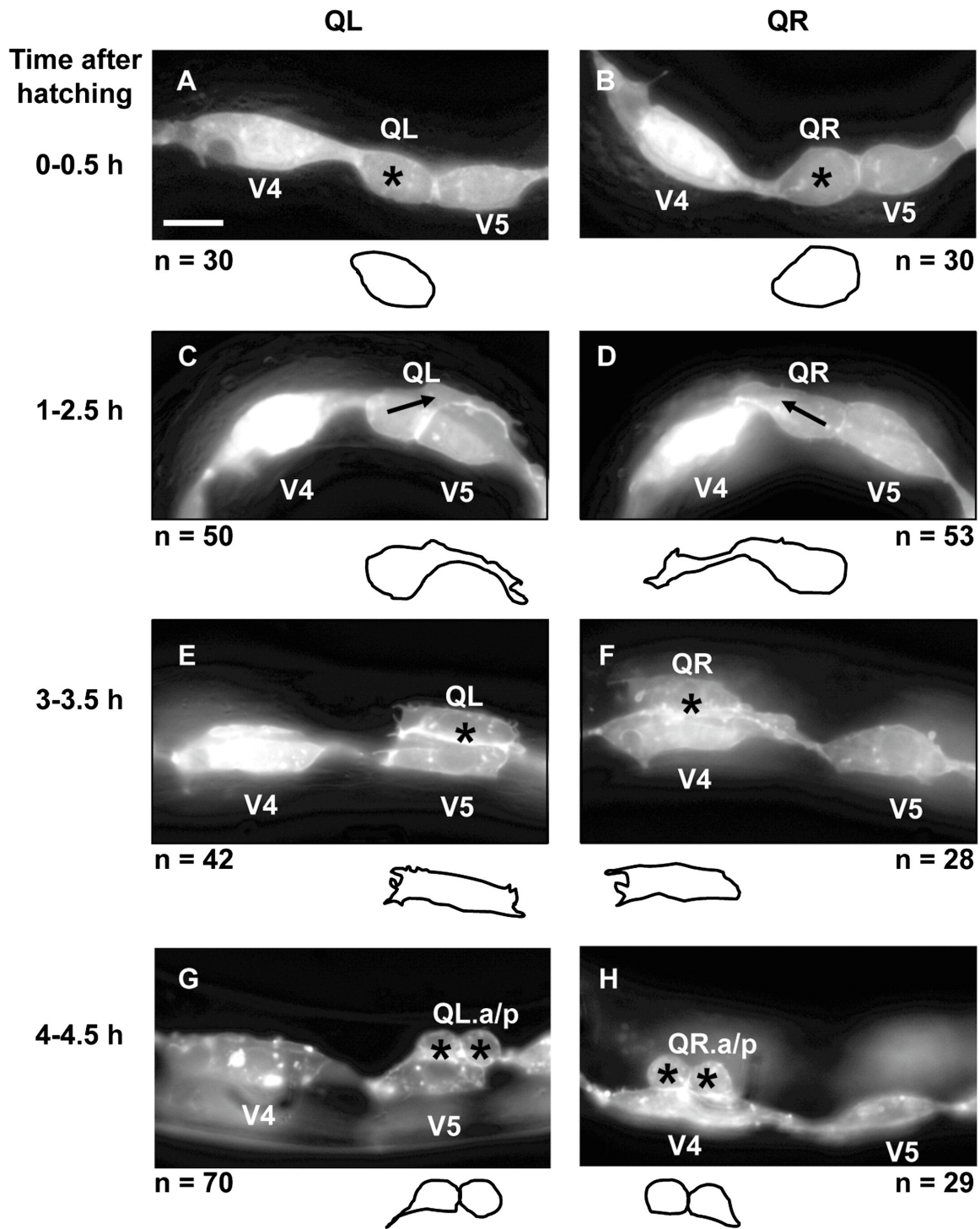
Figure 2.1



**Figure 2.1. The MIG-15 NIK kinase.** MIG-15 contains a STE20 class serine/threonine kinase domain, a proline rich domain (PRD), and a citron/NIK homology (CNH) domain. The effects of the *mu327*, *rh148*, *mu342*, *rh326*, and *rh80* mutations are shown. *qid-7(mu327)* was a G to A missense mutation at position 89 in the *mig-15* open reading frame, resulting in glycine 30 to glutamic acid change. *qid-8(mu342)* was a G to A missense mutation at position 667, resulting in glutamic acid 223 to lysine change.

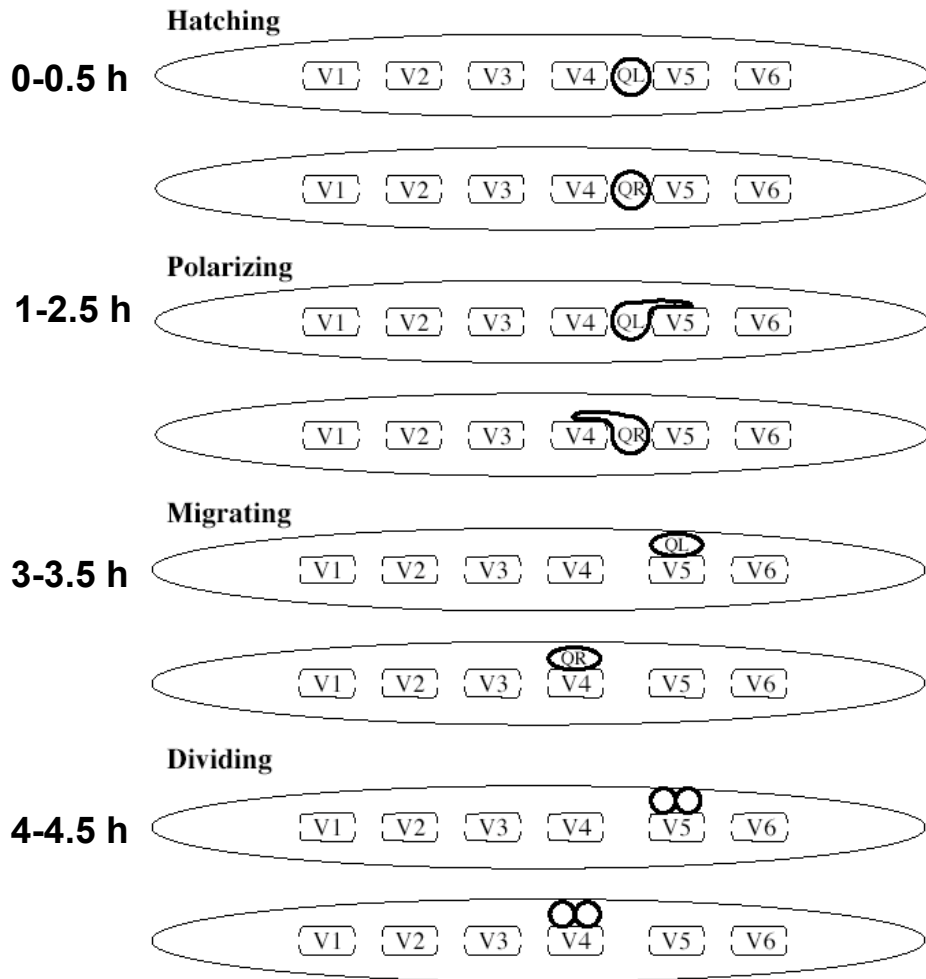


Figure 2.2



**Figure 2.2. Q neuroblast polarization and migration.** (A-H) are panels of epifluorescent micrographs of Q neuroblasts of L1 larvae at given timepoints after hatching expressing the *scm::gfp::caax* marker in the Q cells and the lateral seam cells (V cells). Tracings of the boundaries of the Q neuroblasts in each micrograph are located below each panel. For each time point, the QL neuroblast is found on the left (A,C,E,G) and the QR neuroblast is found on the right (B,D,F,H). The scale bar in (A) represents 5 $\mu$ m for (A-H). (A-B) Unpolarized Q neuroblasts visualized 0-0.5 h after hatching. Asterisks mark the position of the Q neuroblasts. (C-D) Polarization of the Q neuroblasts visualized 1-2.5 h after hatching. QL sent a process posteriorly over the V5L seam cell. QR sent a process anteriorly over the V4R seam cell. Arrows indicate the direction of polarization of the Q neuroblasts. (E-F) Migration of the Q neuroblasts visualized 3-3.5 h after hatching. QL migrated posteriorly over the V5L seam cell. QR migrated anteriorly over the V4R seam cell. (G-H) Division of the Q neuroblasts visualized 4-4.5 h after hatching. QL divided over the V5L seam cell to produce QL.a and QL.p. QR divided over the V4R seam cell to produce QR.a and QR.p. Asterisks mark the position of the Q neuroblast daughters.

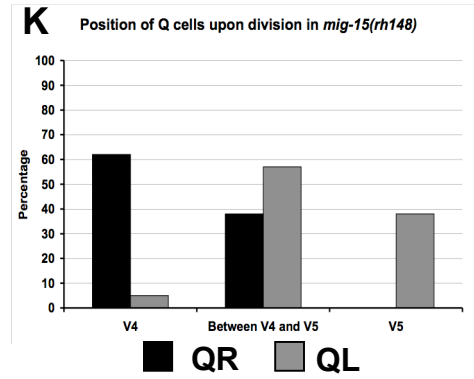
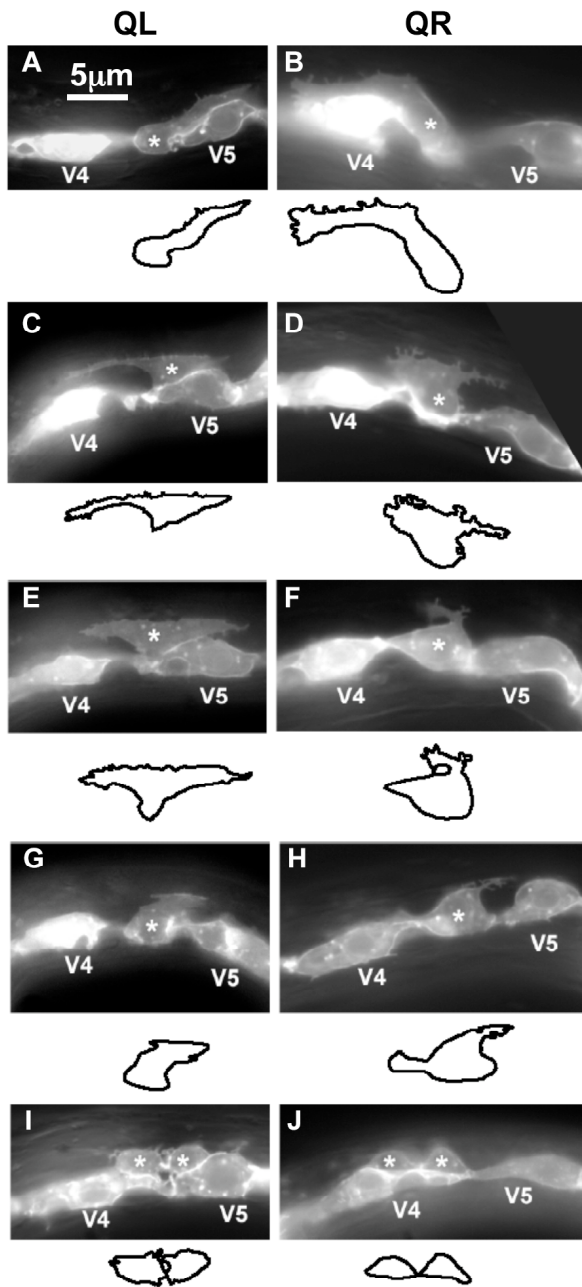
Figure 2.3



**Figure 2.3. Schematic diagram of Q neuroblast polarization and migration.**

A schematic diagram demonstrating the polarization, migration, and division patterns of the Q neuroblasts. For each stage, the time after hatching is listed to the left of the figures for that stage.

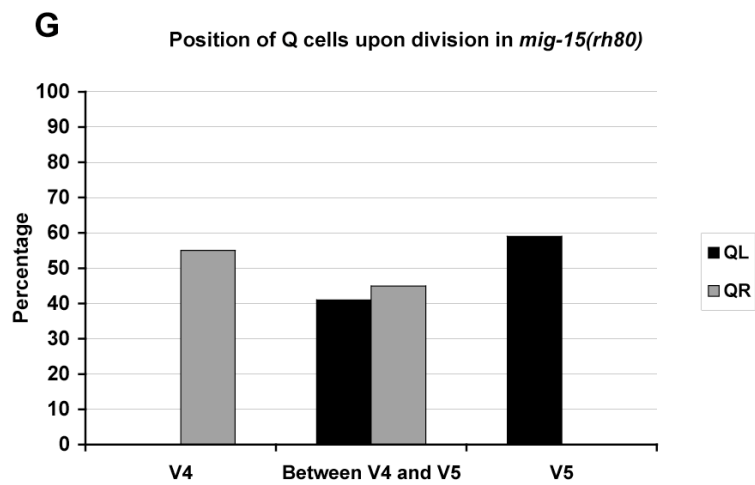
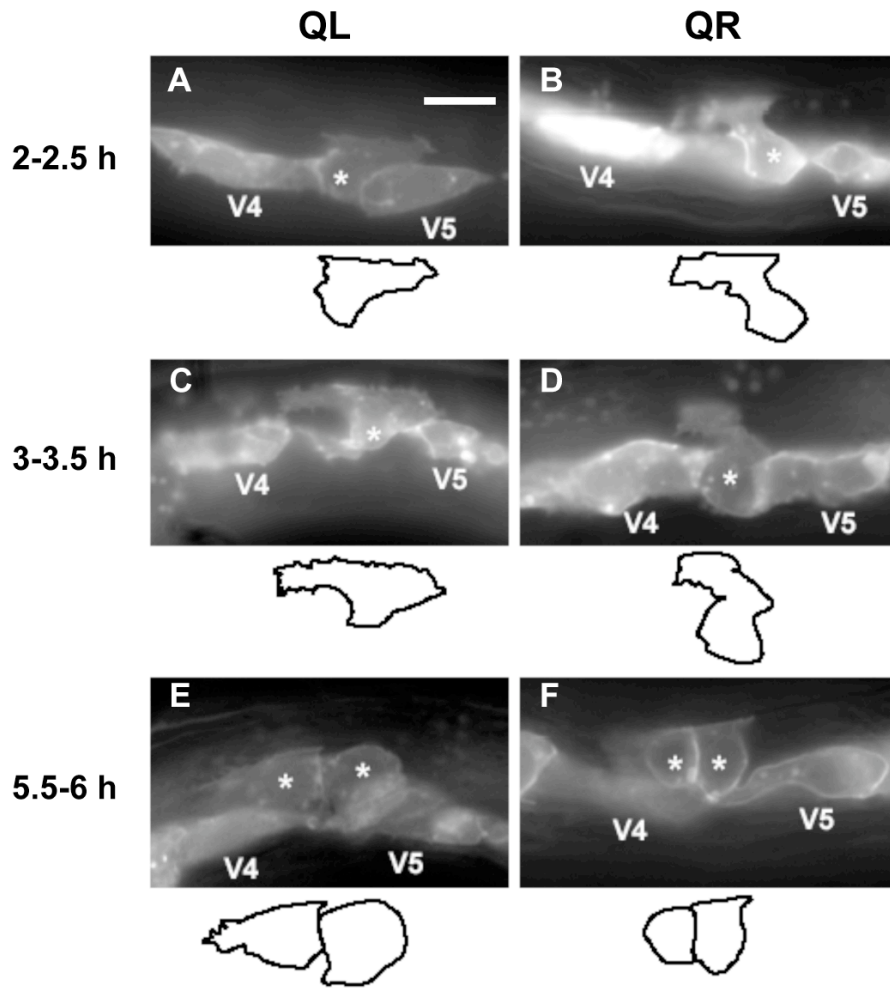
Figure 2.4



**Figure 2.4. *mig-15* NIK kinase hypomorphic mutation affects the polarizations and migrations of the Q neuroblasts.** (A-J) are panels of epifluorescent micrographs of Q neuroblasts of L1 larvae in *mig-15(rh148)* mutants with *scm::gfp::caax* expression. Asterisks mark the position of the Q neuroblast at 3-3.5 h after hatching (A-H) or Q neuroblast descendants at 4-4.5 h after hatching (I-J). Tracings of the Q neuroblasts found in each micrograph are located below each panel. The scale bar in (A) represents 5 $\mu$ m for (A-J). (A) A QL neuroblast polarized normally over the V5L seam cell. (B) A QR neuroblast polarized normally over the V4R seam cell. (C) A QL neuroblast failed to maintain proper posterior polarization, and sent a protrusion to the anterior. (D) A QR neuroblast failed to maintain proper anterior polarization, and sent a protrusion to the posterior. (E) A QL neuroblast sent protrusions to both the anterior and posterior. (F) A QR neuroblast was not strongly polarized in either direction and sent a small, anteriorly-directed protrusion from the posterior of the cell. (G) A QL neuroblast was not strongly polarized in either the anterior or posterior direction, although maintained slight posterior polarization. (H) A QR neuroblast was not strongly polarized in either the anterior or posterior direction and sent a small protrusion posteriorly. (I) A QL neuroblast divided between the V4L and V5L seam cells. (J) A QR neuroblast divided over the V4R seam but was not atop the V4R seam cell. (K) Quantitation of the position of the QL and QR neuroblasts upon division (4-4.5 h after hatching) in *mig-15(rh148)* mutants. Position with respect to the V4 and V5 seam cells is the X axis, and the percentage of Q neuroblast daughters found at those positions is the Y axis. For

QL divisions, 37 animals were scored. For QR divisions, 26 animals were scored.

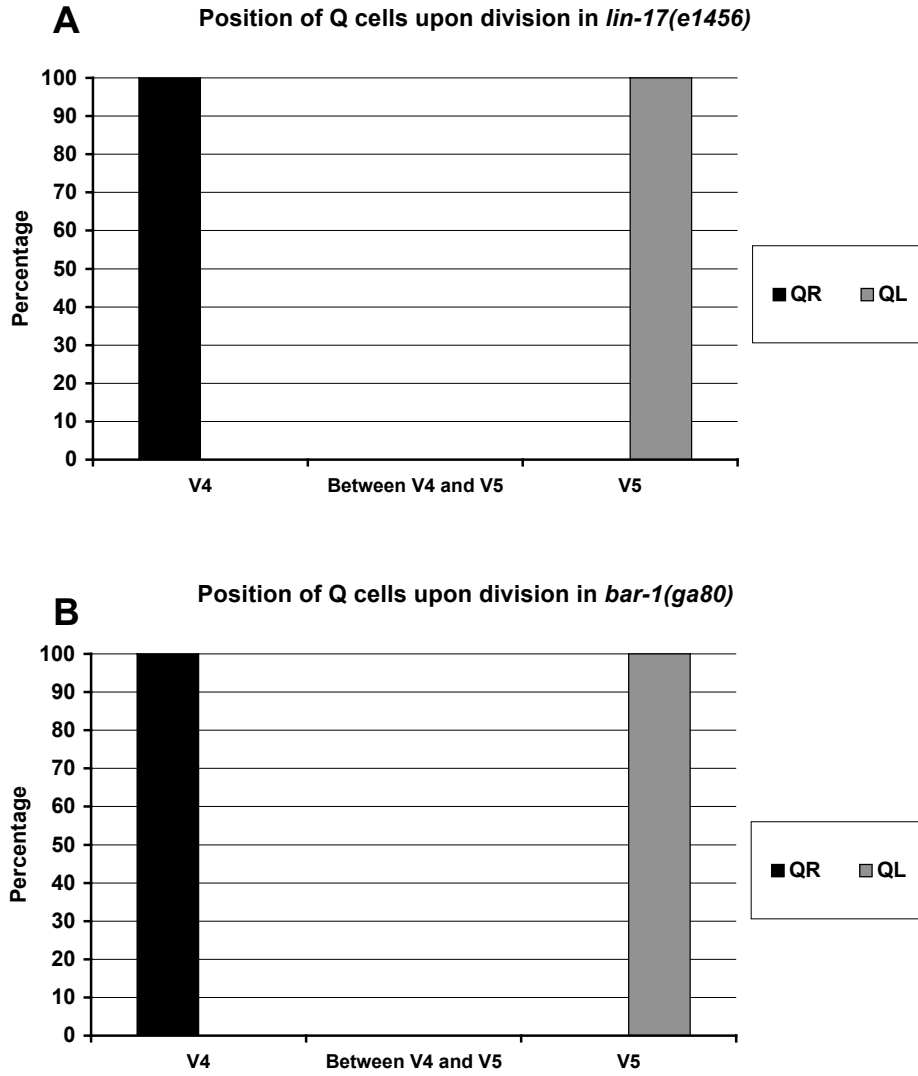
Figure 2.5





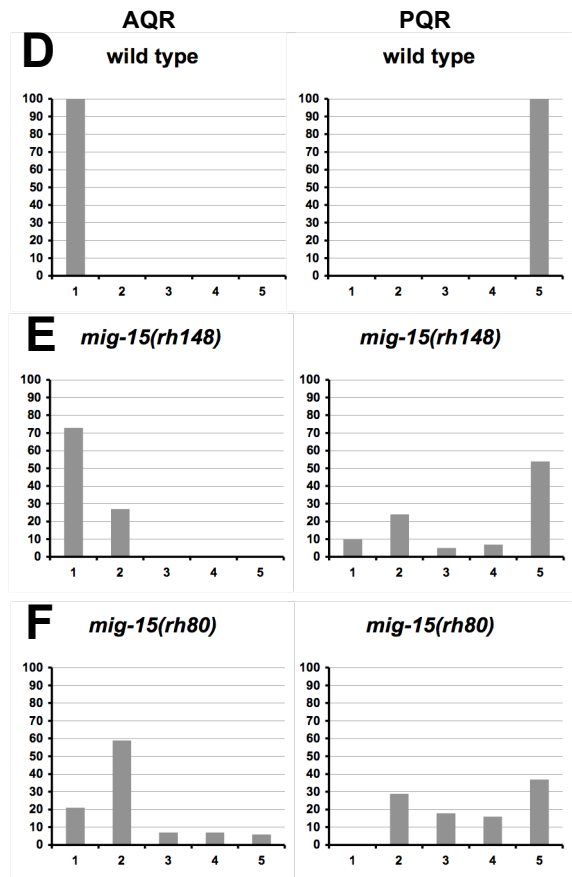
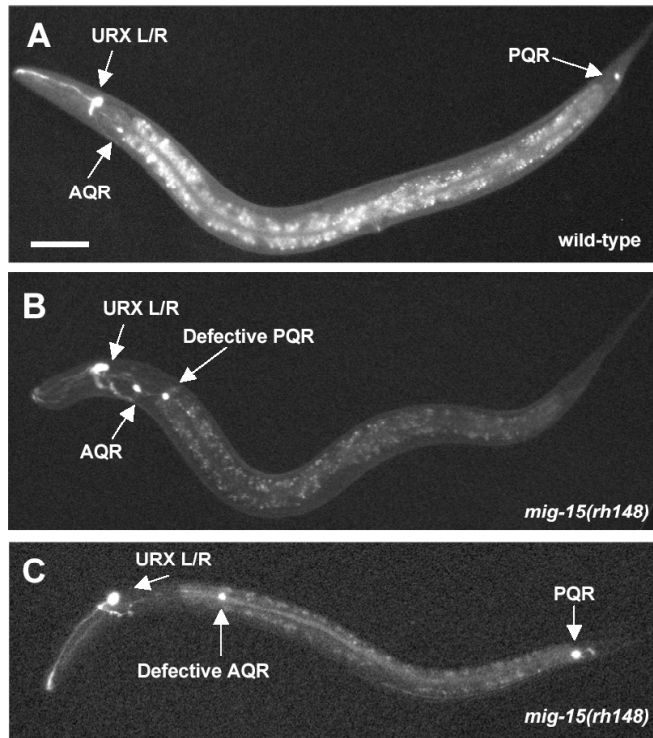
**Figure 2.5. *mig-15* NIK kinase strong loss-of-function mutation affects the polarizations and migrations of the Q neuroblasts.** (A-F) are panels of epifluorescent micrographs of Q neuroblasts of L1 larvae in *mig-15(rh80)* mutants with *scm::gfp::caax* expression. Asterisks mark the position of the Q neuroblast at 2-2.5 h after hatching (A-B) and 3-3.5 h after hatching (C-D) or Q neuroblast descendants at 5.5-6 h after hatching (E-F). Tracings of the Q neuroblasts found in each micrograph are located below each panel. The scale bar in (A) represents 5 $\mu$ m for (A-F). (A) A QL neuroblast polarized posteriorly over the V5L seam cell, but did not extend its protrusion nearly as far as in wild type. (B) A QR neuroblast polarized anteriorly over the V4R seam cell, but did not extend its protrusion nearly as far as in wild type. (C) A QL neuroblast sent protrusions in both anterior and posterior directions. (D) A QR neuroblast did not polarize strongly in either direction, although it sent a small protrusion anteriorly. (E) A QL neuroblast divided between the V4L and V5L seam cells. (F) A QR neuroblast divided between the V4R and V5R seam cells. (G) Quantitation of the position of the QL and QR neuroblasts upon division (5.5-6 h after hatching) in *mig-15(rh80)* mutants. The graph is organized as described in Figure 2.4K. For QL divisions, 41 animals were scored. For QR divisions, 38 animals were scored.

Figure 2.6



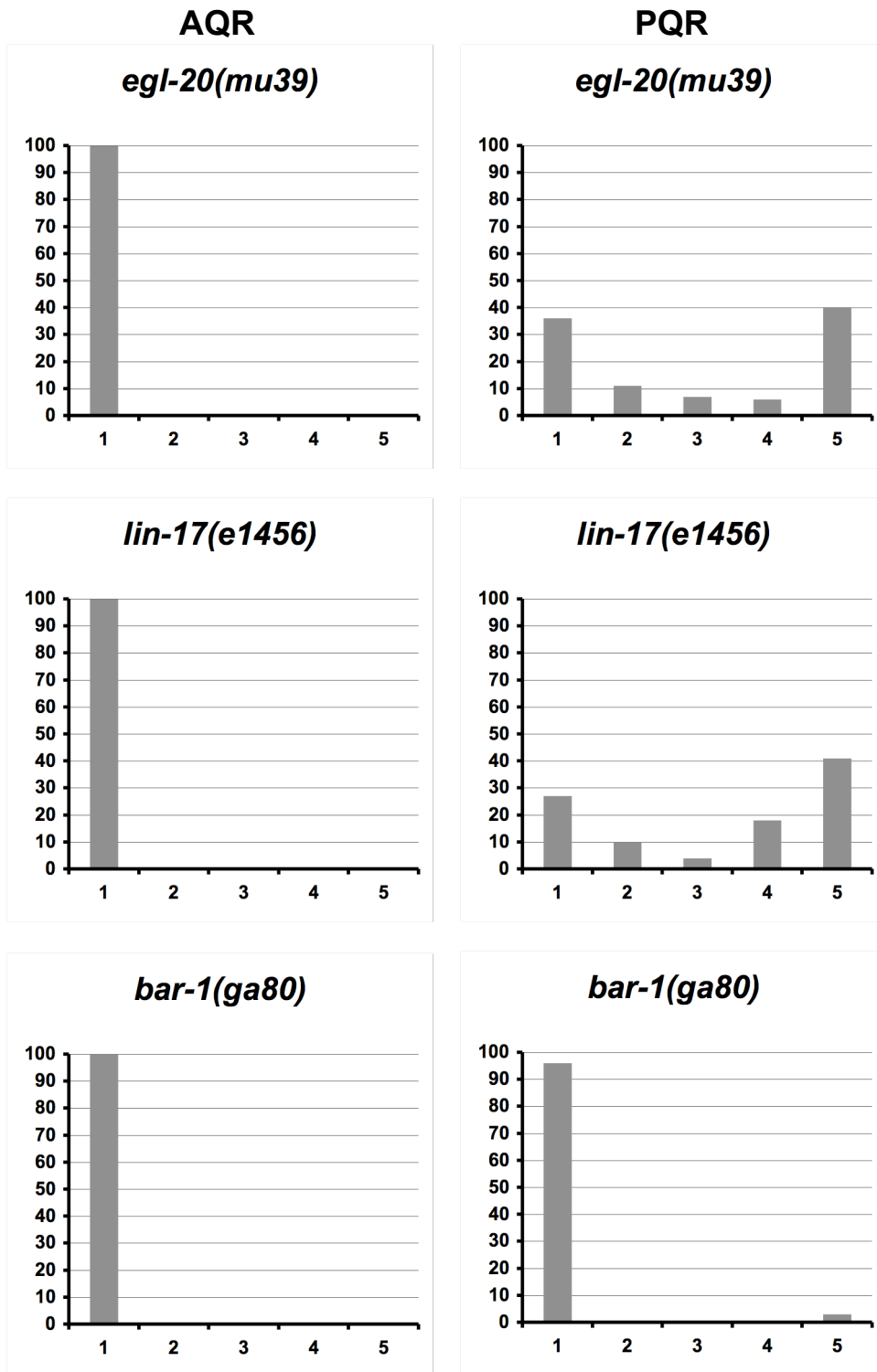
**Figure 2.6. Canonical Wnt signaling does not affect the migrations of the Q neuroblasts.** The graphs are organized as described in Figure 2.4K. (A) Quantitation of the position of the QL and QR neuroblasts upon division (4-4.5 h after hatching) in *lin-17(e1456)* mutants. For QL divisions, 28 animals were scored. For QR divisions, 16 animals were scored. (B) Quantitation of the position of the QL and QR neuroblasts upon division (4-4.5 h after hatching) in *bar-1(ga80)* mutants. For QL divisions, 37 animals were scored. For QR divisions, 17 animals were scored.

Figure 2.7



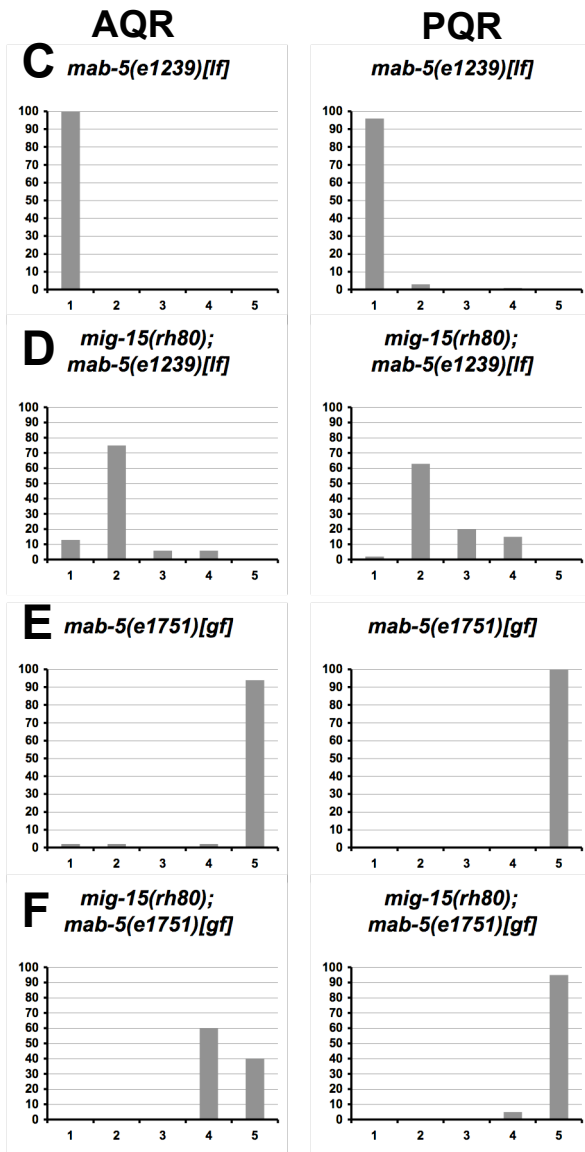
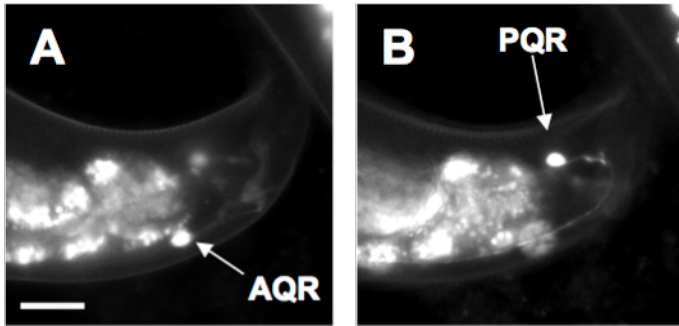
**Figure 2.7. The Q neuroblast descendants AQR and PQR have direction of migration defects and fail to migrate in *mig-15* NIK kinase hypomorphic mutants.** (A-C) are panels of epifluorescent micrographs of AQR and PQR neurons of L4 larvae with *gcy-32::gfp* expression. The scale bar in (A) represents 50 $\mu$ m for (A-C). (A) A wild-type animal with AQR located near the anterior deirid ganglion and PQR near the phasmid ganglion. (B) A *mig-15(rh148)* hypomorphic mutant with AQR located in its normal position. PQR migrated anteriorly, but failed to migrate to the same anterior-posterior position as AQR. (C) A *mig-15(rh148)* mutant with PQR located in its normal position. AQR migrated anteriorly, but failed to migrate completely to reside near the anterior deirid ganglion. (D-F) Quantitation of the final migratory positions of AQR and PQR. Anterior-posterior position of AQR and PQR is the X axis (see Materials and Methods section for description of the classifications of the anterior-posterior positions), and the percentage of AQR and PQR found at those positions in the Y axis. In each case, 100 animals were scored.

Figure 2.8



**Figure 2.8. The PQR neuron has direction of migration defects and fails to migrate in canonical Wnt signaling mutants.** Quantitation of the final migratory positions of AQR and PQR. The graphs are organized as described in Figure 2.7D-F. For *egl-20(mu39)* and *lin-17(e1456)*, 100 animals were scored. For *bar-1(ga80)*, 200 animals were scored.

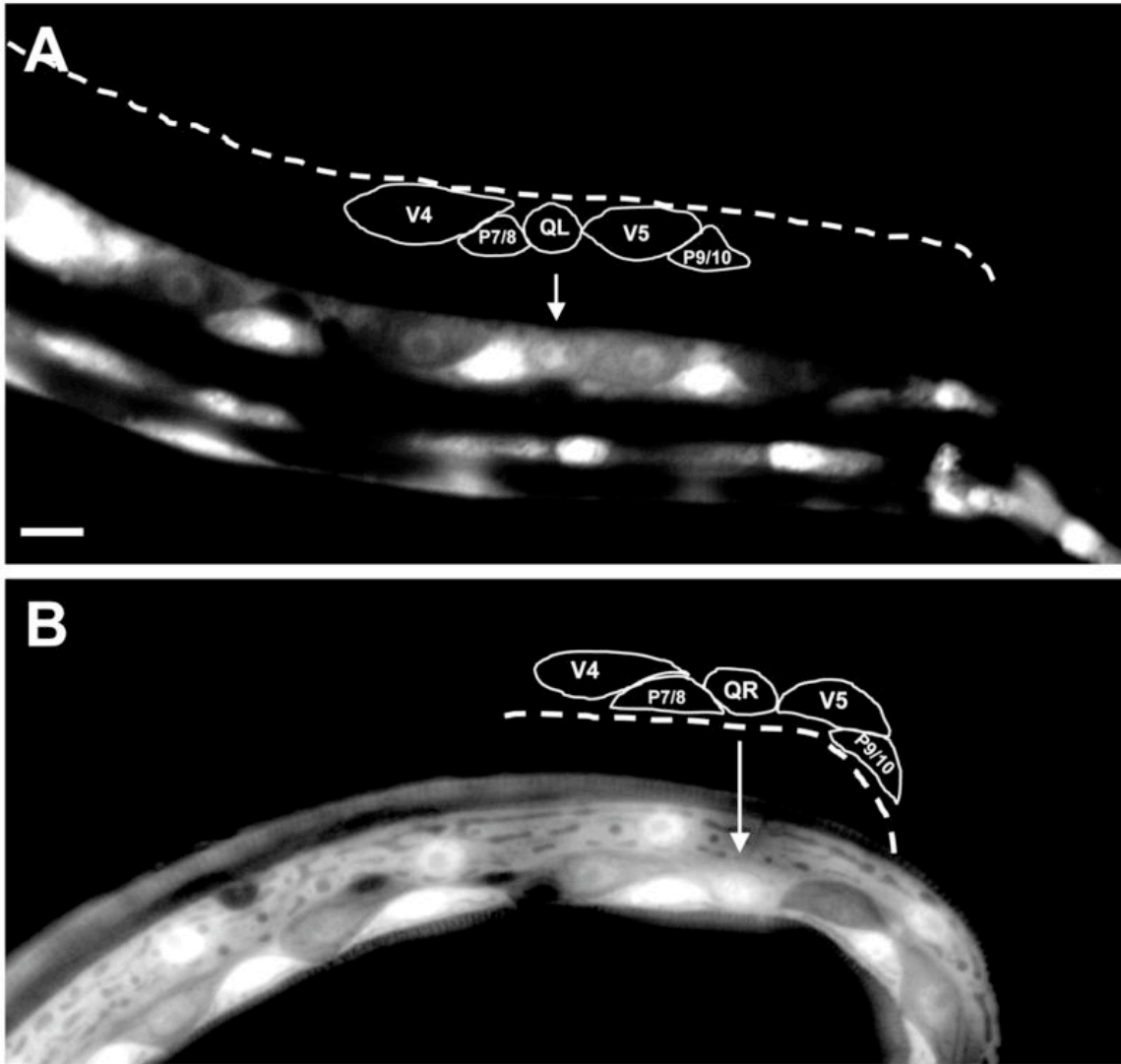
Figure 2.9





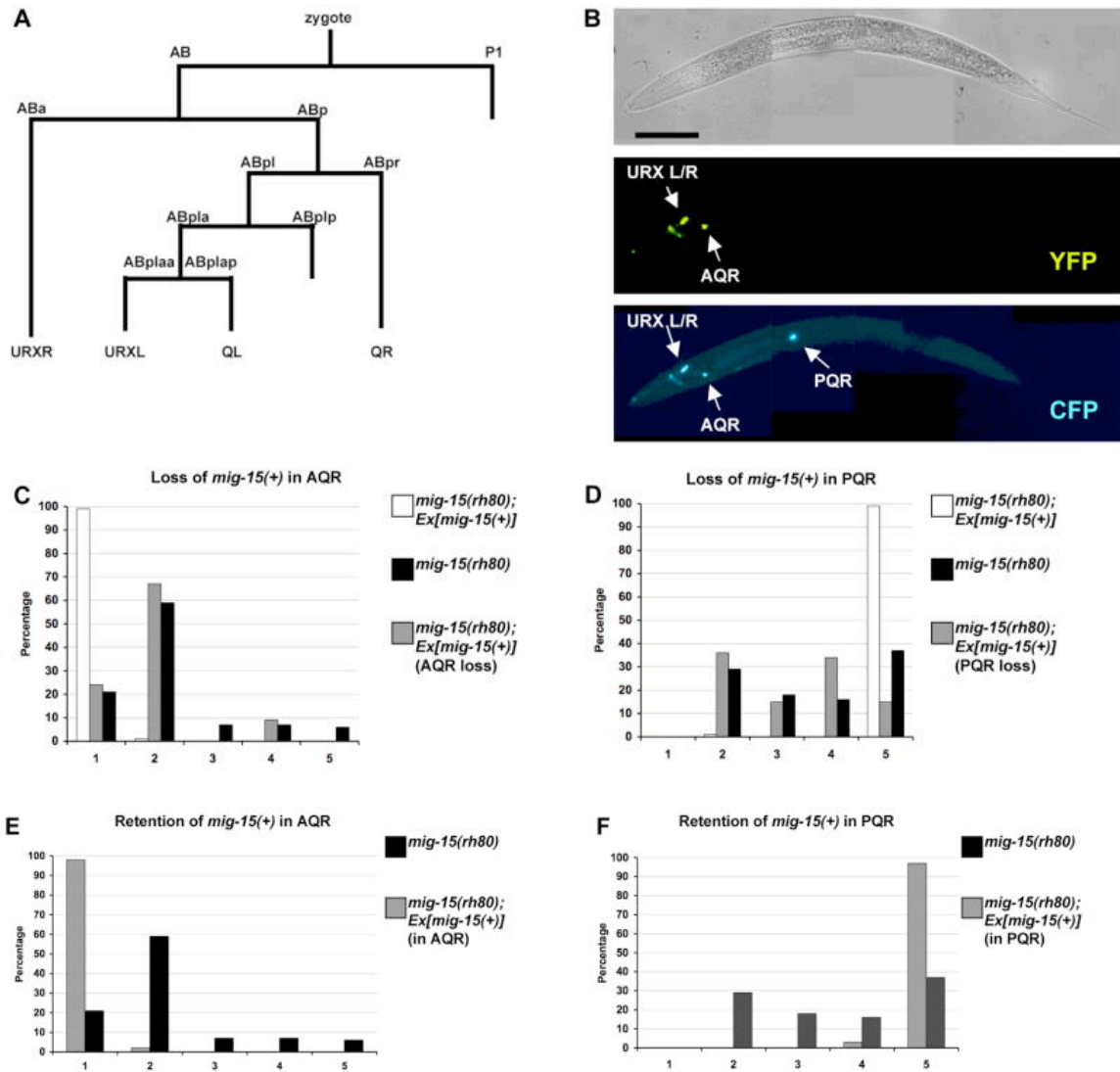
**Figure 2.9. The AQR/PQR direction of migration defects seen in *mig-15* NIK kinase hypomorphic mutants are dependent on MAB-5, whereas the failure to migrate defects are independent of MAB-5.** (A-B) are panels of epifluorescent micrographs of AQR and PQR neurons of a young adult in a *mig-15(rh80)* mutant with *gcy-32::gfp* expression. An AQR neuron (A) reversed the direction of migration and migrated to the tail of the animal near the PQR neuron (B). The scale bar in (A) represents 10 $\mu$ m for (A-B). (C-F) Quantitation of the final migratory positions of AQR and PQR. The graphs are organized as described in Figure 2.7D-F. *mab-5(e1239)[lf]* is a loss-of-function mutation, and *mab-5(e1751)[gf]* is a gain-of-function mutation. For each genotype, 100 animals were scored.

Figure 2.10







**Figure 2.10. *mig-15* is expressed in the Q neuroblasts.** Shown are epifluorescent micrographs of newly-hatched L1 larvae expressing the *mig-15::gfp* transcriptional promoter fusion. Tracings of the Q cells and the surrounding cells are shown above each micrograph. Arrows mark the positions of Q cells. (A) A left ventral-lateral view of an animal with *mig-15::gfp* expression in QL. The lateral seam cells (V cells) and P cells also express *mig-15::gfp*. (B) A right dorsal-lateral view of an animal with *mig-15::gfp* expression in QR. In this animal, the V5 seam cell lost *mig-15::gfp* and showed no fluorescence. The scale bar in (A) represents 5 $\mu$ m for (A-B).

Figure 2.11







**Figure 2.11. MIG-15 NIK kinase acts cell autonomously in AQR and PQR migration.** (A) The cell lineage map for the *gcy-32*-expressing cells. Not all divisions or cells are shown. (B) A mosaic animal that had lost the *mig-15(+)* transgene in the PQR neuron. The top micrograph is a Nomarski image. The middle micrograph shows that this animal has lost the *mig-15(+)* transgene in the PQR neuron as indicated by the lack of YFP expression in PQR. The bottom micrograph shows the position of AQR and PQR using an integrated *gcy-32::cfp* reporter. PQR reversed direction of migration. The scale bar in the top micrograph represents 50 $\mu$ m for all 3 micrographs in (B). (C-F) Quantitation of the final migratory positions of PQR and AQR in *mig-15(rh80)* and in mosaics.

**Table 2.1 *mig-15* polarity maintenance defects (~3-3.5 hours after hatching).**

QL	Normal polarization	Anterior extensions	Anterior/posterior polarization	No strong polarization
Genotype				
<i>mig-15(rh80)</i> (63)	44	9	3	7
<i>mig-15(rh148)</i> (45)	28	7	6	4

QR	Normal polarization	Posterior extensions	Anterior/posterior polarization	No strong polarization
Genotype				
<i>mig-15(rh80)</i> (55)	36	6	6	7
<i>mig-15(rh148)</i> (48)	41	4	0	3

**Table 2.1. *mig-15* polarity maintenance and migration defects (~3-3.5 hours after hatching).** The number of animals scored is listed after each genotype for both QL and QR. The values in each category are the number of animals scored with that listed phenotype.

**Table 2.2 The locations of AQR and PQR with the loss of the *mig-15(+)* transgene in AQR and PQR, but maintained in other tissues.**

	1	2	3	4	5	URXL	URXR		1	2	3	4	5	URXL	URXR
1	A			P		+	+	41		A			P	+	+
2	A	P				+	-	42		A	P			+	+
3	A			P		+	+	43				A	P	+	-
4	A			P		+	-	44		A			P	+	+
5	A	P				+	+	45	A	P				+	-
6	A	P				+	+	46	A				P	+	+
7	A			P		-	+	47	A				P	+	+
8	A	P				-	+	48	A			P		+	+
9	A				P	+	+	49	A			P		+	+
10	A				P	+	+	50	A				P	+	+
11	A			P		-	-	51		A			P	+	+
12	A	P				-	+	52		A			P	+	+
13				A	P	-	+	53	A	P				-	+
14	A				P	-	-	54	A	P				+	+
15	A				P	+	+	55	A			P		-	+
16		A			P	+	+	56	A	P				-	+
17		A			P	+	+	57		A			P	+	+
18	A		P			+	+	58		A			P	+	+
19	A		P			-	+	59		A			P	+	+
20		A			P	+	+	60	A		P			+	+
21		A			P	+	+	61	A	P				-	+
22	A			P		+	+	62	A	P				-	+
23	A			P		+	+	63	A				P	+	+
24		A			P	+	+	64	A		P			+	+
25		A			P	+	+	65	A		P			-	+
26		A			P	+	+	66	A				P	+	+
27		A			P	+	-	67	A	P				+	+
28	A				P	+	-	68	A				P	+	+
29	A	P				-	+	69	A	P				+	+
30	A				P	+	+	70	A		P			-	+
31	A	P				+	+	71	A	P				-	-
32	A			P		-	+	72		A			P	+	+
33		A		P		+	+	73	A			P		+	+
34		A			P	+	+	74		A		P		+	+
35				A	P	+	+	75		A			P	-	-
36		A			P	+	+								
37	A	P				+	+								
38	A			P		+	+								
39	A			P		+	+								
40	A			P		+	+								



**Table 2.2. The locations of AQR and PQR with the loss of the *mig-15(+)* transgene in AQR and PQR, but maintained in other tissues.** The final migratory positions of the AQR and PQR neurons along the anterior-posterior axis of the animal are indicated for AQR and PQR neurons that have lost the expression of the *mig-15(+)* transgene. An A or P indicates the final migratory position of the AQR and PQR neurons, respectively. The columns 1-5 indicate the position along the anterior-posterior axis (see Materials and Methods section for description of the classifications of the anterior-posterior positions). The AQR and PQR designations of A and P are color coded, with green indicating the presence of the *mig-15(+)* transgene in that neuron and blue indicating a loss of the *mig-15(+)* transgene in that neuron. The URXL and URXR columns indicate whether the *mig-15(+)* transgene was present in the left and right URX neurons, with a (+) indicating the presence of the *mig-15(+)* transgene and a (-) indicating the loss of the *mig-15(+)* transgene.

**Table 2.3 The locations of AQR and PQR with the loss of the *mig-15(+)* transgene in other tissues, but maintained in AQR and PQR.**

	1	2	3	4	5	URXL	URXR		1	2	3	4	5	URXL	URXR
1	A				P	+	-	36	A				P	+	+
2	A				P	+	-	37	A				P	+	+
3	A				P	+	-	38	A				P	+	+
4	A				P	+	+	39	A				P	+	+
5	A				P	+	-	40	A				P	+	-
6	A				P	+	+	41	A				P	+	+
7	A				P	+	+	42	A			P		-	+
8	A				P	+	-	43	A				P	+	+
9	A				P	+	-	44	A				P	+	+
10		A			P	+	+	45	A				P	+	+
11	A				P	+	+	46	A				P	+	+
12	A				P	+	+	47	A			P		+	+
13	A				P	+	-	48	A				P	+	+
14		A			P	+	+	49	A				P	+	-
15		A			P	+	+	50	A				P	+	-
16	A				P	+	+	51	A				P	+	+
17	A				P	+	+	52	A				P	+	+
18	A				P	+	+	53	A				P	+	+
19	A				P	+	+	54		A	P			-	+
20	A				P	+	+	55	A				P	+	+
21	A				P	-	+	56	A	P				+	+
22	A				P	+	-	57		A			P	+	+
23	A				P	+	+	58	A				P	+	+
24	A				P	+	+	59	A				P	+	+
25		A			P	-	-	60	A				P	+	+
26	A				P	+	+	61	A				P	+	+
27		A			P	+	+	62	A				P	+	+
28	A				P	+	+	63	A				P	+	+
29	A				P	+	+	64	A				P	+	+
30		A			P	+	+	65	A				P	+	+
31	A			P		+	+	66	A	P				+	+
32	A				P	+	+	67	A				P	+	+
33	A				P	-	-	68		AP				-	+
34	A				P	+	+	69	A				P	+	+
35	A				P	+	+	70	A				P	+	+

**Table 2.3. The locations of AQR and PQR with the loss of the *mig-15(+)* transgene in other tissues, but maintained in AQR and PQR.** The final migratory positions of the AQR and PQR neurons along the anterior-posterior axis of the animal are indicated for AQR and PQR neurons that have maintained the expression of the *mig-15(+)* transgene. The table is organized as described in Table 2.2.

## **Chapter III**

### **The mechanism of action of MIG-15 NIK kinase in neuroblast protrusion extension and migration in *C. elegans***

### 3.1. Abstract

Determining how molecules interact to give neurons the ability to migrate is essential to understanding the development of the nervous system. Nck Interacting Kinases (NIK) have been shown to be involved in numerous processes, including regulation of cell morphology, axon pathfinding, and cell migration. In *C. elegans*, the NIK kinase homolog, MIG-15, is required for the proper migrations of the Q neuroblast lineage neurons. How MIG-15 directs these migrations has yet to be determined. Many molecules, including Wnt signaling components, UNC-40/DCC, DPY-19, INA-1/ $\alpha$ -integrin, and the Rac GTPases, have been shown to be required for the proper migrations of the Q neuroblasts or their descendants. In other organisms, NIK kinases were found to function in several signaling pathways, including those controlling planar cell polarity, cell adhesion via integrins, Jun N-terminal Kinase activation, and ERM phosphorylation. The studies shown here examine the interactions of MIG-15 with the molecules known to play a role in the migrations of the Q neuroblast lineage and molecules that have been shown to interact with other NIK kinases to determine how MIG-15 is directing the migrations of the Q neuroblasts and descendants. The results described here suggest that MIG-15 interacts genetically with both INA-1/ $\alpha$ -integrin and ERM-1/ERM to direct the migrations of the Q neuroblast lineage. Additionally, interactions of CDC-42 and the Rac GTPase MIG-2 with MIG-15 suggest these molecules might be working together to regulate Q descendant migration.

### 3.2. Introduction

The process of cell migration is essential during the development of multicellular organisms. The developing nervous system requires massive amounts of migrations of neurons to form the various components of the central nervous system. Precise control of these migrations is vital. Neurons must be able to receive cues telling these cells when and where to migrate and then, redirect the migratory machinery to allow for these migrations to occur properly. Studying the individual molecules involved in migration and arranging these components into the genetic pathways controlling migration is essential to our understanding of how the nervous system develops. A relatively simple system in which to study neuronal migrations is the Q neuroblast lineage found in the model organism *Caenorhabditis elegans*. The Q neuroblasts are bilateral neuroblasts that undergo anterior-posterior migrations in opposite directions, with QR on the right migrating anteriorly and QL on the left undergoing migrations posteriorly (Chalfie and Sulston, 1981; Sulston and Horvitz, 1977; White et al., 1986). These neuroblasts then divide to ultimately produce three neurons each, with QR giving rise to AQR, AVM, and SDQR and QL giving rise to PQR, PVM, and SDQL. Of these Q neuroblast descendants, AQR and PQR migrate the farthest, with AQR migrating anteriorly to the head of the animal into the anterior deirid ganglion and PQR migrating to the tail of the animal into the phasmid ganglion. Thus, the Q neuroblast lineage provides a system in which to study both directional choices of migration and components that affect the ability of these neurons to complete their long-range migrations.

Previous studies have implicated the MIG-15 Nck Interacting Kinase (NIK) in the migrations of the Q neuroblasts and their descendants (Chapman et al., 2008; Poinat et al., 2002; Shakir et al., 2006; Su et al., 1997). Examination of the Q neuroblasts in *mig-15* mutants showed that MIG-15 is required for the proper extension of protrusions, maintenance of those initial protrusions, and migrations of the Q neuroblasts (Chapman et al., 2008). Additionally, MIG-15 is required cell autonomously in the Q neuroblast descendants AQR and PQR for these neurons to migrate in the proper direction and for these neurons to be able to fully migrate along their proper migratory pathways. Loss of function mutations in *mig-15* cause the Q neuroblasts to fail to maintain proper polarization during a time at which these cells should be migrating and cause these neuroblasts to fail to migrate from their birthplaces before dividing. This failure to migrate before dividing causes subsequent directional defects in the Q cell descendant migrations. The pathways and mechanisms that regulate the function of MIG-15 in neuronal migration have yet to be elucidated. Therefore, to determine how MIG-15 is functioning to control the migrations of the Q neuroblasts and their descendants, a candidate gene approach was taken, examining molecules that have previously been identified to be required for proper migrations of the Q lineage and molecules that had been identified in other systems to interact with NIK homologs.

Previously, numerous factors have been identified that affect the migrations of the Q neuroblasts and descendants. One signaling pathway found to be required for proper migrations of the Q cell descendants is the canonical

Wnt signaling pathway (Chalfie et al., 1983; Eisenmann and Kim, 2000; Harris et al., 1996; Korswagen et al., 2000; Whangbo and Kenyon, 1999). Wnt signaling is required for the proper posterior migrations of the QL descendants, as mutations in Wnt components like *egl-20* Wnt, *lin-17* Frizzled, and *bar-1*  $\beta$ -catenin cause PQR to migrate anteriorly as does AQR (Chapman et al., 2008; Eisenmann, 2005; Eisenmann et al., 1998; Sawa et al., 1996). These Wnt signaling molecules were found to be necessary for the expression of *mab-5*, an Antenneapedia-like Hox gene (Eisenmann, 2005; Kenyon, 1986a; Salser and Kenyon, 1992). MAB-5 has been shown to be expressed in QL and descendants, but not in QR or its descendants (Kenyon, 1986a; Salser and Kenyon, 1992). Additionally, MAB-5 was determined as the factor that directs posterior migration in the QL descendants. The absence of MAB-5 in the QR descendants allows for these neurons to migrate anteriorly (Salser and Kenyon, 1992). Previous studies have shown that MIG-15 does not appear to be acting in the canonical Wnt signaling pathway, as *mig-15* mutants cause defects in the extension of protrusions and migrations of the Q neuroblasts, defects that were not observed for the Wnt signaling pathway mutants (Chapman et al., 2008). Additionally, constitutive expression of MAB-5 could not rescue the *mig-15* mutant failure to fully migrate defects seen in AQR and PQR (Chapman et al., 2008).

Another group of factors found to be required for the proper migrations of the Q neuroblasts are the transmembrane proteins DPY-19 and UNC-40 (Honigberg and Kenyon, 2000). UNC-40/DCC encodes a cell surface receptor



that acts as a receptor for netrin in dorsal-ventral cell migrations and has been shown to act independently of netrin in non-dorsal-ventral migrations (Hedgecock et al., 1990; Keino-Masu, 1996). DPY-19 is a novel transmembrane protein that has been shown to have a homolog expressed in the human brain (Honigberg and Kenyon, 2000). Both of these molecules were shown to be required for the proper polarizations of the Q neuroblasts. Mutations in *dpy-19* and *unc-40* cause a randomization of anterior-posterior polarization of the Q cells, resulting in the Q neuroblasts polarizing in the opposite directions as compared to *wild type* in some of the animals. The directions of the Q neuroblast polarizations were also found to change with time, meaning that a single Q neuroblast was observed extending protrusions in one direction and then later sending out protrusions in the opposite direction. Though DPY-19 and UNC-40 have been identified as proteins involved in receiving the signal that directs the proper direction of polarization for the Q neuroblasts, the ligand that interacts with these transmembrane proteins has yet to be identified.

In addition to the canonical Wnt signaling pathway and the DPY-19 and UNC-40 receptors, integrins have also been shown to be required for the proper migrations of the Q neuroblast descendants (Baum and Garriga, 1997). Previous studies have shown that the QR descendants AVM and SDQR have shortened migrations in hypomorphic alleles of *ina-1*  $\alpha$ -integrin. INA-1 is one of two  $\alpha$ -integrins found in *C. elegans* and is thought to interact with PAT-3, the only  $\beta$ -integrin homolog found in *C. elegans*. PAT-3 and INA-1 are hypothesized to form a heterodimer that binds to laminin, one of the major proteins comprising

the basal lamina on which cells can adhere and migrate (Baum and Garriga, 1997). Therefore, impairing the function of INA-1 could cause defects in the ability of the integrin complex to bind the basal lamina, resulting in the Q neuroblast descendants to fail to complete their full migrations.

Rac GTPases have been shown to be involved in the cell morphology changes and cell migration mediated by the modulation of the actin cytoskeleton (Hall, 1998). Additionally, the Rac GTPases have also previously been implicated in the migrations of the Q neuroblast descendants (Shakir et al., 2006). In *C. elegans*, 3 Rac GTPases have been identified, MIG-2, CED-10, and RAC-2. Mutations in the Rac GTPases *mig-2* RhoG and *ced-10* Rac were shown to have slight defects in the migrations of AQR and PQR alone. RNAi of *rac-2* did not display AQR or PQR migration defects alone, but double mutant combinations of *mig-2* mutants, *ced-10* mutants, and *rac-2* RNAi showed synergistic increases in AQR and PQR migration defects, suggesting redundant functions of these molecules in the migrations of the Q descendants (Shakir et al., 2006). Additionally, analysis of double mutants of *mig-15* with the Rac GTPases found that MIG-15 appears to be interacting with MIG-2 to control the migrations of the AQR and PQR neurons, but no interactions were observed for MIG-15 with CED-10 or RAC-2 (Shakir et al., 2006). Much like the Rac GTPases, another member of the Rho subfamily of small GTPases, CDC-42, has been implicated in the modulation of the actin cytoskeleton to control cell polarity (Hall, 2005). The role of CDC-42 in the Q neuroblasts has yet to be determined, nor has any interactions between MIG-15 and CDC-42 been explored.

In other systems, NIK kinases have also been shown to play roles in multiple pathways that vary between tissues. In *Drosophila melanogaster*, the NIK homolog Misshapen (Msn) has been shown to work upstream of Jun N-terminal Kinase (JNK) to regulate dorsal closure (Su et al., 1998). This interaction of NIK kinases working upstream of JNK was also found for the mammalian NIK molecule in cell culture studies (Su et al., 1997). Additionally, Msn was shown to work downstream of the Frizzled receptor and Dishevelled and upstream of Jun N-terminal Kinase (JNK) in the planar cell polarity pathway to control ommatidial patterning in the developing eye (Paricio et al., 1999). Further studies in *Drosophila* found that Msn interacts with the homolog of the small adaptor protein Nck, called Dreadlocks (Dock), in a JNK independent pathway to control photoreceptor axon targeting (Su et al., 2000). In the rat mammary cell line MTLn3, the mammalian homolog of MIG-15, NIK, was determined to directly bind to moesin and was also shown to phosphorylate ezrin, radixin, and moesin (Baumgartner et al., 2006). These ERM proteins can regulate cell morphology by serving as cross-linkers between membrane-bound proteins and the actin cytoskeleton (Tsukita and Yonemura, 1997). Additionally, the ability of the ERM proteins to localize to lamellipodial protrusions upon induction by epidermal growth factor (EGF) was shown to be dependent on phosphorylation by NIK (Baumgartner et al., 2006). Mammalian cell culture experiments also found that cells expressing kinase-inactive forms of NIK homologs caused cell spreading and NIK homologs affect the surface levels of integrins (Baumgartner et al., 2006; Wright et al., 2003). Though other NIK

homologs have been shown to work in pathways that control planar cell polarity, JNK activation, and ERM phosphorylation, these interactions have not yet been examined for MIG-15 in *C. elegans*.

Although many molecules have been implicated in Q neuroblast migration, possible interactions of these molecules with MIG-15 have not been examined. Additionally, the protein interactions of NIK homologs that have been found in other systems have not yet been tested for MIG-15. Thus, the studies described here attempt to determine the mechanisms of action of MIG-15 in directing the Q neuroblast and descendant migrations. Analysis of mutants that have previously been described to affect Q neuroblast migration and examination of molecules shown to interact with NIK kinases in other systems reveal that MIG-15 interacts genetically with both the  $\alpha$ -integrin INA-1 and the ERM protein ERM-1 in directing Q neuroblast and descendant migration. Additionally, MIG-15 might be working with the RhoG homolog MIG-2 and CDC-42 to control the migrations of the Q neuroblast descendants.

### 3.3. Materials and Methods

**Genetic methods.** All experiments were performed at 20°C using standard techniques (Brenner, 1974; Sulston and Hodgkin, 1988). The following mutations and transgenic constructs were used: X: *lqls48[Pgcy-32::gfp]*, *mig-2(mu28)*, *mig-15(rh148 and rh80)*, *nck-1(ok383 and ok694)*; I: *erm-1(tm677)*, *lqls40[Pgcy-32::gfp]*, *unc-40(e271)*; II: *cdc-42(gk388)*, *mig-5(ok280, rh94, and rh147)*, *mIn1[mIs14 dpy-10(e128)]*; III: *dpy-19(e1259)*, *ina-1(gm86 and gm144)*; IV: *ced-10(n1993)*, *gmls5[ina-1::gfp]*, *jnk-1(gk7)*, *lqls80[scm promoter::gfp::caax]*, *lqls167[scm promoter::phosphomimetic erm-1::cfp]*, *tag-224(ok1036)*. The chromosomal locations of *lqls107[Pmig-15::mig-15-CNH domain]*, *lqls138[Pmig-15::mig-15-S/T kinase domain]*, *lqls163[scm promoter::erm-1::cfp]*, and *lqls169[scm promoter::non-phosphorlatable erm-1::cfp]* were not determined. Extrachromosomal arrays were generated by germ line microinjection and integrated into the genome by standard techniques (Mello and Fire, 1995).

**Synchronization of L1 larvae to visualize Q neuroblast protrusions and migration.** As previously described (Chapman et al., 2008; Honigberg and Kenyon, 2000), L1 larvae were synchronized by washing adults and larvae off of plates containing eggs using M9 buffer. The eggs adhere to the plates during washes, allowing for plates that only contain eggs to be obtained. These eggs were allowed to hatch at 30 min intervals and then were washed off the plates using M9 and collected. These larva were plated on NGM plates seeded with a

bacterial lawn to allow for further development until the specified times to examine the Q neuroblasts at the various stages. For genotypes that have egg-laying defects, gravid adults were collected and subjected to bleach treatment to obtain the eggs (Sulston and Hodgkin, 1988), which were then plated on NGM plates that contained a bacterial lawn.

### **Scoring and analysis of the Q neuroblast protrusions and migrations.**

Animals were analyzed by epifluorescence and confocal microscopy for GFP using a Leica DMR compound microscope with a BD CARV II wide-field light source. Images were captured using IPLab software and a QImaging Rolera mGi camera. The extend of protrusion of the Q neuroblasts were classified into 3 different extents, with strong protrusion indicating that the protrusions extended greater than half of the distance over the respective seam cell, weak protrusions indicating that the protrusions did not extend greater than half the distance over the respective seam cell, and unpolarized indicating that no protrusions were extended in either the anterior or posterior directions. Statistical significance was determined using a student T-test comparing migrations that had occurred properly as in *wild-type* animals.

**Scoring and analysis of the AQR and PQR migration defects.** Animals were analyzed by epifluorescence microscopy for GFP using a Leica DMR compound microscope. Images were captured using Openlab software and a Qimaging Retiga EXi camera. The location of the AQR and PQR neurons were visualized

in L4 larvae to young adults using the transgene *lqls40[Pgcy-32::gfp]* or *lqls48[Pgcy-32::gfp]*. The locations of the neurons after completion of migration were classified into 5 different anterior-posterior positions of the worm, with position 1 = head of the animal to just posterior to the second pharyngeal bulb, 2 = just posterior of the second pharyngeal bulb to slightly anterior of the vulva, 3 = the anterior and posterior regions surrounding the vulva, 4 = slightly posterior to the vulva to just anterior to the anus, 5 = posterior to the anus to the tail of the animal. Statistical significance was determined using a student T-test comparing migrations that had occurred properly as in *wild-type* animals.

***mig-15* RNAi.** The X-5G21 Ahringer RNAi clone was used to knock down *mig-15* function. Polymerase chain reaction (PCR) was used to amplify the *mig-15* RNAi coding segment using T7 primers. dsRNA was synthesized from this dsDNA using the Promega Riboprobe® System-T7. The synthesized dsRNA was microinjected in hermaphrodites. The progeny of the injected hermaphrodites were scored for AQR and PQR migration defects.

***gcy-32*, *erm-1*, *mig-15* transgenes.** The sequences of all plasmids used in this work are available upon request. All coding regions amplified by polymerase chain reaction (PCR) were sequenced to ensure that no mutations had been introduced by PCR. All regions were amplified from N2 genomic DNA unless otherwise noted. The *gcy-32::gfp* transgene *adEX1295* (Yu et al., 1997) was integrated into the genome to generate *lqls40* and *lqls48*. The coding region of

*erm-1* was amplified using the following primers: 5'-ATGTCGAAAAAGCGGTAAGTT and 5'-CCCATATTTTCGTATTGATCGATTC. This fragment was cloned downstream of the *scm promoter* and upstream of the *cfp* coding region to create plasmid pEL635. To create non-phosphorylatable and phosphomimetic mutations in *erm-1*, site directed mutagenesis of plasmid pEL635 was performed using the following primers: 5'-GGACGCGACAAGTACAAGGCTCTCCGTCAAATCCGTGG and 5'-CCACGGATTTGACGGAGAGCCTTGTACTTGTGCGCGTCC for the non-phosphorylatable mutation and 5'-GGACGCGACAAGTACAAGGATCTCCGTCAAATCCGTGG and 5'-CCACGGATTTGACGGAGATCCTTGTACTTGTGCGCGTCC for the phosphomimetic mutation. For the structure function analysis of MIG-15, the entire *mig-15* gene including the *mig-15* coding region plus 4-kb of upstream promoter sequence was amplified and cloned to create pEL445 using primers: 5'-CTCCAATAGTTTGCTCCCGG and 5'-CCAATTTGTCAACCCTGGCTT. To remove the serine/threonine kinase domain, inverse PCR was performed on pEL445 using the following primers: 5'-GATTCCAGCCGGGTCCTGAA and 5'-AAAGAACAACCACATGAGCAAAC. To remove the citron/NIK homology domain, inverse PCR was performed on pEL445 using the following primers: 5'-CTTCCTGATTTCTGGAGCATC and 5'-GGTGGAGGGTCTTGCCAGAT. The *scm::yfp::mig-15* transgene was constructed by amplifying the *mig-15* coding region using the following primers: 5'-ATGTCGTCATCAGGACTCGAC and 5'-TTACCAATTTGTCAACCCTGG. This fragment was cloned downstream of the



*scm promoter* and the *yfp* coding region without a stop codon, with the *mig-15* coding region in frame with the *yfp* coding region.

### 3.4. Results

#### **NCK-1/Nck is not required for proper Q neuroblast descendant migration.**

Previous studies in mammalian cell culture and *Drosophila* have found that NIK kinases interact with the small adaptor molecule Nck (Su et al., 1997; Su et al., 2000). In *Drosophila*, the Nck homolog Dock was shown to interact with Msn to control photoreceptor axon targeting (Su et al., 2000). In *C. elegans*, the relationship between MIG-15 and the Nck homolog NCK-1 had yet to be investigated.

Previous findings through the use of anti-NCK antibodies indicated that two isoforms of NCK-1 exist in *C. elegans* (Mohamed et al., 2007). Two mutant alleles of *nck-1* were examined for defects in the migrations of AQR and PQR. The first of these alleles was *nck-1(ok383)*, which contains a 899 base pair deletion in the second intron of one isoform of *nck-1* and removes a portion of the 5' UTR of the second isoform of *nck-1*. The other allele used was *nck-1(ok694)*, a 1814 base pair deletion that removes a portion of the coding region that includes exons that are common to both isoforms of *nck-1* along with a larger portion of the intron and 5' UTR that were removed with the *ok383* allele, resulting in excretory canal defects consistent with known NCK-1 function (Schmidt et al., 2009). Examination of the AQR and PQR migrations in both of these mutant alleles of *nck-1* showed no defects in the migrations of either neuron (Figs. 3.1A and B). Therefore, the lack of defects in AQR and PQR migration for the *nck-1* mutants suggest that NCK-1 is not required for the proper migrations of the Q neuroblast lineage.

**DPY-19 and UNC-40/DCC control Q neuroblast polarization in a pathway independent of MIG-15/NIK.** The opposite anterior-posterior polarizations of the Q neuroblasts can first be observed morphologically at the stage when these cells extend protrusions in opposite directions, with QR sending protrusions anteriorly and QL sending protrusions posteriorly. Previous studies have identified two transmembrane proteins, DPY-19 and UNC-40/DCC, that are involved in these anterior-posterior polarizations (Honigberg and Kenyon, 2000). Mutants in either of these molecules cause reversals in polarizations, as observed by the Q neuroblasts extending protrusions in the wrong directions. Additionally, Honigberg and Kenyon, 2000, observed that the protrusions of the Q cells can reverse directions between anteriorly and posteriorly directed lamellipodia. Though MIG-15 does not appear to be involved in the initial polarizations of the Q neuroblasts, as the initial protrusions appear to always be extended in the proper anterior-posterior directions, *mig-15* mutants fail to maintain these polarizations, as demonstrated by the protrusions extending in multiple directions during the time at which these neurons should be migrating (Chapman et al., 2008). Like *mig-15* mutants, the *dpy-19* and *unc-40* mutants were observed to repolarize or fail to maintain proper polarization, though these mutants displayed the Q neuroblast polarization defects at an earlier timepoint. The similarities between these phenotypes raise the question of whether MIG-15 could be acting downstream of DPY-19 and UNC-40 to maintain proper polarization of the Q neuroblasts.

Therefore, the AQR and PQR migration patterns were observed for both the *dpy-19(e1259)* and *unc-40(e271)* single mutants (Figs. 3.2A and B). Consistent with the previously found results that *dpy-19* and *unc-40* are required for the proper direction of polarization (Honigberg and Kenyon, 2000), both *dpy-19(e1259)* and *unc-40(e271)* single mutants displayed AQR and PQR neurons that had reversed directions of migration, with AQR being found in the tail and PQR being found in the head of the animal. The *dpy-19(e1259)* mutants were observed to have a stronger effect on both AQR and PQR migrations as compared to *unc-40(e271)* mutant defects (Figs. 3.2A and B).

To determine if MIG-15 is acting downstream of these transmembrane proteins, double mutants of *mig-15(rh148)* with *dpy-19(e1259)* and *unc-40(e271)* were constructed. For both *mig-15(rh148);dpy-19(e1259)* and *mig-15(rh148);unc-40(e271)* double mutants, there was an increase in defects as compared to any of the single mutants alone (Fig. 3.2). The increase in AQR migration defects in the *mig-15;unc-40* double mutants appeared to be slightly stronger than an additive effect. For both AQR and PQR in *mig-15;dpy-19* double mutants and for PQR in *mig-15;unc-40* double mutants, the increase in migration defects appears to be additive and not synergistic, suggesting that MIG-15 is working in either the same pathway as DPY-19 and UNC-40 or that MIG-15 is working in a pathway that is independent of both DPY-19 and UNC-40 in directing the migrations of the AQR or PQR neurons. Defects in the initial direction of protrusions of the Q neuroblasts were not observed for *mig-15* mutants as in *dpy-19* and *unc-40* mutants, and therefore, it is more likely that

MIG-15 is acting in a pathway independent of DPY-19 and UNC-40 to control the migrations of the Q neuroblasts and descendants.

**MIG-15 does not function in the planar cell polarity pathway to control Q neuroblast descendant migrations.** The *Drosophila* NIK kinase Msn has been previously shown to act downstream of the Frizzled receptor and Dishevelled and upstream of the Jun N-terminal Kinase (JNK) in the planar cell polarity pathway to control ommatidial patterning (Su et al., 1998). Though the roles of MIG-15 in protrusion extension and migration of the Q neuroblasts have been shown to be independent of canonical Wnt signaling (Chapman et al., 2008), the possibility of MIG-15 acting in the noncanonical planar cell polarity pathway had not been tested. Therefore, multiple components of the planar cell polarity pathway were examined for involvement in Q cell descendant migrations, including MIG-5/Dishevelled, JNK-1/c-Jun N-terminal Kinase, and TAG-224/Dishevelled associated activator of morphogenesis 1 (Daam1). Of these three molecules, MIG-5/Dishevelled can participate in both canonical Wnt signaling and the planar cell polarity pathway. AQR and PQR migrations were observed for 3 different alleles of *mig-5*, *ok280*, *rh94*, and *rh147*. Both *rh94* and *rh147* result in premature stop codons, with *rh147* thought to be a putative null mutation for *mig-5* (Walston et al., 2006). The *ok280* allele removes the 5' UTR for *mig-5*, along with a portion of the coding region for the adjacent gene *cct-1*, with this *ok280* allele thought to cause a weak hypomorphic mutation of *mig-5*. For the *mig-5(ok280)* mutant, slight PQR migration defects were observed, with PQR

migrating anteriorly and failing to fully migrate to the tail (Fig. 3.3A), similar to the defects observed in other weak loss of function mutant alleles of components of the canonical Wnt signaling pathway (Chapman et al., 2008). With the other 2 alleles, much stronger defects were observed, with the majority of the PQR neurons located in the head of the animal near the wild type position of AQR (Figs. 3.3B and C), similar to what was observed for the null *bar-1(ga80)* allele (Chapman et al., 2008). BAR-1 is the only  $\beta$ -catenin thought to work in canonical Wnt signaling in *C. elegans* and therefore would represent complete knock down of the canonical Wnt signaling pathway, resulting in the PQR neurons migrating anteriorly due to the absence of MAB-5. As for AQR migrations in these *mig-5* mutants, the *mig-5(ok280)* mutant allele showed very weak defects in the ability of AQR to fully migrate to the head of the animal, stopping short in the anterior region of the animal (Figs. 3.3A). Upon examination of the other mutants of the planar cell polarity genes, no migration defects were found for AQR or PQR in the *jnk-1(gk7)* and *tag-224(ok1036)* mutant alleles (Figs. 3.3D and E). These results suggest that the defects seen in the *mig-5* mutant alleles were due to the involvement of MIG-5 in canonical Wnt signaling and not in the planar cell polarity pathway. Taken together, these results also suggest that unlike Misshapen in *Drosophila*, MIG-15 is not functioning in the planar cell polarity pathway to control the migrations of the Q cell descendants AQR and PQR.

**INA-1/ $\alpha$ -integrin is required for Q cell protrusion extension and migration and for Q descendant migration.** Mouse NIK and *C. elegans* MIG-15 interact

physically with  $\beta$ 1-integrin/PAT-3, and NIK has been shown to colocalize with  $\beta$ 1-integrin at the tips of cellular protrusions (Poinat et al., 2002). Genetic studies in *C. elegans* indicate that the  $\alpha$ -integrin INA-1, which is thought to act in a dimer with PAT-3/ $\beta$ 1-integrin, acts in the same pathway as MIG-15 in axon guidance (Poinat et al., 2002). Furthermore, the QR.pa daughters failed to fully migrate in *ina-1* mutants (Baum and Garriga, 1997).

*ina-1(gm86)* is a nonsense mutation in the long chain coding region of INA-1 and is predicted to be a null mutation (Baum and Garriga, 1997). Early Q cell migration was assayed in *ina-1(gm86M+)*. Initial QL and QR protrusions were extended in the correct directions at 1.5-2h after hatching. However, the protrusions were abnormal in that they did not extend as far as in wild-type, usually less than half the length of the adjacent seam cells (Fig. 3.4A and B). This defect is similar to that observed for *mig-15(rh80)*. At 3-3.5h after hatching, when wild-type Q cells have migrated, 54% of QLs and 52% QRs had not migrated, but remained polarized in the proper directions over the V5L and V4R seam cells (Table 3.1). Of the cells that migrated, migrations were much shorter than observed in wild-type: QL migrated to the anterior edge of the V5L seam cell in 38% of animals and QR migrated to the posterior edge of the V4R seam cell in 48% (no QRs migrated normally) (Table 3.1 and Figs. 3.4C and D). At 5-5.5h after hatching, when wild-type QL and QR have divided atop the V5L and V4R seam cells, QL divided between V4L and V5L or at the anterior edge of V5L in 86% of the animals scored (Figs. 3.4E and G). QR divided between V4R and

V5R or at the posterior edge of V4R in 81% of animals scored (Figs. 3.4F and G).

The hypomorphic *ina-1(gm144)* also had weak defects in Q cell migration. Initial Q protrusions were normal in *ina-1(gm144)*. However, 5% of QLs (n = 42) and 6% QRs (n = 36) failed to migrate over their respective seam cells and divided between the V4 and V5 seam cells (Fig. 3.4H). The protrusion extension defects in *ina-1(gm86M+)* and failure to migrate in both *ina-1(gm86M+)* and *ina-1(gm144)* were reminiscent of defects in *mig-15(rh80)*. However, the failure to maintain polarity and to polarize in multiple directions during the time point at which the Q cells should be migrating seen in *mig-15* mutants was not observed in either allele of *ina-1* analyzed.

To determine if these initial defects in migration of the Q cells also had an effect on the migration of the Q cell descendants, AQR and PQR migrations were analyzed in *ina-1(gm144)* and *ina-1(gm86M+)* mutants. Shortened migrations of the QR.pa daughters had already been observed in *ina-1(gm144)* (Baum and Garriga, 1997), but no migration defects have been reported for QL descendants and no reversal of migration defects have been reported for either QL or QR descendant migration. For both *ina-1* alleles, the PQR neuron often failed to fully migrate to the phasmid ganglion as in wild-type (Figs. 3.5A and B). In the null *ina-1(gm86M+)* allele, PQR reversed direction of migration and migrated anteriorly in 3% of animals (Fig. 3.5A). Both *ina-1* alleles showed migration and direction of migration defects for AQR, with 1% and 3% of AQRs in *ina-1(gm144)* and *ina-1(gm86M+)*, respectively, reversing direction of migration and migrating



posteriorly (Figs. 3.5A and B). As described for *mig-15* mutants, posterior migration of AQR is likely due to migration failure of QR and subsequent MAB-5 activation in QR descendants, and anterior migration of PQR is likely due to QL migration failure and subsequent failure to activate MAB-5 in QL (Chapman et al., 2008). The misregulation of MAB-5 in the Q cells is likely the cause of the reversal of the direction of migration of the AQR and PQR neurons in the *ina-1* mutants as well. Also similar to MIG-15, INA-1 controls the ability of the Q descendants to fully migrate to their proper final positions, with AQR and PQR often failing to fully migrate to the head or tail of the animal.

### **Misregulation of *ina-1* $\alpha$ -integrin causes an increase in AQR and PQR**

**defects in *mig-15* mutants.** The similar defects observed in Q neuroblast protrusion and migration for both *ina-1* and *mig-15* mutants raised the question of whether these molecules act together to control the ability of the Q neuroblasts and descendants to migrate. To address this question, double mutants of *mig-15(rh148)* with *ina-1(gm86M+)* were constructed and migrations of AQR and PQR were observed. These double mutants showed an increase in migration defects as compared to either single mutant alone (Compare Figs. 3.5A and C to 3.5D). Although there was not an increase in PQR neurons failing to reach their wild type position in the tail behind the anus, a larger percentage of these neurons failed to migrate at all, resulting in a large percentage of PQR neurons residing in the posterior region of the animal near their birthplace (Fig. 3.5D). Though an increase in migration defects was observed, these results could not

distinguish between an additive effect or the possibility that removing INA-1 was increasing the defects seen in the *mig-15(rh148)* mutants closer to the null state of *mig-15*, with the strong loss of function allele *mig-15(rh80)* exhibiting more severe defects than the *mig-15(rh148);ina-1(gm86M+)* double mutant (Compare Fig. 3.5D to 3.5E). As both *mig-15(rh80)* and *ina-1(gm86M+)* are extremely sick, double mutants of these two alleles could not be constructed and therefore, examination of whether removing INA-1 in a strong MIG-15 loss of function background increases AQR and PQR migration defects as compared to the *mig-15(rh80)* mutant alone could not be performed.

In order to further examine the relationship between MIG-15 and INA-1, overexpression of INA-1 was observed using the transgene *gmls5 [Pina-1::ina-1::gfp]*. The overexpression of INA-1::GFP in the *wild type* background had no effect on AQR and PQR migration (Fig. 3.5F). When INA-1::GFP was overexpressed in the *mig-15(rh148)* mutant background, a strong increase in migration defects was seen for both AQR and PQR as compared to the *mig-15(rh148)* mutant alone (Compare Fig. 3.5G to 3.5C). Taken together, these results could suggest that MIG-15 is required to regulate the adhesion of INA-1 and PAT-3, with MIG-15 being needed to release these integrin adhesions as the removal of *wild type* MIG-15 function causes shortened migrations of both AQR and PQR.

**Members of the Rho subfamily of small GTPases, MIG-2/RhoG and CDC-42 might act with MIG-15/NIK to control Q descendant migrations. Studies**

examining the relationships of the Rac GTPases MIG-2/RhoG and CED-10/Rac with MIG-15 had previously been reported (Shakir et al., 2006). In these studies, MIG-2 was hypothesized to work with MIG-15, as mutation in *mig-2* enhanced the AQR and PQR migration defects of the weak loss of function *mig-15* mutant to that of the strong loss of function *mig-15* allele. Additionally, CED-10 did not appear to have a role in the migrations of the Q descendants. But, only the anterior-posterior directional choice of AQR and PQR were assayed in these experiments and not the extent of the migrations. Therefore, a more detailed approach to these experiments was taken, evaluating the locations of the final positions of the AQR and PQR neurons in mutants of *mig-2* and *ced-10*, along with the mutants of *cdc-42*, another member of the Rho subfamily of small GTPases. Additionally, double mutants of each of these GTPases with *mig-15(rh148)* were constructed to determine if any possible interactions exist between MIG-15 and these three GTPases.

Examinations of the *cdc-42(gk388M+)*, *mig-2(mu28)*, and *ced-10(n1993)* single mutants found only slight migration defects for AQR for all of these mutants and defects in PQR migration for *mig-2(mu28)* and *cdc-42(gk388M+)* (Figs. 3.6A-C), similar to what was found previously for *mig-2* and *ced-10* (Shakir et al., 2006). When double mutants of *mig-15(rh148)* with *mig-2(mu28)* and *cdc-42(gk388M+)* were constructed, defects in AQR and PQR migration strongly increased (Figs. 3.6E and F). For *mig-15(rh148);cdc-42(gk388M+)*, a significant enhancement in defects was seen for both AQR and PQR as compared to the single mutants alone, with only 53% of AQR neurons and 17% of PQR neurons

reaching their wild type positions in the head and tail, respectively (Fig. 3.6E,  $p \leq 0.002$  for both cases). The *mig-15(rh148) mig-2(mu28)* double mutant displayed a similar, yet weaker increase in the defective PQR migrations, though this increase was not significantly different from the defects presented in the two single mutants combined (Fig. 3.6F,  $p \leq 0.098$  for PQR). These results suggest that both CDC-42 and MIG-2 play a role in the migrations of the Q descendants, much like MIG-15. Like *mig-15* mutants, *mig-2* mutants cause a reversal in direction of migration for the PQR neuron, and both *mig-2* and *cdc-42* cause a failure in the extent of migrations of both AQR and PQR, with both cells failing to fully migrate to their wild type positions (Figs. 3.6A and B). Oppositely, the double mutant of *mig-15(rh148);ced-10(n1993)* displayed a significant suppression of PQR migration defects as compared to the defects observed in the two single mutants combined (37% vs. 53% defective; Fig. 3.6G,  $p \leq 0.01$ ). Taken together, these results suggest that MIG-2 and CDC-42 might normally promote migration, whereas CED-10 might normally inhibit migration. Because null mutations of *mig-15* are lethal in combination with *mig-2*, *ced-10*, and *cdc-42* mutants, these studies cannot determine exact relationships of MIG-15 with MIG-2, CED-10, or CDC-42. Since the *mig-2* and *cdc-42* mutants cause an increase in Q descendant migration defects in the *mig-15(rh148)* background that is similar to the strong loss of function *mig-15(rh80)*, these molecules could be working with MIG-15 or in parallel to MIG-15 to control Q descendant migration. Mutations in *ced-10* appear to suppress the *mig-15(rh148)* migration defects,

which could be due to the over-migration phenotype seen for the Q neuroblasts in *ced-10(n1993)* mutants (See Chapter IV).

**Removal of ERM-1/ERM suppresses the QL neuroblast migration defects observed in *mig-15* mutants.** Previous studies in a rat mammary cell line had found that mammalian NIK binds to and phosphorylates ERM proteins (Baumgartner et al., 2006). Additionally, the localization of phosphorylated ERM proteins to lamellipodial protrusions upon induction by EGF is dependent on the kinase activity of NIK. Interestingly, kinase-inactive forms of the NIK protein were shown to cause cell spreading in multiple mammalian cell culture lines (Baumgartner et al., 2006; Wright et al., 2003), similar to the failure to maintain polarization that was observed for the *mig-15* mutants in the Q neuroblasts (Chapman et al., 2008). Therefore, the *C. elegans* homolog of the ERM family of proteins, ERM-1, was examined to determine if ERM-1 plays a role in the extension of lamellipodial protrusions and migration in the Q neuroblasts.

The *erm-1(tm677)* allele used is a 972 base pair deletion and a 2 base pair insertion that occurs in exons 6 and 7 of the coding sequence, causing a frame shift that causes a premature stop (Gobel et al., 2004). This mutation most likely abolishes ERM-1 activity, is lethal to the animals, and thus, requires the mutation to be balanced by a *wild type* copy of *erm-1*. Previous studies have indicated that the maternal contribution of *erm-1* transcripts does have a role in the development of the *erm-1(tm677M+)* homozygous animals which survive to adulthood, as RNAi of *erm-1* causes arrest of larvae at the L1 stage (Gobel et al.,

2004). Examination of the Q neuroblasts in *erm-1(tm677M+)* mutants found no defects in the ability of the Q neuroblasts to fully migrate before dividing (Fig. 3.7C) and only a slight defect in the ability of AQR to extend protrusions at 1-1.5h after hatching (Fig. 3.7A; 4% had not extended protrusions). It is possible that the maternal contribution of *erm-1* transcripts is rescuing any possible defects that could occur in these Q neuroblasts in *erm-1(tm677M+)* animals, though this was not examined here.

To determine if MIG-15 is interacting genetically with ERM-1 in Q neuroblast migration, double mutants of *mig-15(rh148)* with *erm-1(tm677M+)* were constructed. Examination of Q neuroblast divisions found that *erm-1(tm677M+)* appears to suppress the QL migration defects seen in *mig-15(rh148)* mutants at 3-3.5h after hatching (Compare the QL divisions over V5 in Fig. 3.8A to 3.8B;  $p = 0.015$ ), though the *erm-1(tm677M+)* mutation did not suppress the repolarization defects seen in the *mig-15* mutants alone. Additionally, this suppression of migration defects seen for the QL neuroblast was also observed for the PQR neuron as well, with PQR migrating to the *wild type* position in the tail in 61% of the animals scored as compared to 47% in the *mig-15(rh148)* mutants alone (Compare Fig. 3.9C to 3.9B;  $p \leq 0.01$ ). Based on the results presented here and that NIK has been shown to phosphorylate ERM proteins (Baumgartner et al., 2006), these results might suggest a role for ERM-1 downstream of MIG-15. Possibly, the activity of ERM-1 might be upregulated in MIG-15 mutants when phosphorylation of ERM-1 does not occur, causing the Q

neuroblasts and descendants to lose proper polarization, which could then lead to a failure of these cells to complete their proper migrations.

The localization of phosphorylated ERM proteins was found to be dependent on the kinase activity of NIK (Baumgartner et al., 2006). To test the possibility that MIG-15 is functioning similarly as to what was shown for NIK, the localizations of ERM-1 were examined in *wild type* and *mig-15(rh148)* mutants. The *mig-15(rh148)* lesion is thought to inactivate the S/T kinase domain of MIG-15 due to a missense mutation in a conserved residue in the ATP binding pocket (Shakir et al., 2006). Therefore, if MIG-15 is functioning similarly to NIK, it would be expected that the ERM-1::CFP expression in the *wild type* background should display an enrichment in lamellipodial protrusions as compared to the ERM-1::CFP expression seen in the *mig-15* mutant background, since *mig-15(rh148)* mutants should not be able to phosphorylate ERM-1. A transgene consisting of the *scm promoter* driving *erm-1::cfp* was introduced to drive the expression of ERM-1::CFP in the Q neuroblasts along with the seam cells. Expression of ERM-1::CFP was observed outside of the cells that normally express constructs driven by the *scm promoter*, with expression displayed in both the intestine and the excretory canal of the animal (Figs. 3.10C and G). It is possible that these abnormal expression patterns could be the result of an intestine and excretory canal specific enhancer that might be located with an intron in the genomic DNA encoding the *erm-1* locus, though this possibility was not formally examined. A comparison of ERM-1::CFP in the Q neuroblasts in *wild type* versus *mig-15(rh148)* animals found no obvious difference between the localization patterns.

One possibility is that this *scm::erm-1::gfp* transgene might not produce a functional protein, though this is unlikely due to the similar localization patterns found in other ERM studies, including the apical localization of ERM-1 in the intestine and studies showing that ERM proteins localize to cleavage furrows, as seen with this *scm::erm-1::cfp* construct (Figs. 3.10C and G) (Sato et al., 1991; Van Furden et al., 2004). Testing for ability of this construct to rescue mutant defects was not performed, as no migration defects were observed for the Q neuroblasts in the *erm-1(tm677M+)* single mutant and this construct was driven only in the Q neuroblasts and the seam cells by the *scm promoter*. These results suggest that the kinase activity of MIG-15 is not required for the proper localizations of ERM-1, though it cannot be excluded that localization of phosphorylated ERM-1 might differ between *wild type* and *mig-15* mutants.

To determine if the failure of MIG-15 to phosphorylate ERM-1 in *mig-15* mutants is causing the failure of the Q neuroblasts to maintain their initial polarizations, a non-phosphorylatable form of ERM-1 driven by the *scm promoter* was constructed. Neither the non-phosphorylatable ERM-1 protein in a *wild type* background nor the presence of the non-phosphorylatable ERM-1 protein in the *erm-1(tm677M+)* mutant cause AQR or PQR migration defects (Figs. 3.11A and B), though the fact that no migration defects were observed for the non-phosphorylatable ERM-1 protein in the *erm-1(tm677M+)* mutant background could be due to the low n-value scored for this phenotype (n = 18). This suggests that the lack of phosphorylation of ERM-1 is not causing the polarity maintenance defects seen in the *mig-15* mutants. Though ERM-1 seems to have



a role in directing QL and PQR migration as shown by the suppression of these defects when ERM-1 is removed in a *mig-15(rh148)* background, no evidence was obtained in these studies suggesting that MIG-15 affects the phosphorylation of ERM-1 as was published for NIK and ERM in the mammalian cell culture system. However, a phosphomimetic version of the ERM-1 protein driven by the *scm promoter* was constructed, which caused a very low level of AQR and PQR neuron migration defects (Fig. 3.11C). Therefore, it seems that proper phosphorylation of ERM-1 might be required for the migration of the Q neuroblast descendants, though further studies need to be performed to confirm whether phosphorylation of ERM-1 is necessary in the Q neuroblasts to direct their migrations.

**A structure function analysis of MIG-15.** The MIG-15 protein contains 3 conserved domains, a N-terminal serine/threonine kinase domain, a central proline-rich domain, and a C-terminal citron/NIK homology (CNH) domain (Fig. 3.12A). MIG-15 has been shown to directly bind PAT-3/ $\beta$ -integrin through its CNH domain and has been predicted to interact with the Rac GTPases through this same domain (Poinat et al., 2002; Shakir et al., 2006). To further examine the possible functions of MIG-15, a structure function analysis was performed in which the S/T kinase domain and the CNH domain were each individually removed from the *mig-15* coding region. Transgenic animals were made expressing each of these constructs under the endogenous *mig-15* promoter, with transgenic line *lqls107* containing a MIG-15 protein with the CNH domain

removed and transgenic line *lqls138* containing a MIG-15 protein with the S/T kinase domain removed (Fig. 3.12).

Removal of the CNH domain caused weak defects in the migrations of PQR in a *wild type* background (Fig. 3.13A). When this form of MIG-15 without the CNH domain was introduced into the *mig-15(rh148)* mutant background, a statistically significant increase in defects in the migration of the PQR neuron were observed as compared to *mig-15(rh148)* alone (Compare Fig. 3.13D to 3.13B;  $p \leq 0.001$ ). This raises the question of whether *lqls107* is functioning as a dominant negative. To address this issue, *lqls107* was also introduced into the *ina-1(gm86M+)* background to observe if an increase in defects in AQR and PQR migration is present. Since *ina-1(gm86M+)* was shown to have defects in AQR and PQR migration, placing *lqls107* with the *ina-1* mutant should determine if this increase in defects is due to *lqls107* inhibiting migration of the AQR and PQR neurons in general or in a MIG-15 dependent manner. Since no significant increase in AQR or PQR migration defects was found for *ina-1(gm86M+);lqls107*, it appears that the removal of the CNH domain from MIG-15 causes an increase in defects in *mig-15(rh148)* mutants specific to the function of MIG-15 (Fig. 3.13C and E).

Animals containing a form of MIG-15 with the S/T kinase domain removed (*lqls138*) had weak defects in the migrations of both AQR and PQR in a *wild type* background (Fig. 3.13F). This transgene was integrated into the X chromosome, the same chromosomal location as the *mig-15* locus. Due to complications with the transgene or integration, *lqls138* could not be made homozygous in the *mig-*

*15(rh148)* mutant background. Therefore, determination of the AQR and PQR migration defects for *lqls138* could not be determined for animals with their endogenous *mig-15* mutated.

### 3.5. Discussion

**NCK-1/Nck and the planar cell polarity pathway do not appear to be required for proper Q cell descendant migration.** NIK kinases have been shown to interact with the small adaptor molecule Nck through their proline-rich domains (Su et al., 1997; Su et al., 2000). To date, MIG-15 has not been shown to directly interact with the *C. elegans* homolog of Nck, NCK-1. Animals with mutations in *nck-1* did not exhibit any defects in the migrations of the AQR or PQR neurons. These results indicate that NCK-1 does not play a role in directing the migrations of the AQR or PQR neurons, which could also suggest that NCK-1 is not required for the earlier Q neuroblast migrations either.

The role of MIG-15 in directing Q neuroblast protrusion and migration was previously found to be independent of canonical Wnt signaling (Chapman et al., 2008), but noncanonical Wnt signaling pathways were not tested. In *Drosophila*, Misshapen has been shown to work downstream of the Frizzled receptor and Dishevelled and upstream of the Jnk pathway in the planar cell polarity pathway (Paricio et al., 1999). Therefore, the roles of members of the planar cell polarity in Q neuroblast descendant migrations were investigated. Mutations in MIG-5/Dishevelled showed defects in AQR and PQR migration, though these defects are hypothesized to be due to role of MIG-5/Dishevelled in canonical Wnt signaling and not planar cell polarity, as JNK-1/JNK and TAG-224/Daam1, members of the planar cell polarity pathway, do not exhibit AQR or PQR migration defects.

**MIG-15 does not appear to be working genetically with DPY-19 and UNC-40/DCC.** Examination of the AQR and PQR neuron migrations in *dpy-19* and *unc-40* mutants suggests that MIG-15 is likely working in a pathway independent of DPY-19 and UNC-40. The reversals in the directions of migration of AQR and PQR found for both *dpy-19* and *unc-40* mutants were consistent with the previous findings that *dpy-19* and *unc-40* cause reversals in Q neuroblast polarizations (Honigberg and Kenyon, 2000). When *dpy-19* and *unc-40* mutations were each introduced individually into a *mig-15(rh148)* background, an increase in AQR and PQR migrations defects was observed as compared to any of the single mutants alone. This increase in defects does appear to be only an additive effect and since *mig-15* mutants display Q neuroblast defects that are different than the defects observed for the Q cells in *unc-40* and *dpy-19* mutants, these results suggest that MIG-15 is not acting downstream of UNC-40 or DPY-19 to control Q neuroblast and descendant migration. Interestingly, the *mig-15(rh148);dpy-19(e1259)* double mutants displayed a greater proportion of increased defects in PQR migration as compared to the *mig-15(rh148);unc-40(e271)* double mutants, though this might be due to a larger percentage of PQR migration defects in the *dpy-19(e1259)* single mutants as compared to the *unc-40(e271)* mutants.

**MIG-15 might be regulating adhesion of integrins to control the migrations of the Q neuroblasts and descendants.** Integrins have been showed repeatedly to be required for cell migrations. Thus, it is not surprising to find that

a mutation that abolished the function of INA-1/ $\alpha$ -integrin would result in defects in migration of the Q neuroblasts. The Q neuroblasts in *ina-1* mutants display defects in the ability to extend protrusions and defects in migration, similar to what was observed for the *mig-15(rh80)* mutants. But unlike the strong loss of function mutant of *mig-15*, *ina-1(gm86M+)* did not cause the Q neuroblasts to fail to maintain their initial polarizations. These results would require that MIG-15 must be working with some molecule other than INA-1 to maintain the initial polarity of the Q neuroblasts.

Looking at the migrations of the AQR and PQR neurons, double mutants of *mig-15(rh148)* with *ina-1(gm86M+)* cause an increase in defects in the migrations of both AQR and PQR as compared to the single mutants alone, though the increase in the defects might be an additive effect. One interesting point of data was that overexpression of INA-1::GFP caused an increase in AQR and PQR migration defects in the *mig-15(rh148)* mutant background. Since no defects were observed for the overexpression of INA-1::GFP in a wild type background, these results suggest that MIG-15 might be regulating the adhesion of the integrins in Q neuroblast descendant migration. Since adhesions of integrins are regulated by phosphorylation of their cytoplasmic tails, MIG-15 could be regulating cell adhesion by phosphorylation of integrins through its N-terminal serine/threonine kinase domain. Previously, MIG-15 has also been shown to directly bind to PAT-3/ $\beta$ -integrin through the C-terminal citron/NIK homology domain of MIG-15, which could allow for the S/T kinase domain of MIG-15 to interact with the cytoplasmic tail of INA-1 or possibly PAT-3 (Poinat et

al., 2002). Another possibility is that the interaction of MIG-15 with PAT-3 could require the activity of the kinase domain in MIG-15, which is thought to be inactivated in the *rh148* mutation. Without this kinase activity, MIG-15 might not be able to interact with PAT-3 and regulate integrin adhesion. Though it is out of the scope of this project, it would be interesting to determine if MIG-15 is responsible for the phosphorylation of either INA-1 or PAT-3 *in vivo*.

**MIG-2/RhoG and CDC-42 might be functioning with MIG-15 to control Q descendant migrations.** Mutations in *mig-2*, *ced-10*, and *cdc-42* each caused weak defects in the migrations of AQR and/or PQR. When double mutants of these 3 GTPases with mutations in *mig-15* were constructed, an increase in AQR and PQR migration defects were seen in the *mig-15;cdc-42* and *mig-15 mig-2* double mutants. Mutations in *mig-2*, *cdc-42*, and *mig-15* each cause defects in the extent of migrations of the Q descendants, suggesting a role for each of these molecules in the ability of the Q neuroblasts to fully migrate. Due to the restriction of using only a weak loss of function allele for *mig-15* and since the increases in AQR/PQR migration defects in these *mig-15 mig-2* and *mig-15;cdc-42* double mutants are similar to the Q descendant migration defects seen in the *mig-15* strong loss of function mutation, a linear relationship could not be ruled out. Therefore, these results are consistent with MIG-15 interacting with MIG-2 and CDC-42 into either a linear or parallel pathways.

Double mutants of *mig-15* with *ced-10* displayed a suppression of PQR migration defects as compared to the *mig-15* mutants alone. This suppression

could be due to the over-migration defects observed for the *ced-10* mutants in the Q neuroblasts. Loss of function *ced-10* mutations cause an over-migration of the Q neuroblasts before dividing, resulting the QR neuroblasts dividing more anteriorly and the QL neuroblasts dividing more posteriorly as compared to the wild type division positions (See Chapter IV). Since CED-10 normally inhibits migration and MIG-15 promotes migration of the Q neuroblasts, loss of function mutations in each of these could partially cancel out these defects. This could allow the QL neuroblast to migrate posteriorly enough to receive a sufficient amount of the EGL-20/Wnt signal to turn on MAB-5/Hox, which then directs the posterior migrations of the QL descendants. This proper directing of the migrations of the QL descendants posteriorly could then be the reason fewer PQR neurons are found anteriorly in the *mig-15;ced-10* double mutants. Additionally, the role of CED-10 in the Q lineage migrations appears to be strongest in the Q neuroblasts, as the proportions of Q descendants that failed to fully migrate appear similar between the *mig-15;ced-10* double mutant and the *mig-15* single mutant. This explanation of CED-10 playing a role in the migrations of the Q neuroblasts is also consistent with the lack of suppression of the AQR migration defects seen for the *mig-15;ced-10* double mutant, as a failure of the QR neuroblast to migrate in *mig-15* mutants rarely results in directional migration defects of the QR descendants due to the QR neuroblast being inherently less sensitive to the Wnt signal needed to turn on MAB-5/Hox than the QL neuroblast (Whangbo and Kenyon, 1999).



### **ERM-1/ERM might act downstream of MIG-15 in Q neuroblast migration.**

Mutation in *erm-1* did not result in the cell spreading phenotype as was observed for the *mig-15* mutants. Only slight defects were observed for *erm-1* mutants during the protrusion extension and migration stages in the Q neuroblasts. As stated previously, there is a possibility that the reason for a lack of defects in these *erm-1(tm677M+)* mutants could be due to maternal rescue. Interestingly, loss of ERM-1 function in the *mig-15* mutant background suppressed the QL and PQR migration defects. Although a decrease in PQR migration defects were seen in the *mig-15;erm-1* double mutant, this finding could be a result of the suppression of the QL migration defects, as the decrease in anteriorly directed PQR neurons in the double mutant roughly correlates to the 31.8% of QL neuroblasts that no longer fail to migrate in these double mutants as compared to the *mig-15* mutant alone. These results could suggest that ERM-1 is acting downstream of MIG-15, consistent with the findings that NIK binds to and phosphorylates ERM proteins (Baumgartner et al., 2006). Though, it cannot be ruled out by these experiments that ERM-1 could be acting upstream of MIG-15 to inhibit MIG-15 function and that removing ERM-1 could allow for the residual activity of the protein produced from the *mig-15(rh148)* weak loss of function allele to facilitate the Q cell descendants in migrating towards their proper locations.

Localization of ERM-1 was found to be independent of the kinase activity of MIG-15. These experiments vary from those performed in the cell culture experiments, as they had assayed phosphorylated ERM proteins (Baumgartner

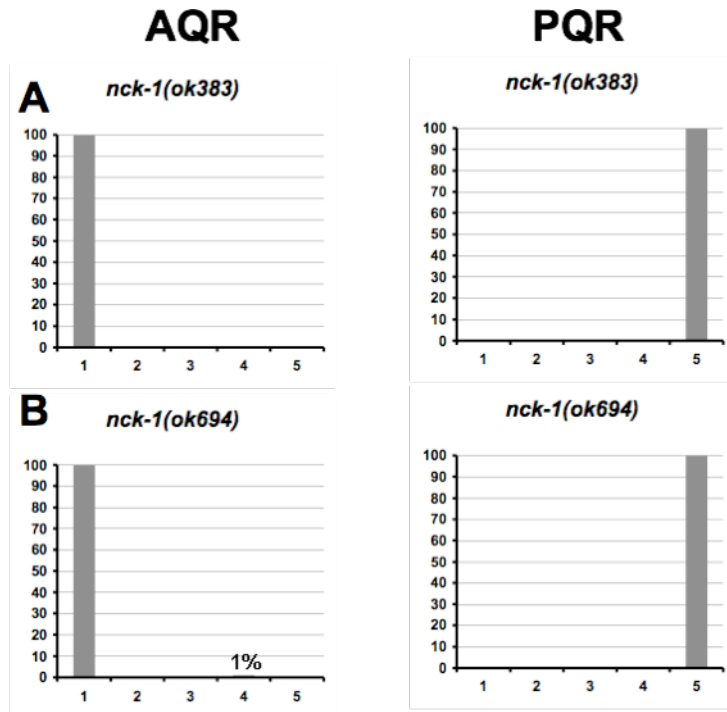
et al., 2006). Phosphorylation of ERM-1 did not seem to be required in the Q descendant migrations either, as AQR and PQR neurons expressing a non-phosphorylatable form of ERM-1 did not display migration defects. Thus, the interaction of MIG-15 with ERM-1 that causes suppression of QL and PQR migration defects remains to be determined.

**The structure function analysis.** Removal of the S/T kinase domain and CNH domain of MIG-15 individually caused migration defects in AQR and/or PQR, even in the presence of a wild type MIG-15 protein. When the CNH domain was removed in the *mig-15(rh148)* mutant background, an increase in AQR/PQR migration defects were observed as compared to the *mig-15* mutant alone. This is interesting, as the *mig-15(rh148)* mutant allele contains a wild type version of the CNH homology, but has a missense mutation in the S/T kinase domain in a conserved residue in the ATP binding pocket, thought to remove the kinase function (Shakir et al., 2006). When trying to construct a fluorescently tagged version of MIG-15, it was found that C-terminal fusions of MIG-15 with GFP or mCherry were lethal to *wild type* animals (results not shown). Though, a N-terminal fusion of CFP to MIG-15 was viable (results not shown). Taken together, it seems that blocking the function of the CNH domain is deleterious to the animals. Removal of the CNH domain could allow for the N-terminal portion of MIG-15 to interact with the normal binding partners of MIG-15. These interactions could block the residual activity of the protein produced by the *mig-15(rh148)* locus, causing an increase in Q descendant migration defects.

Production of a MIG-15 protein with the S/T kinase domain removed could not be done in the absence of wild type MIG-15, though it is expected that this construct would work similarly to the *mig-15(rh148)* allele, as this mutation is thought to inactivate the kinase domain of MIG-15.

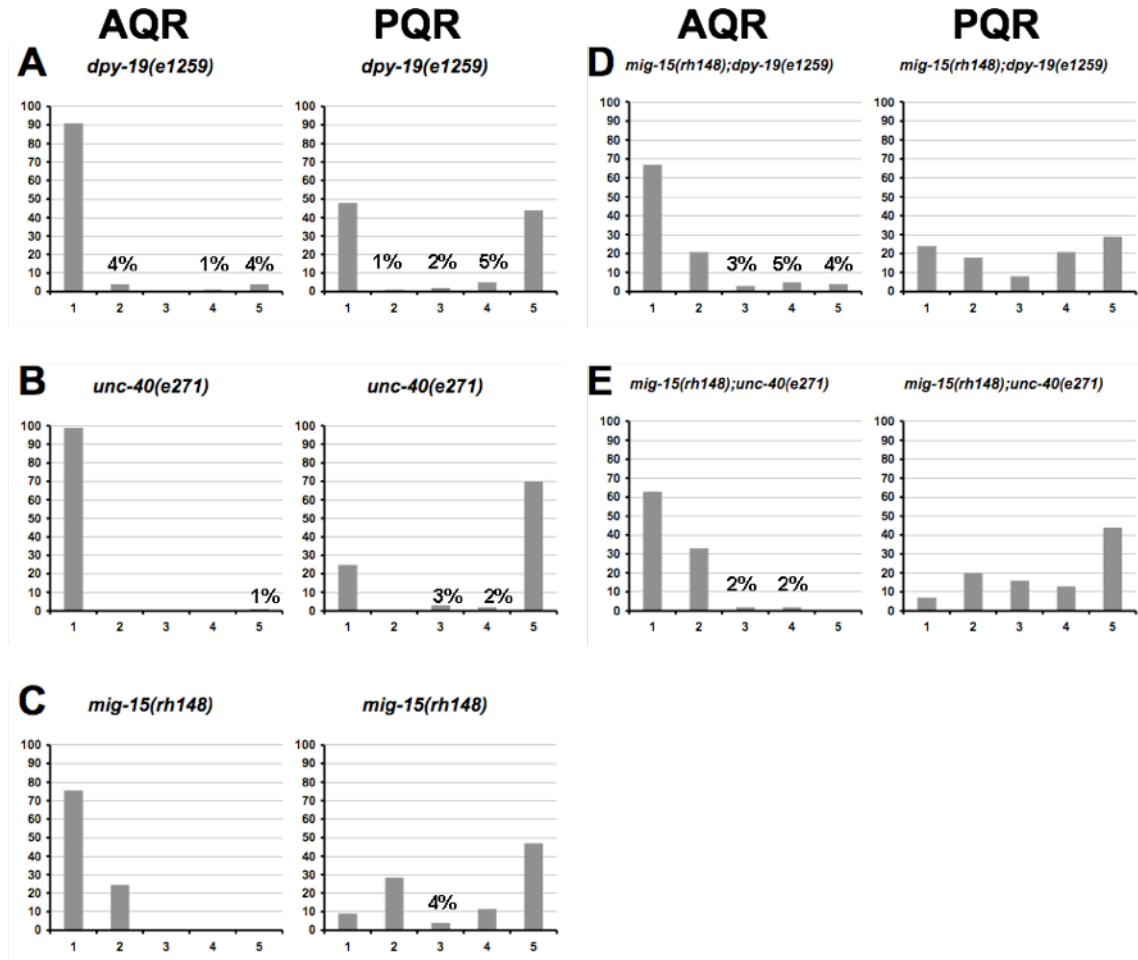
Taken all together, these results indicate that MIG-15 might be acting with numerous molecules to control the migrations of the Q neuroblasts and their descendants. MIG-15 displays interactions with molecules involved in cell adhesion and actin cytoskeleton modulation. The nature of the interactions of MIG-15 with INA-1, ERM-1, MIG-2, and CDC-42 have yet to be determined. Experiments aimed at identifying which proteins directly bind to MIG-15 and which proteins are phosphorylation targets of MIG-15 would provide insight into how MIG-15 is functioning with these molecules and possibly others that have yet to be determined as interacting partners of MIG-15. As human orthologs of NIK kinases have been found to be upregulated in tumor cell lines, determination of how NIK kinases control migration will provide insight into not only how the nervous system develops, but will also increase our understanding of tumor cell invasion.

Figure 3.1



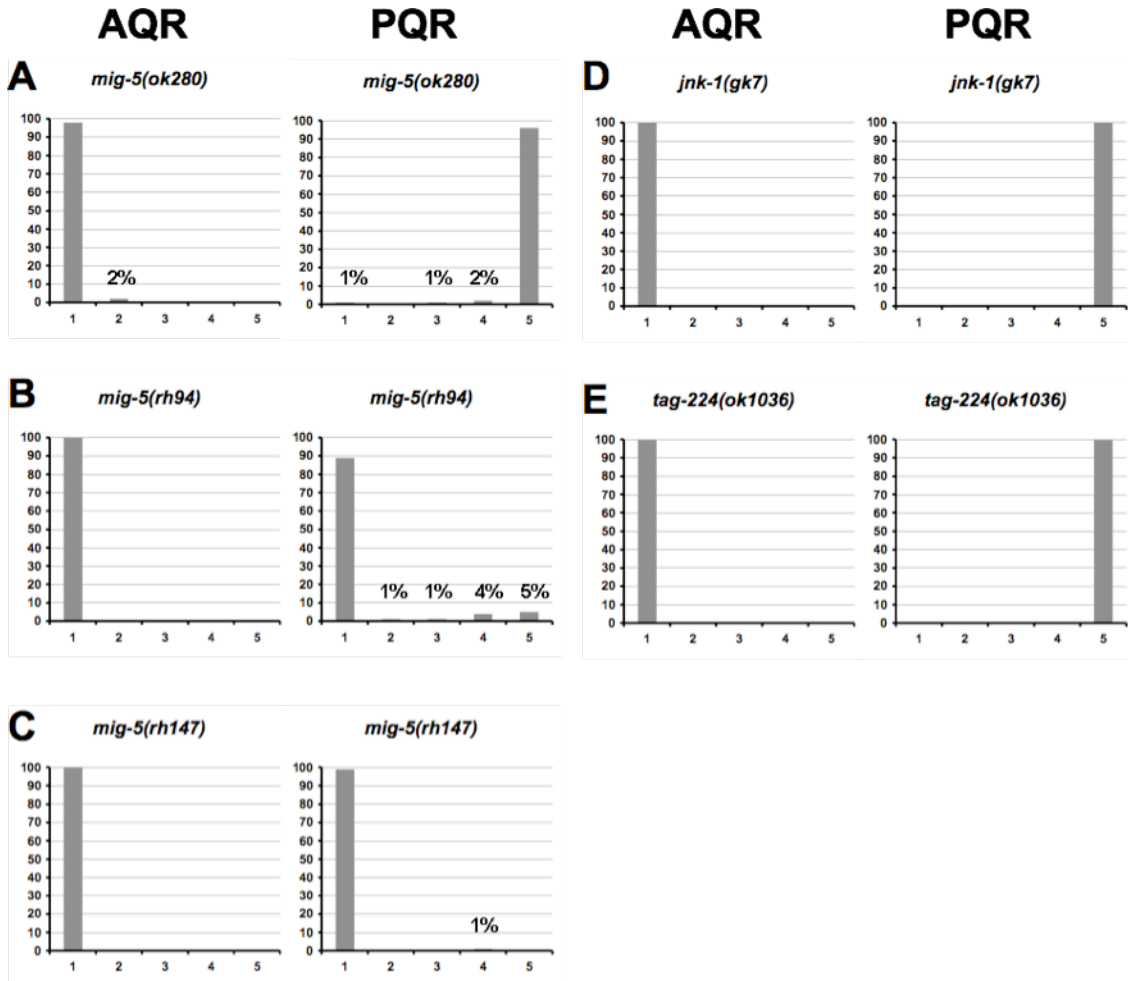
**Figure 3.1. NCK-1/Nck is not required for the migrations of the Q neuroblast descendants AQR and PQR.** (A-B) Quantitation of the final migratory positions of the AQR and PQR neurons. The x-axis represents the anterior-posterior position of the AQR and PQR neurons after completion of migration (see Materials and Methods section for description of the classifications of the anterior-posterior positions). The y-axis represents the percentages of the AQR and PQR neurons that were observed at each anterior-posterior position. For all cases,  $n \geq 100$ .

Figure 3.2



**Figure 3.2. Mutations in *dpy-19* and *unc-40* increase the AQR and PQR migration defects seen in *mig-15(rh148)* mutants.** (A-E) Quantitation of the final migratory positions of the AQR and PQR neurons. The graphs are organized as described in Figs. 3.1A-D. For all cases except *mig-15(rh148)*, n = 100. For *mig-15(rh148)*, n = 200.

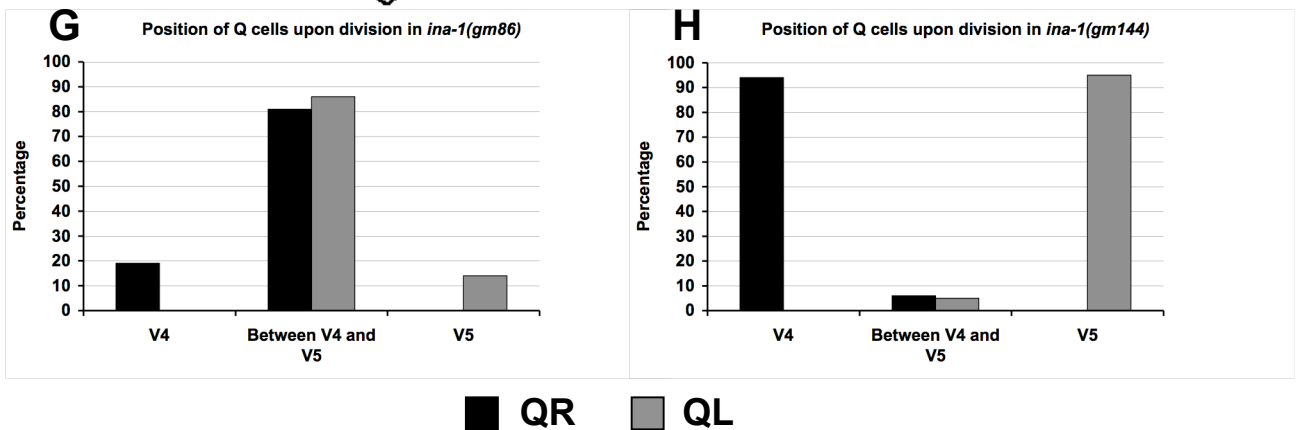
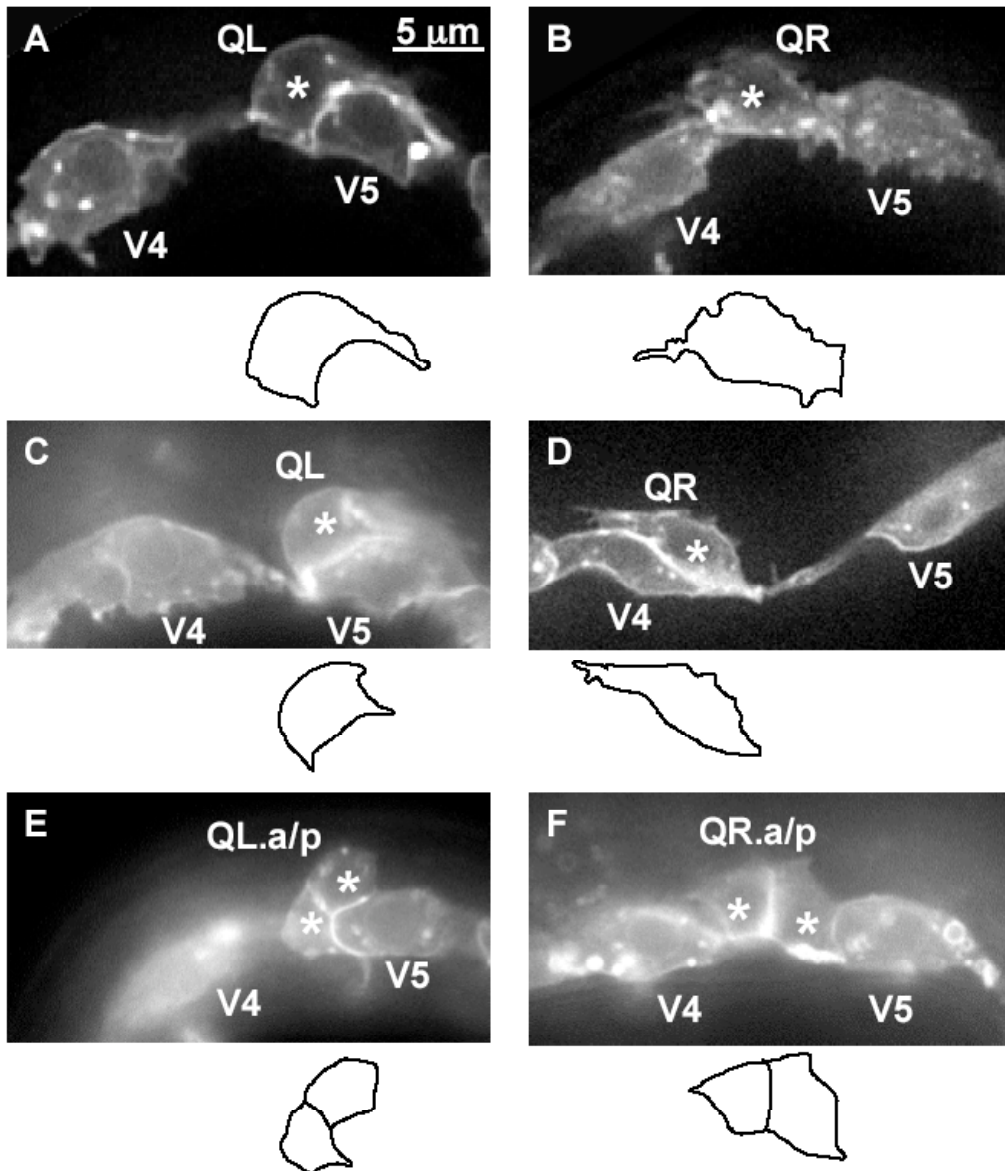
Figure 3.3





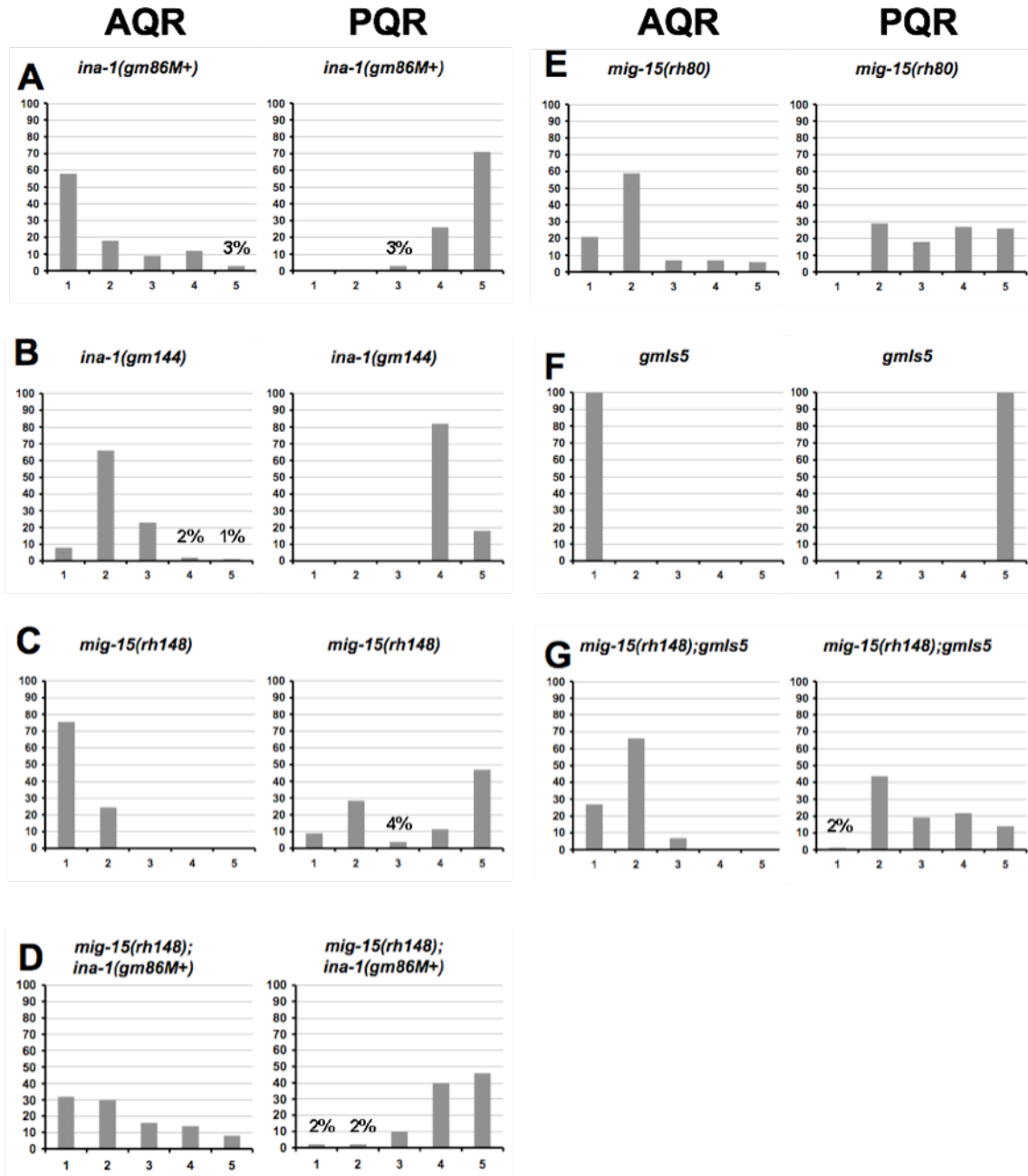
**Figure 3.3. The planar cell polarity pathway does not control the migrations of AQR and PQR.** (A-E) Quantitation of the final migratory positions of the AQR and PQR neurons. The graphs are organized as described in Figs. 3.1A-D. For all cases,  $n \geq 100$ .

Figure 3.4



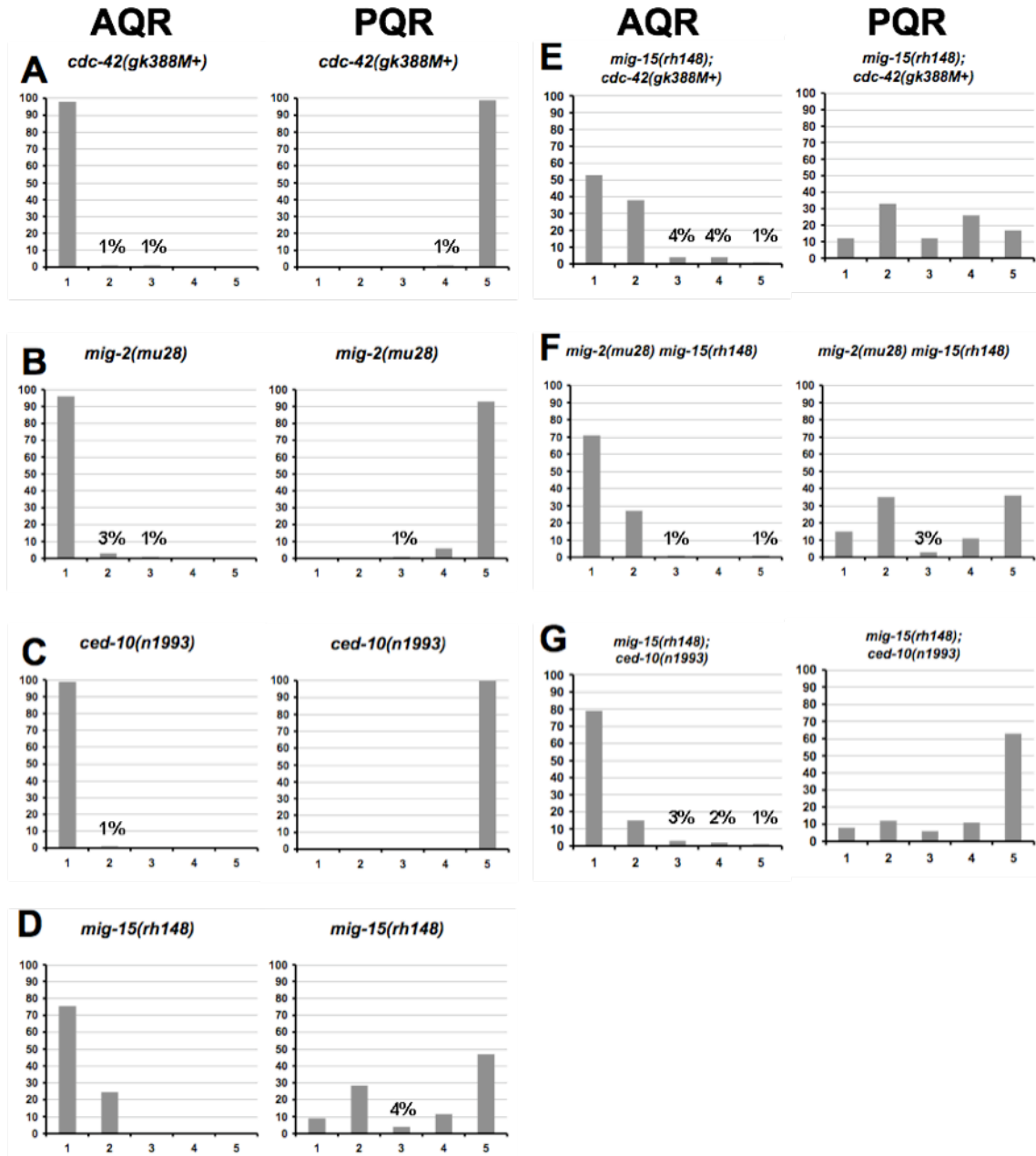
**Figure 3.4. *ina-1*  $\alpha$ -integrin null mutations affect the extension of protrusions and migrations of the Q neuroblasts.** (A-F) Confocal micrographs of Q neuroblasts of *ina-1(gm86M+)* L1 larvae with *scm::gfp::caax* expression. Asterisks mark the locations of the Q neuroblasts and the Q neuroblast descendants. Tracings of the Q neuroblasts located in each panel have been provided below each panel. The scale bar in (A) represents 5 $\mu$ m for panels (A-F). (A) A QL neuroblast polarizes and sends protrusions posteriorly, though this protrusion was reduced in size as compared to wild type. (B) A QR neuroblast polarizes and sends protrusions posteriorly, though this protrusion was reduced in size as compared to wild type. (C) A QL neuroblast migrates posteriorly to the anterior edge of the V5L seam cell. (D) A QR neuroblast migrates anteriorly to the posterior edge of the V4R seam cell. (E) A QL neuroblast divides at the anterior edge of the V5L seam cell. (F) A QR neuroblast divides without migrating from its birth place between the V4R and V5R seam cells. (G-H) Quantitation of the positions of the Q neuroblasts upon dividing. The x-axis represents the anterior-posterior positions of the dividing Q cells with respect to the V4 and V5 seam cells. The y-axis represents the percentage of animals with Q neuroblasts dividing at each anterior-posterior position. For all cases, n  $\geq$  21.

Figure 3.5



**Figure 3.5. Loss of function of INA-1 and overexpression of INA-1::GFP increase the AQR and PQR migration defects in a *mig-15(rh148)* mutant background.** (A-G) Quantitation of the final migratory positions of the AQR and PQR neurons. The graphs are organized as described in Figs. 3.1A-D. For A, B, E, F, and G, n = 100. For *mig-15(rh148)*, n = 200. For *mig-15(rh148);ina-1(gm86M+)*, n = 50.

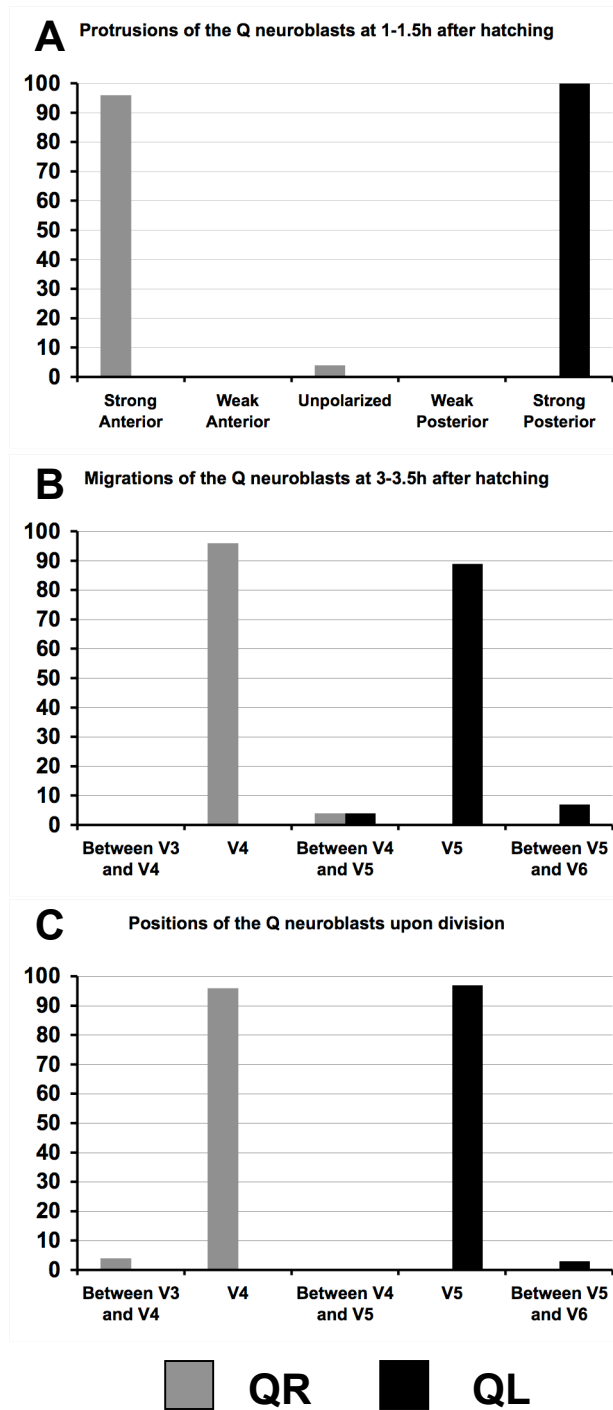
Figure 3.6



**Figure 3.6. Mutations in the Rac GTPases MIG-2 and CED-10 and in CDC-42 cause in increase in migration defects in a *mig-15(rh148)* mutant**

**background.** (A-G) Quantitation of the final migratory positions of the AQR and PQR neurons. The graphs are organized as described in Figs. 3.1A-D. For all cases except *mig-15(rh148)*, 100 animals were scored. For *mig-15(rh148)*, n = 200.

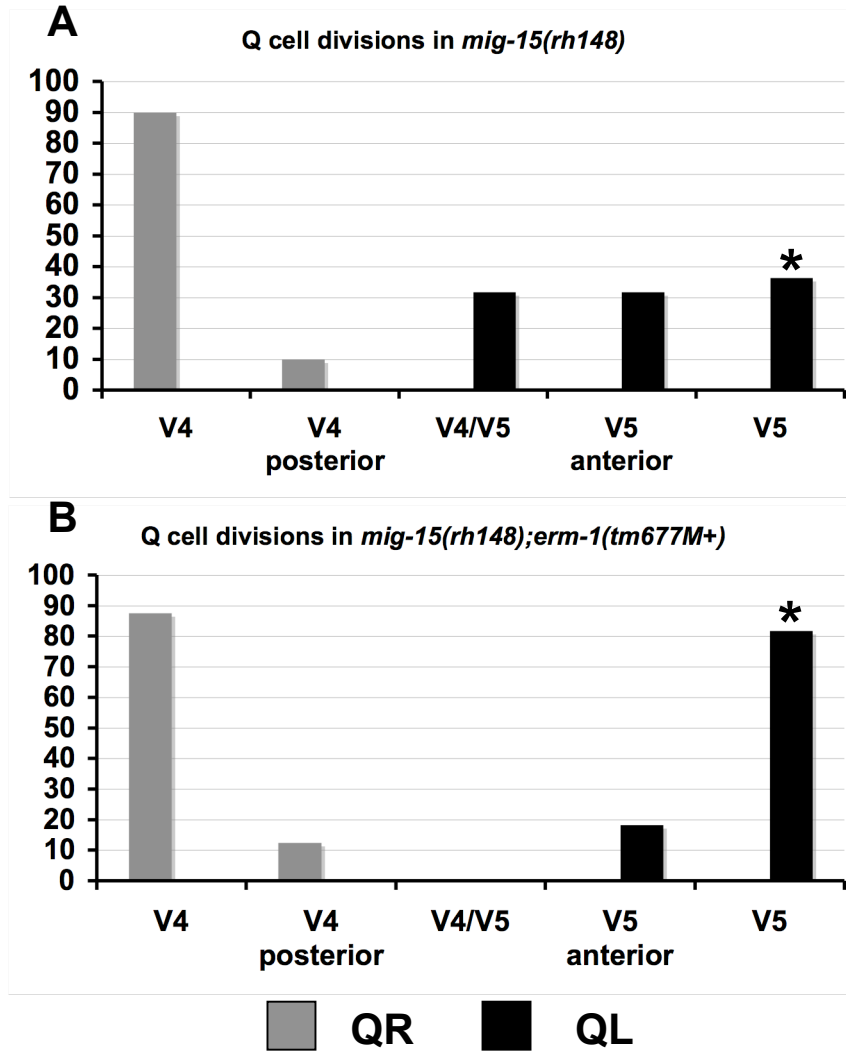
Figure 3.7





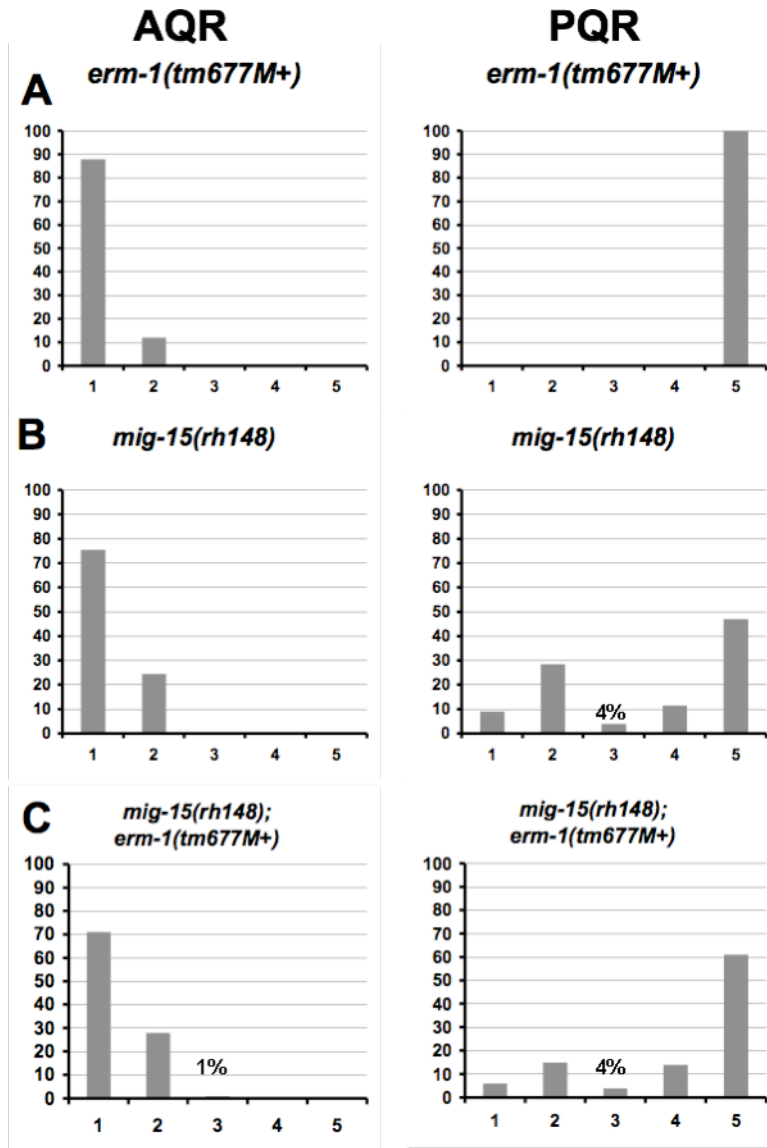
**Figure 3.7. The *erm-1(tm677M+)* mutation does not cause strong defects in Q neuroblast extension of protrusions or migrations.** (A) Quantitation of the direction and extent of protrusions during the polarization stage of the Q neuroblasts at 1-1.5h after hatching. The x-axis represents the direction and extent of polarization of the Q neuroblasts. The y-axis represents the percentage of Q neuroblasts polarized in each of the categories along the x-axis. For both QL and QR, n = 25. (B) Quantitation of the positions of the Q neuroblasts at 2.5-3.5h after hatching. The x-axis represents the direction and extent of migration of the Q neuroblasts. The y-axis represents the percentage of Q neuroblasts that had migrated to each of the categories along the x-axis. For both QL and QR, n  $\geq$  25. (C) Quantitation of the positions of the Q neuroblasts upon dividing. The x-axis represents the anterior-posterior positions of the dividing Q cells with respect to the V4 and V5 seam cells. The y-axis represents the percentage of animals with Q neuroblasts dividing at each anterior-posterior position. For both QL and QR, n  $\geq$  25.

Figure 3.8



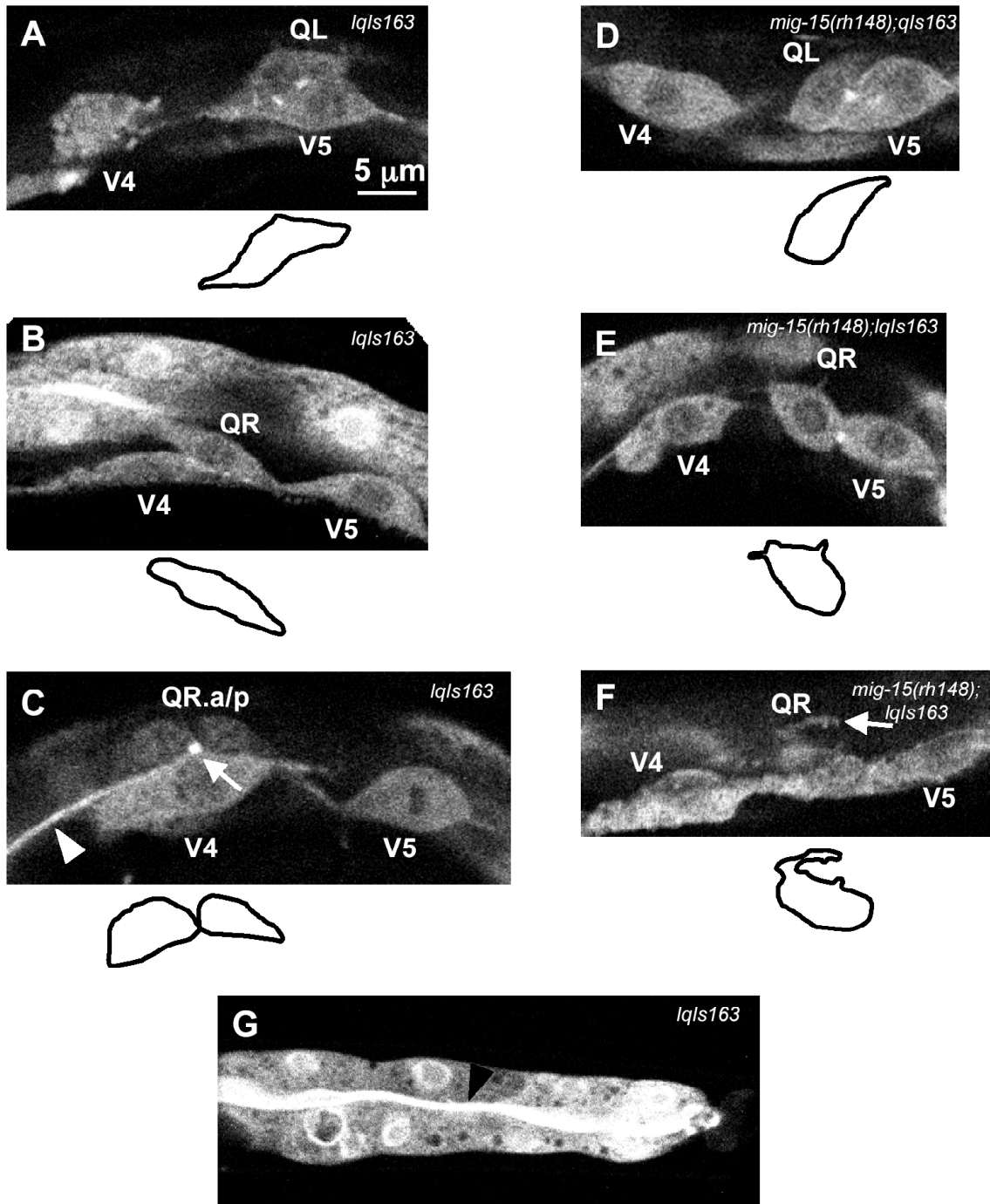
**Figure 3.8. Loss of function *erm-1* mutation suppresses the QL migration defects observed in *mig-15* mutants.** (A,B) Quantitation of the positions of the Q neuroblasts upon dividing. The graphs are organized as described for Fig.3.7C. For *mig-15(rh148)*,  $n \geq 20$  for both QL and QR. For *mig-15(rh148);erm-1(tm677M+)*,  $n \geq 8$  for both QL and QR. The asterisks indicate a significant difference between the two indicated values ( $p = 0.015$ ).

Figure 3.9



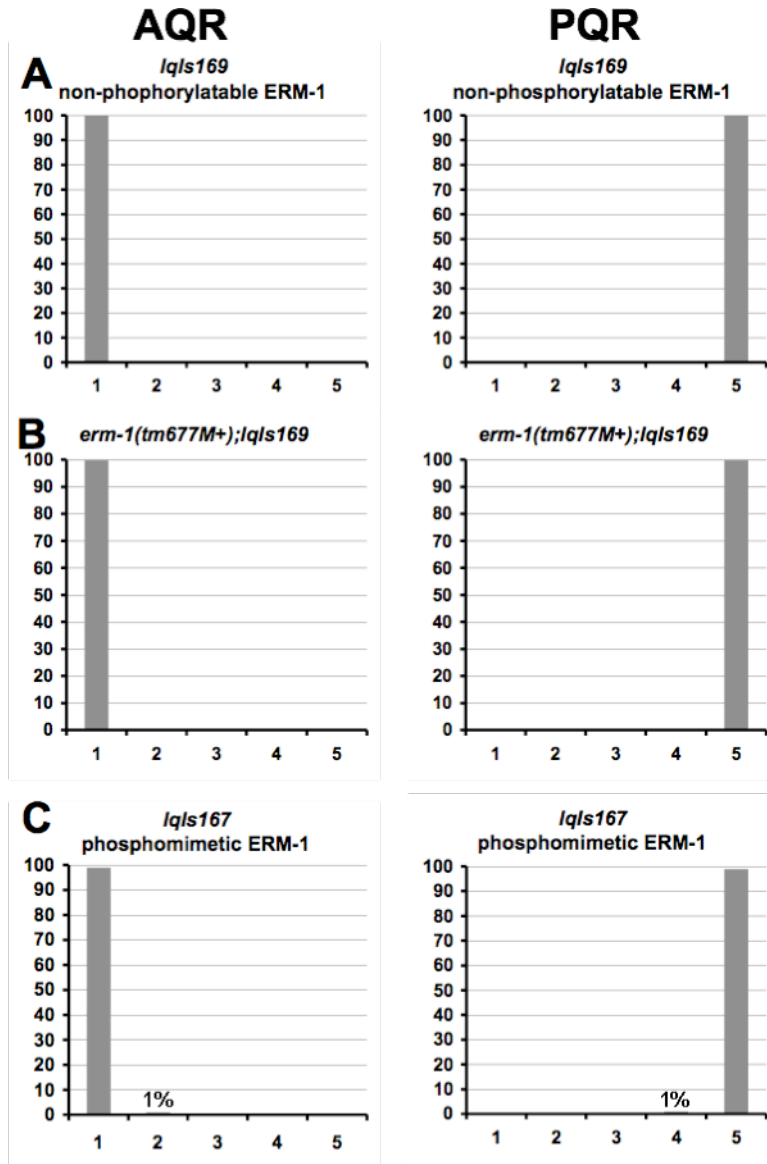
**Figure 3.9. *erm-1* ERM mutant suppresses the PQR migration defects observed in *mig-15(rh148)* mutants.** (A-C) Quantitation of the final migratory positions of the AQR and PQR neurons. The graphs are organized as described in Figs. 3.1A-D. For all cases except *mig-15(rh148)*, n = 100. For *mig-15(rh148)*, n = 200.

Figure 3.10



**Figure 3.10. Localization of ERM-1 in the Q neuroblasts is not disrupted in *mig-15(rh148)* mutants.** (A-G) Fluorescent confocal micrographs of L1 larvae expressing the *scm::erm-1::cfp* translational fusion. Tracings of the Q neuroblasts located in each panel have been provided below each panel for (A-F). The scale bar in (A) represents 5 $\mu$ m for panels (A-G). (A,B) Expression of the *scm::erm-1::cfp* translational fusion visualized at 2-2.5h after hatching in a *wild type* background. (C) Expression of the *scm::erm-1::cfp* translational fusion visualized at 4-4.5h after hatching in a *wild type* background. The arrow indicates strong ERM-1::CFP expression at the cleavage furrow. The arrowhead indicates expression of ERM-1::CFP in the excretory canal. (D-F) Expression of the *scm::erm-1::cfp* translational fusion visualized at 2-2.5h after hatching in a *mig-15(rh148)* mutant background. The arrow in (F) indicates that normal levels of ERM-1::CFP expression are seen in misdirected protrusions in the *mig-15(rh148)* mutant background. (G) Expression of ERM-1::CFP observed in the intestine of animals expressing the *scm::erm-1::cfp* construct in a *wild type* background. The arrowhead indicates strong expression of ERM-1::CFP in the lumen of the intestine.

Figure 3.11

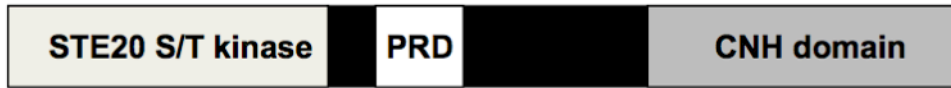




**Figure 3.11. Lack of phosphorylation of ERM-1/ERM does not cause AQR and PQR neuron migration defects.** (A-C) Quantitation of the final migratory positions of the AQR and PQR neurons. The graphs are organized as described in Figs. 3.1A-D. For *lqls169* and *lqls167*, n = 100. For *erm-1(tm677M+);lqls169*, n = 18.

Figure 3.12

**A** Wild type MIG-15



**B** *lqls107*



**C** *lqls138*



**Figure 3.12. Schematic diagram of the MIG-15 structure function**

**constructs.** (A) Diagrams of the domain structure for the wild type MIG-15 protein. (B) Diagram of the plasmid construct of the MIG-15 protein with the CNH domain removed used to generate the *lqls107* transgenic line. (C) Diagram of the plasmid construct of the MIG-15 protein with the S/T kinase domain removed used to generate the *lqls138* transgenic line.

Figure 3.13

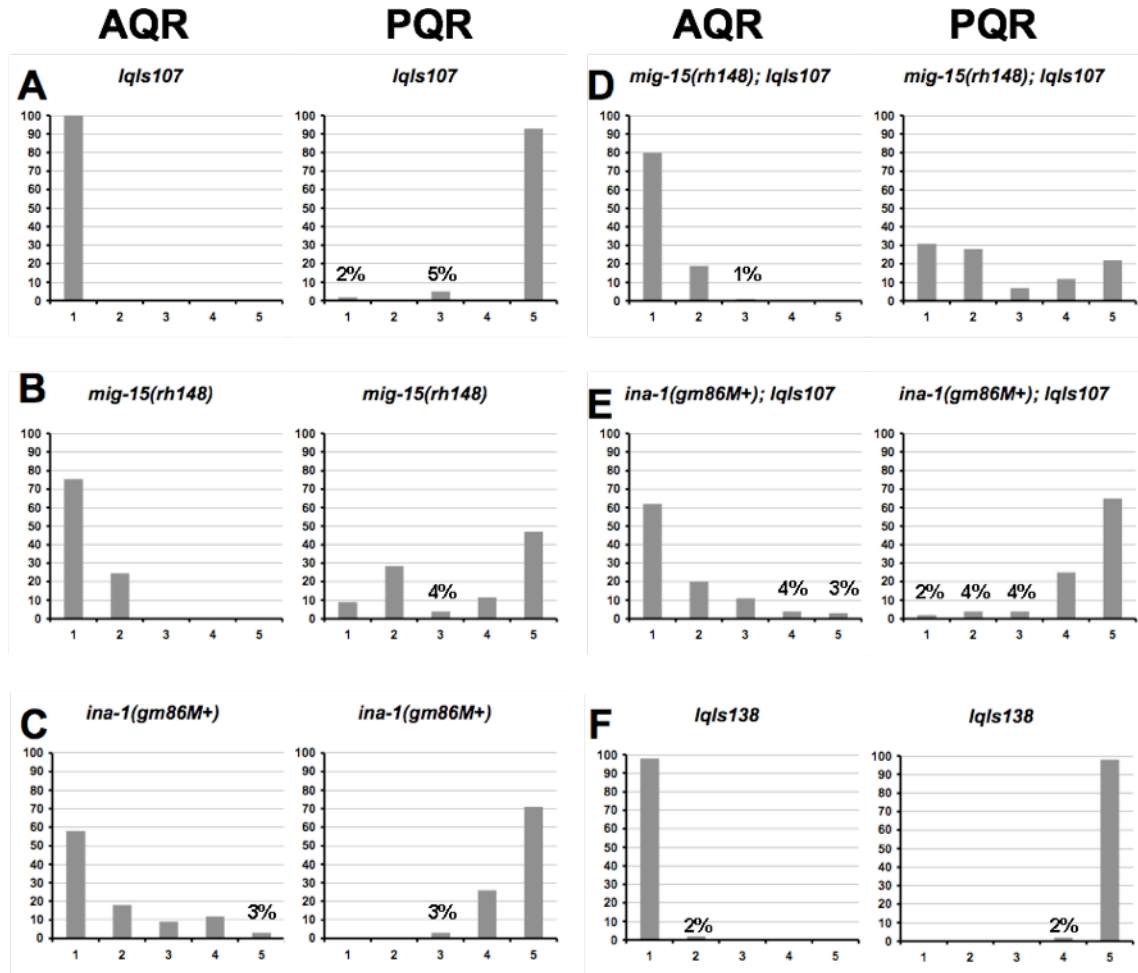





**Figure 3.13. Removal of the citron/NIK homology domain from the *mig-15* coding region causes PQR migration defects in *wild type* animals and increases the PQR migration defects observed in *mig-15(rh148)* mutants.**




(A-F) Quantitation of the final migratory positions of the AQR and PQR neurons.

The graphs are organized as described in Figs. 3.1A-D. For all cases except *mig-15(rh148)*, n = 100. For *mig-15(rh148)*, n = 200.

**Table 3.1 *ina-1* Q cell migration defects (~3-3.5 hours after hatching).**

QL	Normal migration	Shortened migration	No migration
Genotype (n)			
wild-type (42)	100%	0%	0%
<i>ina-1(gm86M+)</i> (24)	8%	38%	54%

QR	Normal migration	Shortened migration	No migration
Genotype			
wild-type (28)	100%	0%	0%
<i>ina-1(gm86M+)</i> (21)	0%	48%	52%

**Table 3.1. *ina-1* Q cell migration defects (~3-3.5 hours after hatching).** The number of animals scored is listed after each genotype for both QL and QR. The values in each category are the percentages of neurons scored that had normal migrations, shortened migrations, or did not migrate.

## **Chapter IV**

**Rac GTPases and the UNC-73/Trio and PIX-1/ $\beta$ PIX Rac GTP  
exchange factors mediate neuroblast protrusion and migration  
in *C. elegans***



#### 4.1. Abstract

Nervous system development is highly dependent on cell migration. In *Caenorhabditis elegans*, numerous neuroblasts must undergo migration in order to form a properly functioning nervous system. In order for these migrations to occur properly, actin cytoskeleton reorganization must take place. The Rac GTPases and CDC-42 have been implicated in the pathways that drive actin cytoskeleton reorganization. Studies shown here examine the roles of the Rac GTPases MIG-2 and CED-10 and CDC-42 in the migration of the QL and QR neuroblasts. MIG-2 and CED-10 were found to act in parallel to control the ability of the Q neuroblasts to extend protrusions and migrate. Surprisingly, CDC-42 was not found to affect the migrations of the Q neuroblasts. UNC-73, the putative GEF for MIG-2 and CED-10, also displayed defects in Q neuroblast protrusion and migration, but the defects were less severe than the *mig-2;ced-10* double mutant, suggesting another possible GEF for these proteins. PIX-1 was found to also be required for proper Q neuroblast protrusion and migration. Double mutants of *pix-1* with *mig-2* caused a synergistic increase in protrusion and migration defects, whereas *pix-1;ced-10* double mutants did not display a large increase in defects, suggesting that PIX-1 could be serving as another possible GEF for CED-10 in Q neuroblast protrusion and migration.

## 4.2. Introduction

The development of the vertebrate nervous system requires extensive amounts of neuronal migration. These neurons must migrate away from their birthplaces to form the various portions of the central nervous system. In order for these migrations to occur, numerous pathways must be activated in order for cells to be able to determine the proper pathway of migration, provide the motile force, and identify the precise stopping point of these migrations. The motile force necessary for these migrations is in part supplied through the reorganization of the actin cytoskeleton (Insall and Machesky, 2009). One family of proteins that have been repeatedly implicated in modulation of the cytoskeleton is the Rho subfamily of GTPases, including Rho, Rac, and Cdc42 (Hall, 1998; Raftopoulou and Hall, 2004; Ridley et al., 2003).

Small GTPases can act as molecular switches, cycling between active and inactive states. These GTPases are in an active state when bound to GTP and inactive when bound to GDP. Several molecules work with the small GTPases to modulate their activity. Guanine nucleotide exchange factors (GEFs) interact with the small GTPases to facilitate the exchange of GDP for GTP, which in turn activates the GTPases. GTPase-activating proteins (GAPs) act in an opposite manner, inactivating the GTPases by activating the GTPase activity of these small GTPases leading to the hydrolysis of GTP to GDP. As small GTPases have been found to interact with a wide variety of effector proteins, GEFs and GAPs are able to control the activation of an extensive

number of signaling pathways through their interactions with these small GTPases.

Extensive studies have been performed examining the roles of the Rac GTPases and Cdc42 in cell motility (Hall, 1998; Raftopoulou and Hall, 2004; Ridley et al., 2003). Rac GTPases and Cdc42 have been found to interact with effector proteins that then modulate the actin cytoskeleton, allowing for directed migration. The effectors that transduce these signals to alter the cytoskeleton vary between the specific Rac GTPases and Cdc42. Cdc42 has been shown to directly bind to members of the Wiskott-Aldrich Syndrome Protein (WASP) family, leading to the activation of the Arp2/3 complex that initiates the addition of branched actin filaments at the leading edge of the cell (Aspenstrom et al., 1996; Higgs and Pollard, 2000; Kolluri et al., 1996; Machesky and Insall, 1998; Welch, 1999). Additionally, Cdc42 has been found to be required for filopodia extension and cell polarity necessary for directed cell movement (Heasman and Ridley, 2008; Nobes and Hall, 1995). Likewise, numerous reports have found that the Rac GTPases lead to the generation of membrane ruffling necessary for the advancement of migrating cells (Heasman and Ridley, 2008).

Though an extensive number of studies have been reported describing the roles of these small GTPases in cell migration, most of these studies have been performed in cell culture with constitutively active and dominant negative forms of the Rac GTPases and Cdc42 (Heasman and Ridley, 2008). These studies have provided an immense amount of information about how these GTPases function in directing migration, but alteration of the activities of the GTPases have brought

about confounding results. As such, here we present *in vivo* studies examining the endogenous functions of the Rac GTPases CED-10/Rac and MIG-2/RhoG along with CDC-42 in neuroblast migration in the nematode *Caenorhabditis elegans*.

Understanding the functions of the Rac GTPases and Cdc42 in neuronal migration also requires examining the molecules that regulate these GTPases, including guanine nucleotide exchange factors specific to these molecules. Numerous GEFs have been found to be involved in the regulation of Cdc42 and the Rac GTPases during cell migration. Particularly of interest is the UNC-73/Trio Rac GTPase GEF, which has been shown to be involved in both migration of neurons and the extension of neurites in *C. elegans* (Kubiseski et al., 2003; Lundquist et al., 2001; Steven et al., 1998; Wu et al., 2002). UNC-73/Trio consists of numerous domains, including two GEF domains, with the first of which thought to interact solely with Rac proteins (Steven et al., 1998). As such, UNC-73 has been shown to work upstream of the Rac GTPases CED-10/Rac and MIG-2/RhoG in axon pathfinding and neuronal migration (Lundquist et al., 2001; Steven et al., 1998). Additionally, studies examining UNC-73 in the Q neuroblasts have found that UNC-73 is required for lamellipodial extension (Honigberg and Kenyon, 2000).

In order to examine the *in vivo* roles of the Rac GTPases and CDC-42 in the migrations of the nervous system, the effects of mutations in the Rac GTPases *ced-10* and *mig-2* and *cdc-42* were studied for the migrations of the Q neuroblasts and their descendants in the nematode *C. elegans*. Observations of

mutants in these Rho subfamily GTPases found opposing roles for these molecules in the migrations of the Q neuroblasts. CED-10/Rac appears to be required for limiting the protrusions and migrations of the Q neuroblasts, whereas MIG-2/RhoG and CDC-42 are required for the ability of the Q neuroblasts to migrate. Examination of mutants in *unc-73* found that UNC-73/Trio, a GEF for both CED-10 and MIG-2, is required for lamellipodial protrusions, as shown previously (Honigberg and Kenyon, 2000). In addition, examination of the other DH containing GEFs found that PIX-1/ $\beta$ PIX also plays a role in the migration of the Q neuroblasts and descendants. Double mutant analysis of *pix-1* with *ced-10* and *mig-2* found that PIX-1 might be working upstream of CED-10, but in parallel to MIG-2 in directing the migrations of the Q neuroblast lineage. PIX-1 has previously been found to act in parallel to CED-10 and MIG-2 in gonad morphogenesis (Lucanic and Cheng, 2008), suggesting that Rac GEFs can interact with different Rac GTPases in a cell specific manner.

In sum, our results indicate that the endogenous functions of the Rac GTPases in directing neuronal migration vary between Rac molecules and that the Rac GEFs UNC-73/Trio and PIX-1/ $\beta$ PIX act in parallel signaling pathways to control neuroblast migrations of the developing nervous system *in vivo*.

### **4.3. Materials and Methods**

#### **Genetic Methods**

All experiments were performed at 20°C using standard techniques (Brenner, 1974; Sulston and Hodgkin, 1988). The following mutations and transgenic constructs were used: X: *mig-2(mu28)*, *pix-1(ok982)*; I: *lqls40[Pgcy-32::gfp]*, *unc-73(rh40)*; II: *cdc-42(gk388)/mln1[mls14 dpy-10(e128)]*; IV: *ced-10(n1993)*, *lqls80[scm promoter::gfp::caax]*. Extrachromosomal arrays were generated by germ line microinjection and integrated into the genome by standard techniques (Mello and Fire, 1995).

#### **Synchronization of L1 larvae to visualize Q cell polarization and migration.**

Methods used for synchronization of L1 larvae were previously described in Honigberg and Kenyon, 2000 and Chapman, et al., 2008. Synchronized L1 larvae were obtained by washing NGM plates containing eggs with M9 buffer at 30-minute intervals. The collected larvae were placed on NGM plates with a bacterial lawn to allow for continued development until the specified time of imaging. Eggs were isolated from egg-laying-defective worms by bleach treatment of gravid adults (Sulston and Hodgkin, 1988).

#### **Epifluorescence microscopy and visualization of Q cell protrusion and**

**migration.** The protrusions and migrations of the Q neuroblasts were visualized in L1 larvae using the transgene *lqls80[scm promoter::gfp::caax]*. Animals were analyzed using a Leica DMR compound microscope with a BD CARV II wide-

field light source. Images were captured using IPlab software and a QImaging Rolera mGi camera. The extent of protrusion of the Q neuroblasts were classified into 3 different extents, with strong protrusion indicating that the protrusions extended greater than half of the distance over the respective seam cell, weak protrusions indicating that the protrusions did not extend greater than half the distance over the respective seam cell, and unpolarized indicating that no protrusions were extended in either the anterior or posterior directions. Statistical significance was determined using a student T-test comparing protrusions and migrations that had occurred properly as in *wild-type* animals.

**Scoring and analysis of AQR and PQR migration defects.** The location of the AQR and PQR neurons were visualized in L4 larvae to young adults using the transgene *lqls40[Pgcy-32::gfp]*. The locations of the neurons after completion of migration were classified into 5 different anterior-posterior positions of the worm, with position 1 = head of the animal to just posterior to the second pharyngeal bulb, 2 = just posterior of the second pharyngeal bulb to slightly anterior of the vulva, 3 = the anterior and posterior regions surrounding the vulva, 4 = slightly posterior to the vulva to just anterior to the anus, 5 = posterior to the anus to the tail of the animal. Statistical significance was determined using a student T-test comparing migrations that had occurred properly as in *wild-type* animals.

**Cell specific RNAi of *cdc-42*.** The sequences of the primers and plasmids used for these experiments are available upon request. The coding region for *cdc-42*

was amplified from N2 genomic DNA by polymerase chain reaction (PCR) and sequenced to ensure that no mutations were introduced by PCR. The coding region was placed downstream of the seam cell promoter from the seam cell marker (*scm*) plasmid pRT1 in both orientations (Terns et al., 1997). Both plasmids were digested with blunt end restriction enzymes and allowed to self-ligate, removing the N-terminal portion of the coding regions in each case. These two plasmids were injected together, along with two additional plasmids containing *scm promoter::gfp::caax* and *Pgcy-32::cfp*. The resulting extrachromosomal array was integrated into the genome to generate *lqls171*. This transgenic line *lqls171* did not cause defects similar to *cdc-42* mutants, suggesting that this construct is not effectively knocking down *cdc-42* transcript levels.



#### 4.4. Results

**Q neuroblasts extend protrusions and migrate in opposite directions.** The Q neuroblasts make an ideal system in which to study neuroblast polarization, extension of lamellipodial and filopodial protrusions, and migration (Chapman et al., 2008). The bilateral Q neuroblasts are born between the V4 and V5 seam cells and are the sister cells of the V5 seam cell (Chalfie and Sulston, 1981; Sulston and Horvitz, 1977). At hatching, the Q neuroblasts are round, unpolarized cells. Between 1-2.5h after hatching, the Q neuroblasts polarize in opposite directions by extending robust protrusions in the direction of polarization, with the QR neuroblast sending out protrusions anteriorly over the V4R seam cell and the QL neuroblast sending out protrusions posteriorly over the V5L seam cell (Fig. 4.1A and B). Between 3-3.5h, the Q neuroblasts cell bodies then follow these protrusions and migrate over the adjacent seam cells. Between 4-4.5h after hatching, the Q cells have completed their migrations and divide, with the QR and QL neuroblasts dividing atop the V4R and V5L seam cells, respectively (Fig. 4.1C and D). These polarizations, protrusion extensions, and migrations are highly characteristic in wild type animals, with very little variation from animal to animal (Figs. 4.1E and F).

After the initial divisions of the Q neuroblasts, the daughter cells continue migrating and undergo additional rounds of division and programmed cell death to ultimately produce three neurons each, with QL producing SDQL, PVM, and PQR, and QR producing SDQR, AVM, and AQR (Sulston and Horvitz, 1977; White et al., 1986). Of these neurons, AQR and PQR are the descendants that

migrate the farthest, with AQR migrating into the anterior deirid ganglion in the head and PQR migrating into the phasmid ganglion in the tail (Sulston and Horvitz, 1977; White et al., 1986; Chapman et al., 2008) (Fig. 4.1G).

Observations of wild-type AQR and PQR migrations again showed that the migrations of the Q cell lineage do not display much deviation in the final locations of these neurons after migration, with the AQR always migrating to the head region of the animal near the second pharyngeal bulb and the PQR always migrating to the tail of the animal behind the anus (Fig. 4.1H).

**CED-10/Rac limits Q neuroblast protrusion whereas MIG-2/RhoG is required for robust Q neuroblast protrusion.** To determine if the Rac GTPases and CDC-42 are involved in Q neuroblast polarization, protrusion or migration, the protrusions of the Q cells were examined in each of *ced-10(n1993)*, *mig-2(mu28)*, and *cdc-42(gk388M+)* single mutants. *ced-10(n1993)* did not strongly affect direction of polarization or protrusion, as all of the observed Q neuroblasts at 1-1.5h had extended robust protrusions in their respective directions in the *ced-10(n1993)* mutants (Fig. 4.2A). In 5% of *ced-10(n1993)* mutants, the QL protrusion actually extended completely over V5 and touched V6, a phenotype never observed in wild-type (Fig. 4.3A).

MIG-2/RhoG has previously been shown to affect Q descendant migration, but its role in Q neuroblast polarization and migration has not been determined (Ou and Vale, 2009; Shakir et al., 2006). The *mig-2(mu28)* did not affect direction of polarization but did cause weak defects in protrusion, with a

small but significant proportion of both QL and QR failing to extend protrusions in any direction at 1-1.5h after hatching (Figs. 4.2B and see example in 4.3C).

Wild-type Q cells never failed to extend protrusions in this manner.

All of the Q cells in the *cdc-42(gk388M+)* mutants extended protrusions in the correct direction, though in a small percentage the protrusions were shorter and less robust than those of wild-type and did not extend greater than half of the distance over the respective seam cell (weakly polarized versus strongly polarized; Figs. 4.2C and 4.3B). These data indicate that CED-10/Rac, MIG-2/RhoG, and CDC-42 are not involved in the direction of protrusion of the Q neuroblasts. While the effects were weak, these data also indicate that MIG-2/RhoG and to a lesser extent CDC-42 are required for robust Q neuroblast protrusion. That some *ced-10(n1993)* QL protrusions extended further than wild-type suggests that CED-10/Rac might have a role in limiting protrusion.

**CED-10/Rac limits Q neuroblast migration whereas MIG-2/RhoG and CDC-42 are required for migration.** Next, migration of the Q neuroblasts was observed by examining the location of the division of the Q cells at 4-4.5h with respect to the surrounding seam cells. In *ced-10(n1993)*, a small but significant percentage of the QR and QL neuroblasts divided at a location farther from their normal division points atop V4 and V5: 15% of QR cells divided between the V3R and V4R seam cells; and 11% of QL divided between the V5L and V6L seam cells (Fig. 4.4A). This suggests that in *ced-10(n1993)* mutants, the Q cells migrated too far before division. This is consistent with the observation reported

above that some QL protrusions at 1-1.5h extended too far in *ced-10(n1993)* mutants, although in the case of division position, the effect was also observed in QR. These results suggest that CED-10/Rac might normally be required to limit Q neuroblast protrusion and migration.

In contrast to *ced-10(n1993)*, a reduction in the distance of migration prior to division was observed for both the *cdc-42(gk388M+)* and the *mig-2(mu28)* single mutants, with the Q neuroblasts dividing between the V4 and V5 seam cells. In most cases, the cells migrated a short distance to either the posterior edge of V4R for QR or the anterior edge of V5L for QL (Figs. 4.4B and C, and 4.5A), though these defects in migration for QL were not significantly different than wild type. Rarely, the cells apparently did not migrate at all and divided directly between V4 and V5 (Fig. 4.5B). Only QL was affected in *mig-2(mu28)*, whereas both QL and QR were affected in *cdc-42(gk388M+)*.

Taken together, these results suggest that each of these single mutants have only a small effect on Q cell polarizations or migrations individually. Both MIG-2/RhoG and CDC-42 appear to be required for the protrusion and migration of the Q neuroblasts. Conversely, CED-10/Rac appears to be involved in limiting Q neuroblast protrusion and migration, as the Q cells in the *ced-10(n1993)* were observed to migrate past their normal stopping points before dividing.

**Single mutations in *ced-10/Rac*, *mig-2/RhoG*, and *cdc-42* have weak effects on Q cell descendant migrations, AQR and PQR.** The neuronal descendants of the Q neuroblasts AQR (from QR) and PQR (from QL) undergo long-range

migrations to the anterior and posterior (Fig. 4.1G and H) (Chalfie and Sulston, 1981; Sulston and Horvitz, 1977). To determine if these GTPases are involved in AQR and PQR long-range migration, the final positions of the AQR and PQR neurons once they had completed their migrations were observed in *ced-10(n1993)*, *mig-2(mu28)*, and *cdc-42(gk388M+)* single mutants.

Two distinct aspects of AQR and PQR migration were scored: the direction of migration and the extent of migration to their normal destinations. Directional migration defects seen for AQR and PQR have been shown to be dependent on the expression of MAB-5/Hox (Chalfie and Sulston, 1981; Kenyon, 1986b; Salser and Kenyon, 1992). MAB-5 is a Hox transcription factor that is induced in QL and QL descendants and directs the further posterior migration of the QL descendants. In the absence of MAB-5/Hox, the QL descendants migrate anteriorly despite an initial posterior QL migration. The expression of MAB-5 is controlled by canonical Wnt signaling, with an EGL-20/Wnt signal being secreted from the posterior of the animal (Chalfie et al., 1983; Eisenmann and Kim, 2000; Harris et al., 1996; Herman, 2001; Kenyon, 1986b; Korswagen et al., 2000; Salser and Kenyon, 1992; Whangbo and Kenyon, 1999). Previous results suggest that the initial migrations of the Q neuroblasts affect their responses to the posterior EGL-20/Wnt signal (Chapman et al., 2008). By migrating posteriorly, the QL neuroblast encounters the EGL-20/Wnt signal and turns on the expression of MAB-5. By migrating anteriorly, the QR neuroblast might avoid the posterior EGL-20/Wnt signal. Failure of QL to migrate posteriorly over V5L could result in QL not receiving a robust EGL-20/Wnt signal and not expressing

MAB-5/Hox, causing the QL descendants (e.g. PQR) to migrate anteriorly. Additionally, if QR fails to migrate anteriorly, it might be exposed to a stronger EGL-20/Wnt signal that activates MAB-5/Hox in QR and descendants, resulting in posterior migration of the QR descendants (e.g. AQR). QR appears to be inherently less sensitive to the EGL-20/Wnt signal (Whangbo and Kenyon, 1999), possibly explaining the weaker defects in AQR direction defects compared to PQR (see below).

*ced-10(n1993)* and *cdc-42(gk388)* had very little effect on AQR and PQR migration (Figs. 4.6A and C). *mig-2(mu28)* had the strongest effect on AQR and PQR migration, with 4% of the AQR neurons failing to fully migrate to the wild type location in the head of the animal and 7% of PQR neurons failing to migrate properly to the wild type location in the tail (Fig. 4.6B). One point of interest is that 1% of the PQR neurons in *mig-2(mu28)* had reversed direction of migration and migrated anteriorly to the area surrounding the vulva, a defect never observed in wild type. *mig-2(mu28)* displayed a low percentage of QL cells that failed to migrate posteriorly (Fig. 4.4B). Possibly, these QL cells failed to receive the EGL-20/Wnt signal and thus PQR migrated anteriorly. Thus, the slightly stronger Q migration defects in *mig-2* mutants might result in stronger AQR and PQR migration defects, including reversal of PQR direction. No AQR or PQR directional defects were observed in *ced-10(n1993)* or *cdc-42(gk388M+)*, consistent with their weaker effects on Q migration compared to *mig-2(mu28)*. These *mig-2(mu28)* defects are consistent with previous reports of Q descendant migration defects in *mig-2* mutants (Ou and Vale, 2009; Shakir et al., 2006).

**CED-10/Rac and MIG-2/Rac act synergistically to control protrusion and migration of the Q neuroblasts.** Previous studies have shown that CED-10/Rac and MIG-2/RhoG act in parallel pathways to control axon pathfinding (Lundquist et al., 2001; Shakir et al., 2006). Neither single mutation alone had strong axon pathfinding defects. Additionally, shown here and in Shakir et al., 2006, CED-10/Rac and MIG-2/RhoG also act in parallel pathways in directing AQR and PQR migration. Since only weak defects in polarization and migration were observed for the Q neuroblasts in single mutants, *mig-2(mu28); ced-10(n1993M+)* were analyzed to determine if they act redundantly in Q migration.

At 1-1.5h after hatching when in wild type animals the Q neuroblasts would be polarized and extending protrusions in opposite directions, most of the Q cells in the *mig-2(mu28);ced-10(n1993M+)* double mutants did not extend obvious protrusions in either anterior or posterior directions (Fig. 4.2D) (60% of QR and 80% of QL). Of the Q cells that did send out protrusions, the QL protrusions were always directed posteriorly and the QR protrusions were always directed anteriorly, as in wild type.

Looking later after migration had occurred, the divisions of the Q cells were observed at 4-4.5h after hatching. A strong failure to migrate atop the neighboring seam cells before division was observed in the *mig-2(mu28);ced-10(n1993M+)* double mutants (Fig. 4.4D; 56% of QR and 100% of QL). *mig-2(mu28)* alone had significantly fewer defects in QL migration and neither *ced-10(n1993)* nor *mig-2(mu28)* had defects in QR migration. Most of the *mig-*

*2(mu28); ced-10(n1993M+)* Q cells did not migrate at all before dividing and divided directly between V4 and V5. No defects in direction of QL or QR migration were apparent. These results suggest that CED-10/Rac and MIG-2/RhoG are required redundantly in parallel pathways for Q cell protrusion and migration, but are not required for direction of polarization.

**CED-10/Rac and MIG-2/Rac act synergistically in AQR and PQR neuronal migration.** Previous studies indicated that CED-10/Rac and MIG-2/RhoG act redundantly in the migration of the Q descendants AQR and PQR (Shakir et al., 2006). These studies relied on an *osm-6::gfp* transgene that was expressed in AQR and PQR but also in other neurons in the head and tail, making it difficult to unambiguously determine the positions of AQR and PQR. To confirm these results and to refine the defects in AQR and PQR migration in *mig-2(mu28); ced-10(n1993M+)* double mutants, we used the *gcy-32::gfp* transgene. *gcy-32::gfp* is expressed in AQR, PQR and the two URX neurons and allows unambiguous identification of AQR and PQR (Chapman et al., 2008).

As shown above, *mig-2(mu28);ced-10(n1993M+)* double mutants exhibited a large number of Q neuroblasts that had failed to migrate before dividing (Fig. 4.4D). Indeed, many (37%) of the PQR neurons migrated anteriorly rather than posteriorly in *mig-2(mu28);ced-10(n1993M+)*, consistent with the initial failure of QL migration (Fig. 4.6D). No AQR directional defects were observed, consistent with the idea that QR is inherently less sensitive to the EGL-20/Wnt signal than is QL (Whangbo and Kenyon, 1999).



Additionally, defects in the extent of AQR and PQR migration were observed in *mig-2(mu28);ced-10(n1993M+)* (Fig. 4.6D). For example, the majority of PQR neurons remained in the posterior of the animal near their birthplace (Fig. 4.6D). Many AQR migrations also stopped short of their wild type position (Fig. 4.6D). Together, these data indicate that CED-10/Rac and MIG-2/RhoG redundantly affect Q descendant neuronal migrations. The directional defects might be due to initial defects in Q cell migration, and the defects in extent of migration might indicate a requirement of these CED-10/Rac and MIG-2/RhoG in neuronal migration.

**Mutations in *cdc-42* enhance the Q neuroblast protrusion defects observed in *ced-10* mutants.** CDC-42 has been shown to be involved in establishing cell polarity and to be involved in directional migration in cell culture (Heasman and Ridley, 2008; Mackay and Hall, 1998). Since only weak defects in migration were observed for the Q cell descendants for the *cdc-42* single mutants, double mutants were constructed of *ced-10(n1993)* and *mig-2(mu28)* with *cdc-42(gk388M+)* to determine if a stronger role for CDC-42 could be observed in this sensitized background. As Cdc42 is involved in many aspects of cell polarization, protrusion and migration in other systems, it was a surprise to find that CDC-42 had only weak effects on Q cell protrusion and migration even in double mutant combinations, as described below (Heasman and Ridley, 2008; Mackay and Hall, 1998).

In *cdc-42(gk388M+);ced-10(n1993)* animals, 2% of both QL and QR failed to extend obvious protrusions at 1-1.5h (Fig. 4.2E), a defect not observed in either single mutant alone (compare to Figs. 4.2A and C). The proportion of all defects was not significantly increased, however. Protrusions were always in the correct direction. At 4-4.5h, *cdc-42(gk388M+);ced-10(n1993)* did not have significantly different defects in migration and division position compared to either single alone (Fig. 4.4E). No defects in direction migration were observed. These data suggest that CDC-42 might act weakly in parallel to CED-10 in Q protrusion but not migration, or that CDC-42 and CED-10 might act in the same pathway to control Q neuroblast protrusion and migration. As was observed with the *ced-10(n1993)* single mutant, a small percentage of the Q cells had migrated past the wild type positions before dividing in the *cdc-42(gk388M+);ced-10(n1993)* double mutant, again suggesting that CED-10/Rac also inhibits over-migration of the Q neuroblasts.

In *mig-2(mu28);cdc-42(gk388M+)* at 1-1.5h, Q protrusion defects were not significantly different than the additive effects of either mutant alone (Fig. 4.2F). At 4-4.5h after hatching, examination of the divisions of the Q cells showed a slight increase in migration defects in *mig-2(mu28);cdc-42(gk388M+)* double mutants compared to *mig-2(mu28)* and *cdc-42(gk388M+)* alone, but these differences were not statistically significant (Fig. 4.4F). No defects in direction of protrusion or migration were observed.

In sum, none of the effects of CDC-42 on Q protrusion and migration were as strong as those observed in the *mig-2(mu28);ced-10(n1993M+)* double

mutant. While the effects were weak, these data could indicate that CDC-42 might act in parallel to CED-10/Rac in Q cell protrusion and MIG-2/RhoG in Q neuroblast migration. However, a linear relationship between CDC-42 and CED-10 and between CDC-42 and MIG-2 could not be ruled out by the results presented here. Interestingly, no defects in direction of Q polarization were observed, which might have been expected based on the previous studies suggesting that CDC-42 is involved in polarization and directional migration (Heasman and Ridley, 2008; Mackay and Hall, 1998).

**CDC-42 acts with CED-10/Rac and MIG-2/RhoG in Q descendant migration.**

*cdc-42(gk388M+)* strongly and significantly enhanced the AQR and PQR extent of migration defects of *mig-2(mu28)* (Fig. 4.6F). Neither AQR nor PQR direction defects were observed, possibly reflecting the weak effects of Q protrusion and migration in these double mutants. For the *cdc-42(gk388M+);ced-10(n1993)* double mutants, a significant synergistic increase in defects was also observed, though not to the same extent as in the *mig-2(mu28);cdc-42(gk388M+)* double mutants (Fig. 4.6E). This effect was most pronounced in PQR. As in the *mig-2(mu28);cdc-42(gk388M+)* double mutants, the *cdc-42(gk388M+);ced-10(n1993)* double mutants did not display AQR/PQR directional migration defects, possibly reflecting the weak Q protrusion and migration defects in the double mutant.

When summarizing all of these data with CED-10/Rac, MIG-2/RhoG, and CDC-42, it is clear that CED-10/Rac and MIG-2/RhoG are central players in Q protrusion and migration, whereas CDC-42 has only weak effects: CDC-42 acts

in parallel to CED-10/Rac in protrusion and in parallel to MIG-2/RhoG in migration. All three of these GTPases also act redundantly to control migration of the neuronal descendants of the Q neuroblasts, with CED-10/Rac and MIG-2/RhoG again having the greatest effect and CDC-42 having a lesser effect. The weak effects of CDC-42 are surprising. A caveat with all experiments with CDC-42 is that the *cdc-42(gk388)* allele is lethal and must be balanced over a wild-type copy. Therefore, activity from the wild-type maternal copy of the gene might be enough to mediate most effects on Q cell protrusion and migration.

**The UNC-73/Trio GEF is required for robust Q cell protrusion.** UNC-73/Trio has two Dbl-homology guanine nucleotide exchange factor domains (DH-GEF domains) (Steven et al., 1998). DH1 acts as a GEF for both CED-10/Rac and MIG-2/RhoG, but not CDC-42 (Debant et al., 1996; Steven et al., 1998). The DH2 GEF domain of UNC-73 is specific for Rho. The Rac GEF activity of UNC-73 is required for axon pathfinding and interacts with CED-10/Rac and MIG-2/RhoG (Lundquist et al., 2001; Shakir et al., 2006). An allele of *unc-73* that is thought to perturb both Rac and Rho GEF activities of the protein has been shown to have defects in Q neuroblast protrusion and migration (Honigberg and Kenyon, 2000). The *unc-73(rh40)* allele is a missense mutation in the DH1 Rac GEF domain that biochemically attenuates the Rac GEF activity of the protein specifically (Steven et al., 1998). Given that *ced-10(n1993)* and *mig-2(mu28)* affect Q protrusion and migration, we tested the effect of the *unc-73(rh40)* mutation on Q cell protrusion and migration.

At 1-1.5h after hatching, *unc-73(rh40)* mutants displayed protrusion defects for both QL and QR, with a small percentage of both QL and QR neuroblasts failing to extend any protrusions (Fig. 4.7C). No defects in direction of protrusion were observed in *unc-73(rh40)*. Comparing these data to that of the *mig-2(mu28);ced-10(n1993M+)* double mutants (Fig. 4.2D), the *unc-73(rh40)* mutants were weaker. Intriguingly, the protrusions observed for *unc-73(rh40)* mutants look very thin compared to wild-type, resembling finger-like filopodial protrusions rather than the robust lamellipodia-like protrusions in wild-type (Figs. 4.7A and B). These thin, finger-like protrusions were rarely if ever observed in *mig-2*, *ced-10*, *cdc-42*, or any double mutant combination of the three. These results suggest that Rac GEF function of UNC-73 is required to extend protrusions and is required for robust lamellipodial protrusion when they do form in *unc-73(rh40)* mutants.

Though the protrusions that the Q neuroblasts normally follow during migration were much less robust in the *unc-73(rh40)* mutants, the Q cells were still able to migrate correctly in most of the *unc-73(rh40)* animals observed. Examining the location of division at 4-4.5h after hatching, most of the QL and QR neuroblasts had fully migrated before dividing over V5L and V4R, respectively, with the remaining neuroblasts migrating to the edges of the seam cells adjacent to their birthplaces before dividing (Fig. 4.7D).

These results suggest that the UNC-73/Trio Rac GEF is playing a role in robust Q cell protrusion. Some Q cells failed to extend any protrusion in *unc-73(rh40)*, similar to but weaker than *mig-2;ced-10* double mutants. The thin,

finger-like protrusions in *unc-73(rh40)* were not observed in *mig-2;ced-10* doubles. This might represent a distinct, non-Rac-mediated role of UNC-73 in protrusion. More likely, given that the Rac GEF activity is specifically affected in *unc-73(rh40)*, is that the thin protrusions are due to reduced but not eliminated CED-10/Rac and MIG-2/RhoG activity in *unc-73(rh40)* mutants.

*unc-73(rh40)* also affected AQR and PQR migration (Fig. 4.7E). The reversal defects of PQR were weak, and the extent of migration defects were stronger, but not as strong as the *mig-2;ced-10* double mutants. These results suggest that UNC-73/Trio is not the only Rac GEF that controls the activity of both CED-10 and MIG-2 in protrusion and migration of the Q neuroblasts.

**PIX-1/ $\beta$ -PIX is required for QL neuroblast protrusion and migration.** The *C. elegans* genome encodes 19 DH GEF domain containing proteins, including UNC-73/Trio. Mutations and/or RNAi of each of the 19 were analyzed for AQR and PQR migration defects. In addition to the already determined role of UNC-73 in Q descendant migration, only one of the other 19 DH GEF domain containing genes was found to cause migration defects when mutated singly in the Q descendants, the guanine nucleotide exchange factor gene *pix-1*. The *pix-1(ok982)* deletion allele was found to have weak defects in PQR migration (6%; Fig. 4.8C). PIX-1 is similar to the PAK (p21-activated kinase) Interacting Exchange Factor, and has been shown previously to act in a Rac-independent pathway with GIT and PAK in *C. elegans* gonadal distal tip cell migration (Lucanic and Cheng, 2008). As described below, *pix-1(ok982)* alone caused

weak defects in protrusion and migration of the QL and QR neuroblasts, and QL migration defects.

At 1-1.5h after hatching, *pix-1(ok982)* mutants displayed weak defects in protrusion for QL and QR (Fig. 4.8A), with all neuroblasts polarized in the correct directions. The most common defect was weak protrusion that did not extend as far as wild-type. *pix-1(ok982)* animals did not display the thin-finger-like protrusions as did *unc-73(rh40)*.

At 4-4.h, migration defects were observed for only the QL neuroblast, and not the QR neuroblast (Fig. 4.8B): 30% of QL failed to fully migrate posteriorly over V5L before dividing, and 1/44 did not migrate at all (i.e. divided at its birthplace).

As described above, *pix-1(ok982)* caused 6% of PQR neurons to not complete their migrations (Fig. 4.8C). Migration of AQR was mostly wild type (Fig. 4.8C), but 1 out of 100 animal scored had a reversal in the direction of migration for AQR, with the final location of migration just anterior to the anus near the location of the PQR neuron (Fig. 4.8C). In sum, these results suggest the possibility that the PIX-1 GEF acts with the UNC-73/Trio GEF in Q protrusion and migration.

**PIX-1/ $\beta$ PIX and UNC-73/Trio act synergistically in controlling protrusion and migration of the Q neuroblasts.** To determine if UNC-73/Trio and PIX-1/ $\beta$ PIX have redundant roles in Q neuroblast migration, a double mutant of *pix-1(ok982)* and *unc-73(rh40)* was constructed. The Rac double *mig-2(mu28);ced-*

*10(n1993)* was maternal-effect lethal, whereas the *pix-1(ok982);unc-73(rh40)* double mutant was viable and fertile.

Examination of the protrusions of the Q neuroblasts at 1-1.5h indicated that PIX-1 and UNC-73 act in parallel pathways to control protrusion of these cells. The defects in protrusion of both QR and QL were much stronger than either single mutant alone (Compare Fig. 4.9A with 4.8A and 4.7C). At 1-1.5h after hatching, many of the Q cells in *unc-73(rh40);pix-1(ok982)* had no visible protrusions. No defects in direction of protrusion were observed. In *unc-73(rh40);pix-1(ok982)*, 37% of QL neuroblasts and 44% of QR neuroblasts had long protrusions similar to wild-type. This is still much less severe than the *mig-2(mu28);ced-10(n1993M+)* double mutant, with a mere 4% of QL and 8% of QR neuroblasts extending robust protrusions. Many of the *unc-73(rh40);pix-1(ok982)* mutants displayed thin and finger-like protrusions in a proportion similar to that of *unc-73(rh40)* alone.

At 4-4.5h after hatching, a synergistic increase in Q neuroblast migration defects was seen in the *pix-1(ok982);unc-73(rh40)* double mutants as compared to the single mutants alone (Fig. 4.9B). As seen for the *pix-1(ok982)* single mutants, the QL neuroblast was affected much more strongly than QR, with QL migration defects observed more than twice as often as in the QR neuroblast (Fig. 4.9B). That *unc-73(rh40);pix-1(ok982)* animals display a synergistic increase in Q protrusion and migration defects indicates that UNC-73/Trio and PIX-1/ $\beta$ PIX might act in parallel to control Q protrusion and migration.



**PIX-1/ $\beta$ PIX acts with CED-10/Rac, but in parallel to MIG-2/RhoG to control protrusion and migration of the Q neuroblasts.** The finding that PIX-1 and UNC-73 act in parallel to control Q protrusion and migration raises question of whether PIX-1 is acting with or in parallel to CED-10 and MIG-2 in the Q neuroblasts, as UNC-73 has been shown to act as a GEF for both CED-10 and MIG-2 (Lundquist et al., 2001; Steven et al., 1998). To determine the genetic relationships between PIX-1 and the Rac GTPases CED-10 and MIG-2, double mutants were constructed and the Q neuroblasts were examined.

Double mutants of *pix-1(ok982)* with *mig-2(mu28)* display synergistic increases in defects in both protrusion and migration of the Q neuroblasts as compared to the defects observed for the single mutants combined (Fig. 4.10A and B). Examination of the Q neuroblast protrusions found that 43% of QL and 35% of QR neuroblasts either failed to extend protrusions or only extended small protrusions in the *mig-2 pix-1* double mutant, a substantial increase in defects as compared to a combined percentages of defects (15.5% for QL and 2.5% for QR) seen for the single mutants alone (compare Fig. 4.10A to 4.2B and 4.8A). But as observed for the single mutants alone, the protrusions that were present in the *mig-2 pix-1* double mutants were always in the proper directions. Defects in the location of divisions of the Q neuroblasts in the *mig-2 pix-1* double mutant again showed a large increase in defects as compared to the combination of defects seen in both of the single mutants, with 56% of QL and 20% of QR neuroblasts failing to fully migrate to their proper locations before dividing in the double mutant as compared to the combined defects observed for 35% of QL

neuroblasts scored and no defects seen for QR migration in either single mutant (compare Fig. 4.10B to 4.4B and 4.8B). This increase in migration defects was also observed for the migrations of AQR and PQR, with the *mig-2 pix-1* double mutant again showing an increase in defects as compared to the combination of defects observed for the single mutants (compare Fig. 4.10C to 4.6B and 4.8C). These results suggest that PIX-1 and MIG-2 are working in parallel pathways to control the migrations of the Q neuroblasts and their descendants.

Examination of the *pix-1(ok982);ced-10(n1993)* double mutants found that PIX-1 and CED-10 do not display a large increase in defects in the migrations of the Q neuroblasts or the Q descendants as compared to the single mutants (compare Fig. 4.10 with Figs. 4.4A, 4.6A, and 4.8). Examination of the protrusions in the *pix-1;ced-10* double mutant found an increase in neurons that had not polarized or had only weakly polarized at 1-1.5h after hatching. The *pix-1;ced-10* double mutants were developmentally delayed as compared to wild type animals, with the divisions of the Q neuroblasts occurring approximately 30 minutes later at 4.5-5h after hatching. Based on this finding, the extension of strong protrusions might occur at a later time point as well. Observations of the locations of Q neuroblast divisions found that both QL and QR migrations were not significantly different than the combination of the defects seen for the single mutants, with the double mutants only displaying 27% QL and 7% QR migration defects (Figure 4.10E). Likewise, there was no synergistic increase in migration defects observed for the AQR and PQR neurons in the *pix-1;ced-10* double mutants (Figure 4.10F). The migration defects for the AQR neuron were not

significantly different than the combination of the defects observed for both of the single mutants ( $p = 0.3$ ). As for the PQR neuron, the migration defects in the *pix-1;ced-10* double mutant were slightly increased as compared to the combination of defects observed for the *pix-1* and *ced-10* single mutants ( $p = 0.03$ ). Though there was an increase in protrusion extension defects that might be due to the time point at which these neurons were scored, the lack of a synergistic increase in the later migration events of the Q neuroblasts and the Q neuroblast descendants suggest that PIX-1 and CED-10 might be acting in the same pathway to control the migrations of the Q neuroblasts and their descendants. Taken the results shown here and the previous findings that UNC-73 serves as a GEF for CED-10 and MIG-2 together (Lundquist et al., 2001; Steven et al., 1998), it appears that CED-10 is acting downstream of both UNC-73 and PIX-1, whereas MIG-2 is acting downstream of UNC-73 in parallel to the PIX-1/CED-10 pathway to control the migrations of the Q neuroblast descendants.

#### 4.5. Discussion

**The Rac GTPases CED-10/Rac and MIG-2/RhoG have opposite effects on the protrusion extension and migration of the Q neuroblasts.** Loss of function mutations in the Rac GTPases *ced-10* and *mig-2* do not cause defects in the direction of polarization of the Q neuroblasts. Of the Q neuroblasts that do extend protrusions, these processes are always oriented in the proper direction of polarization, with QR extending protrusions anteriorly and QL extending protrusions posteriorly. These mutants do however affect the size of the protrusions that are extended, with *ced-10(n1993)* mutants observed to extend protrusions that are increased in size as compared with *wild type* Q cell protrusions. As shown in Figure 4.3A, the Q neuroblast protrusions extended past the adjacent seam cell where they normally terminate in *wild type* animals, continuing to extend these protrusions onto the next seam cell, with the QL protrusion touching the V6L seam cell in 5% of animals scored. Opposite defects were observed for *mig-2(mu28)*, with a small percentage of the Q neuroblasts failing to extend any protrusions at 1-1.5h after hatching. Thus, it seems that CED-10 might normally limit the extension of protrusions, whereas MIG-2 might promote protrusion extension in the Q neuroblasts.

Similar to what was seen during the polarization stage of the Q neuroblasts, *ced-10* and *mig-2* mutants also displayed opposite effects on the migrations of the Q neuroblasts. For *ced-10(n1993)*, the Q neuroblasts often migrated past the stopping point where *wild type* Q cells divide, but continued migrating to between the V3R and V4R seam cells for QR and between the V5L

and V6L seam cells for QL before dividing. For *mig-2(mu28)*, failure of the Q neuroblasts to fully migrate before dividing was observed, with 5% of the QL neuroblasts dividing at the anterior edge of V5L instead of on top of the V5L seam cell as in *wild type*. Taken together, these data suggest that CED-10 normally plays an inhibitory role in the protrusions and migrations of the Q neuroblasts with CED-10 limiting the length of protrusions and migrations of the Q cells. MIG-2 appears to be required for full extension of protrusions and for complete migrations of the Q neuroblasts.

**CED-10/Rac and MIG-2/RhoG also have redundant roles in directing the Q neuroblast protrusion and migration.** Though CED-10 and MIG-2 appear to have opposite roles in directing protrusion extension and migration in the Q neuroblasts, these molecules also seem to have redundant roles in both of these processes as well. Double mutants of *ced-10* with *mig-2* show a synergistic increase in protrusion and migration defects. During the 1-1.5h after hatching timepoint, the majority of both QL and QR neuroblasts had failed to extend any protrusions at all, suggesting that CED-10 might be functioning redundantly with MIG-2 to promote the initiation of Q neuroblast protrusion in addition to the role of CED-10 in limiting the length of protrusion extension. CED-10 and MIG-2 also appear to be working redundantly in directing the migrations of the Q neuroblasts, with 100% of the QL and 56% of the QR neuroblasts failing to migrate over their respective seam cells before dividing. Thus, it appears as though CED-10 and MIG-2 are acting in parallel pathways to control both

protrusion extension and migration of the Q neuroblasts. In addition, functional redundancy of CED-10 and MIG-2 has previously been observed for the roles of these two Rac GTPase molecules in axon pathfinding (Lundquist et al., 2001; Shakir et al., 2006). Though these two molecules appear to be acting in parallel in three different morphological processes, these three processes of protrusion extension, neuronal migration, and axon pathfinding might all be controlled by the same signaling pathway in which the Rac GTPases CED-10/Rac and MIG-2/RhoG function. As the Rac GTPases are required for lamellipodial protrusion, defects in migration and axon pathfinding seen in these mutants could be a consequence of the lack of lamellipodial protrusions.

**CDC-42 acts with CED-10/Rac and MIG-2/RhoG to control the migrations of the Q neuroblast descendants.** Loss of function *cdc-42* mutants displayed weak defects in the protrusions and migrations of the Q neuroblasts, similar to the defects observed for *mig-2* mutants, suggesting that CDC-42 is required for promoting protrusion extension and migration in the Q cells. Double mutants of *cdc-42* with *mig-2* did not display a significant increase in defects in protrusion and migration of the Q cells as compared to the defects of the two single mutants combined, suggesting that CDC-42 might be working in the same pathway as MIG-2 or in independent pathways to control Q neuroblast protrusion and migration. Another possibility, since a small increase in defects was observed for the migrations of the Q neuroblasts in the *mig-2;cdc-42* double mutants, is that MIG-2 and CDC-42 could be working in parallel pathways. The defects observed

for the migrations of the Q cell descendants would suggest the latter, as a synergistic increase in migration defects was observed for both the AQR and PQR neurons in the *mig-2;cdc-42* double mutants.

Double mutants of *ced-10* with *cdc-42* also displayed a weak increase in defects in protrusion extension of the Q neuroblasts as compared to the two single mutants alone. No increase in defects was observed for this double mutant in the migrations of the Q neuroblasts. Again, like for the *mig-2;cdc-42* double mutants, a synergistic increase in migration defects was observed for the PQR neuron in the *cdc-42;ced-10* double mutant. These results might suggest that CDC-42 and CED-10 are working in parallel pathways to control the migrations of the Q neuroblast descendants. As for in the Q neuroblasts, CDC-42 and CED-10 might also be working in parallel pathways to control protrusion extension, but a linear relationship could not be ruled out by these experiments.

One caveat of these experiments is that the *cdc-42* mutant used here has to be maintained over a *wild type* copy of *cdc-42*. Therefore, maternal contributions of *cdc-42* RNA could be rescuing any defects that might be present in the Q neuroblasts. The *cdc-42* mutants did not display much difference in the amount of defects in the early Q neuroblast migrations versus those observed for the later Q descendant migrations, though defects in either migration was rare, as seen for the *ced-10* and *mig-2* single mutants. However, when mutation in *cdc-42* was introduced into the *ced-10* and *mig-2* mutant backgrounds, the proportion of increased defects seen for the later migration events of AQR and PQR was much larger than the increase in defects seen for the Q neuroblast

migrations. This could be a result of the limitation of the maternal contribution of *cdc-42* RNA, with the amount of CDC-42 present during the later migration events substantially reduced as compared to the earlier migration events, leading to an increase in migration defects. Another possibility is that an increased requirement for CDC-42 function is necessary for the proper migrations of the Q neuroblast descendants, resulting in many more defects in the migration of the AQR and PQR neurons as compared to the Q neuroblasts when knocking down CED-10 or MIG-2, molecules that are acting redundantly to direct the migrations of the Q neuroblast descendants.

**UNC-73/Trio does not act alone as the GEF for the Rac GTPases in Q neuroblast migration.** Previous studies have determined UNC-73 to act as a guanine nucleotide exchange factor (GEF) for the CED-10 and MIG-2 Rac GTPases (Lundquist et al., 2001; Steven et al., 1998). Thus, the *unc-73(rh40)* allele, a mutation thought to inactivate the GEF activity for Rac GTPases, was examined for Q neuroblast protrusion and migration defects (Steven et al., 1998). Examination of the Q neuroblast protrusions found that these structures were much reduced in size as compared to *wild type*. These protrusions in the *unc-73* mutants were highly branched and more filopodial-like than lamellipodial-like, suggesting that UNC-73 is required for lamellipodial extensions. The presence of filopodial-like, thin Q neuroblast protrusions were not observed in the *mig-2;ced-10* double mutants, though the lack of these structures could be due to the Rac GTPase double mutant causing much more severe defects in protrusion



extension, with the majority of the Q neuroblasts not sending out any protrusions at 1-1.5h after hatching. In addition to the *unc-73* protrusion defects being less severe than those seen for the *mig-2;ced-10* double mutants, a similar relationship was observed for the Q neuroblast and Q neuroblast descendant migration defects, in which the *unc-73* mutants displayed migration defects that were much weaker than observed for the *mig-2;ced-10* double mutant. Thus, these results suggest that UNC-73 is not acting as the only GEF for CED-10 and MIG-2 in the Q neuroblasts.

**PIX-1/ $\beta$ PIX functions as a GEF for CED-10/Rac in Q neuroblast protrusion and migration.** Examination of another Rac GTPase GEF found that PIX-1/ $\beta$ PIX has a role in the protrusion extension and migration of the Q neuroblasts and in the migration of the Q descendants. Additionally, double mutants of *unc-73* with *pix-1* displayed a synergistic increase in protrusion and migration defects in the Q neuroblasts. These results suggest that PIX-1 and UNC-73 are acting in parallel pathways to control the protrusion and migration of the Q neuroblasts.

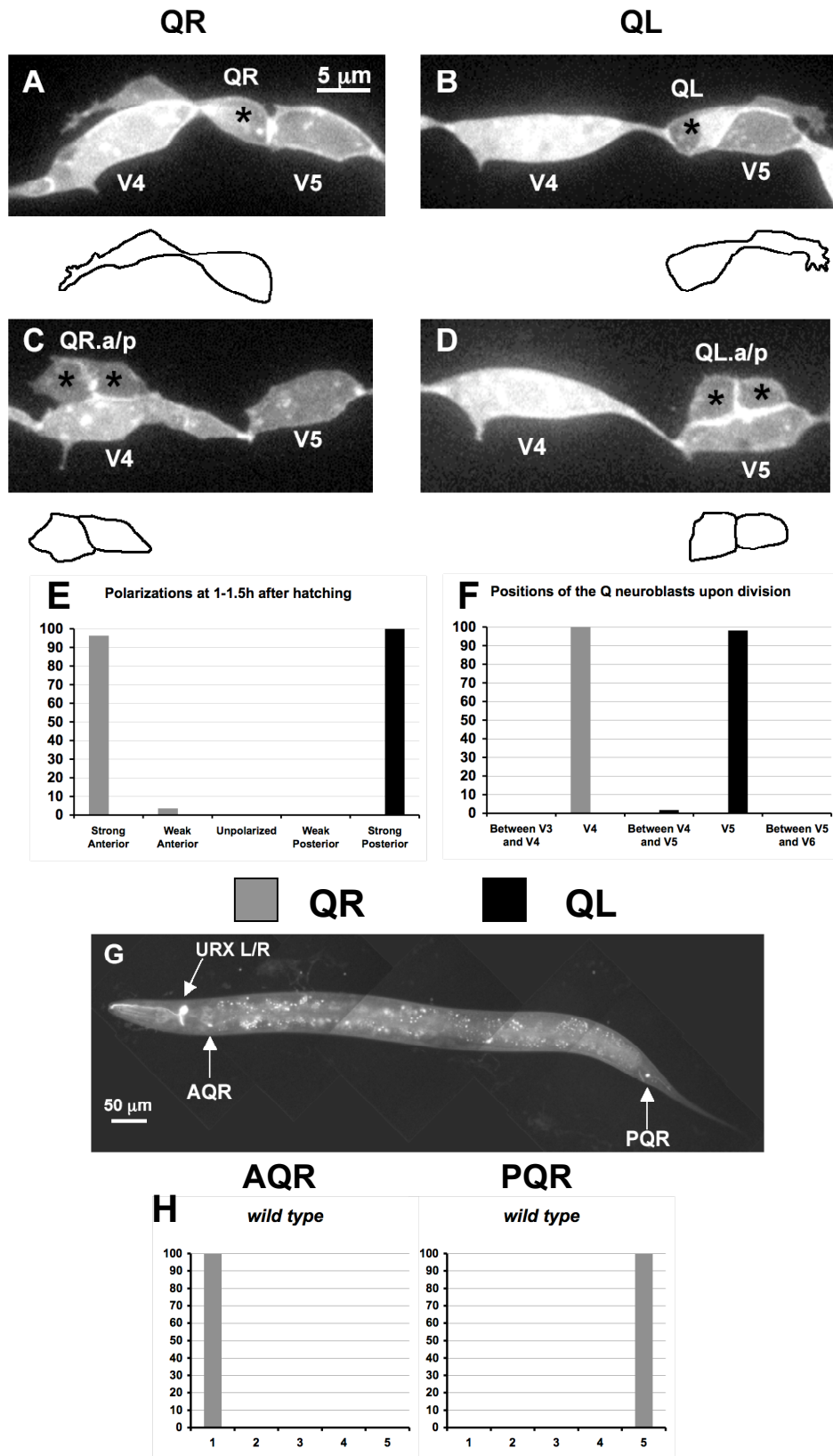
One point of interest was that of the Q neuroblasts observed during the division stage in the *pix-1;unc-73* double mutants, 2/28 of the observed QL neuroblasts had divided on the posterior edge of V4L, a phenotype that was not observed for any of the single mutants examined here. Though this would indicate an anterior migration of the QL neuroblasts before division, another possible explanation could be that it appears as though the V4 seam cells extend posteriorly to make contact with the V5 seam cells after the initiation of migration

of the Q neuroblasts. This could cause neuroblasts that had failed to migrate to appear to have migrated anteriorly, even if these cells had not migrated at all. This could also partially explain the differences between the QL and QR migration defects seen in many of the mutants observed here, as the defects in protrusion extension are mostly similar between the QL and QR neuroblasts for all mutants, whereas the defects in migration were typically stronger for the QL neuroblasts in the same mutants.

As UNC-73 has been shown to function as a GEF for MIG-2 and CED-10 and UNC-73 and PIX-1 are shown here to act in parallel to control Q neuroblast protrusion and migration, PIX-1 could be acting in parallel to the UNC-73/CED-10/MIG-2 pathway or PIX-1 could be acting as a GEF for CED-10 and/or MIG-2 as does UNC-73 (Lundquist et al., 2001; Steven et al., 1998). To differentiate between these possibilities, double mutants of *pix-1* with *ced-10* and *mig-2* were built. Interestingly, only *mig-2 pix-1* double mutants displayed a synergistic increase in Q neuroblast defects, whereas the *pix-1;ced-10* double mutants were observed to have only a small increase in defects compared to either of the single mutants alone. Taken together, these results suggest that PIX-1 might be working upstream of CED-10 in a linear pathway and that PIX-1 and CED-10 are working in a parallel pathway to MIG-2 to control Q neuroblast protrusion and migration. Interestingly, previous studies have found that PIX-1 functions in a pathway that is parallel to the Rac GTPases CED-10 and MIG-2 in gonad morphogenesis (Lucanic and Cheng, 2008). The results shown here suggest

that PIX-1 can also function in a linear pathway with the Rac GTPase CED-10 indicating that the relationship of PIX-1 with the Rac GTPases is tissue specific.

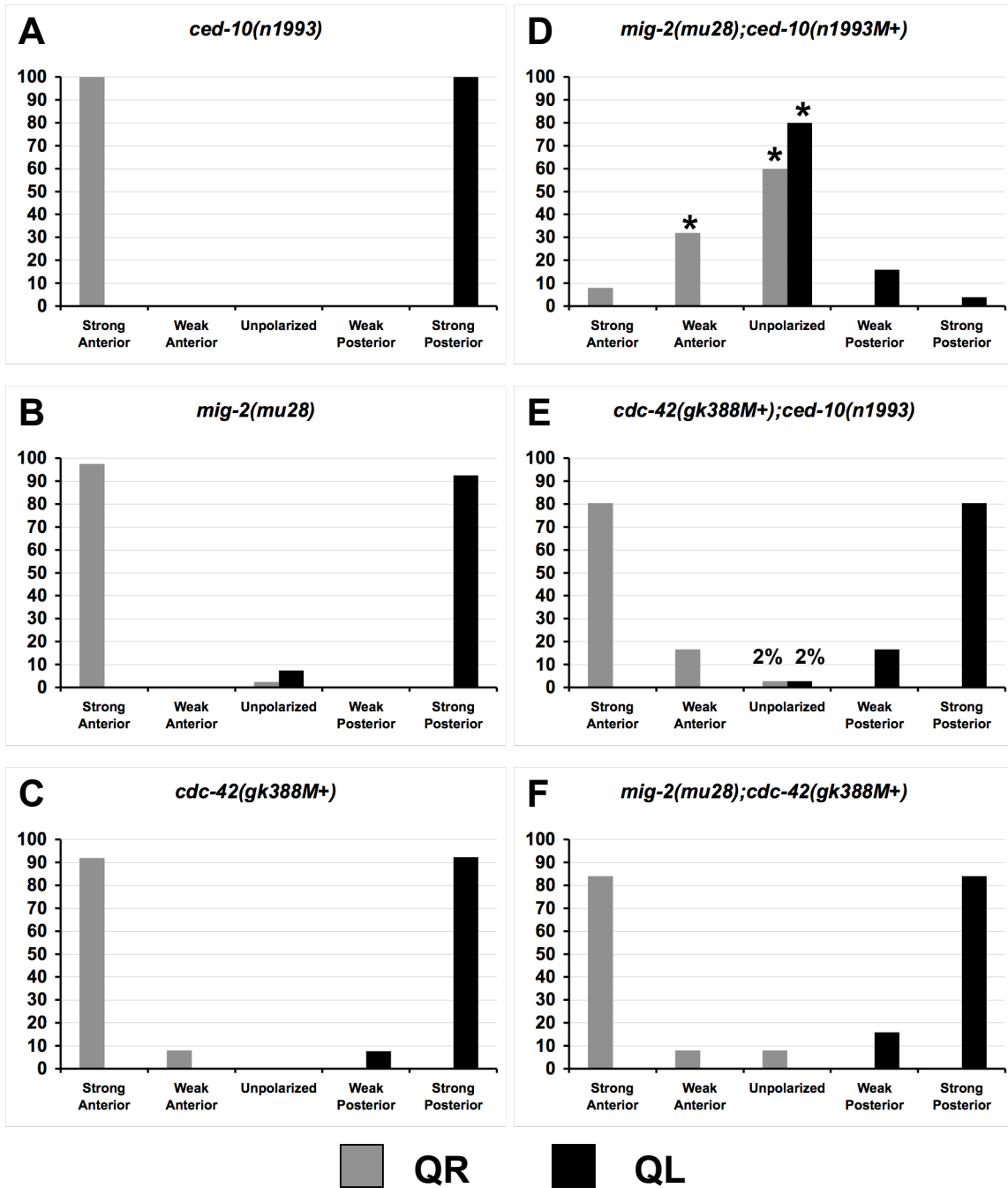
Figure 4.1



**Figure 4.1.** Protrusions and migrations of the Q neuroblasts and migrations of the AQR and PQR neurons in *wild type* animals. (A-D) Confocal fluorescent micrographs of Q neuroblasts in *wild type* L1 larvae visualized with *scm::gfp::caax* expression. Asterisks mark the position of the Q neuroblasts and the Q neuroblast descendants. Tracings of the Q neuroblasts and the Q neuroblast descendants are located beneath each micrograph. The scale bar in (A) represents 5 $\mu$ m for (A-D). (A) A QR neuroblast polarizes, sending out protrusions anteriorly over the V4R seam cell at 1-1.5h after hatching. (B) A QL neuroblast polarizes, sending out protrusions posteriorly over the V5L seam cell at 1-1.5h after hatching. (C) A QR neuroblast divides over the V4R seam cell after migrating anteriorly at 4-4.5h after hatching. (D) A QL neuroblast divides over the V5L seam cell after migrating posteriorly at 4-4.5h after hatching. (E) Quantitation of the direction and extent of protrusions during the polarization stage of the Q neuroblasts at 1-1.5h after hatching in *wild type* animals. The x-axis represents the direction and extent of polarization of the Q neuroblasts. See Materials and Methods for classifications of extent of protrusion. The y-axis represents the percentage of Q neuroblasts polarized in each of the categories along the x-axis. For both QR and QL polarizations, n = 55. (F) Quantitation of the location of the Q neuroblasts at division with respect to the adjacent seam cells in *wild type* animals. The x-axis represents the location of the Q neuroblasts at division with respect to the adjacent seam cells. The y-axis represents the percentage of Q neuroblasts located at those positions. For both QR and QL polarizations, n  $\geq$  29. (G) Epifluorescent micrograph of the AQR and

PQR neurons in a *wild type* L4 larvae visualized with *Pgcy-32::gfp*. The scale bar in (G) represents 50 $\mu$ m. (H) Quantitation of the final migratory positions of the AQR and PQR neurons in *wild type* animals. The x-axis represents the final position of the AQR and PQR neurons along the anterior-posterior axis of the animal as described in the Materials and Methods section. The y-axis represents the percentage of AQR and PQR neurons located at those positions along the anterior-posterior axis. For both cases, n = 100.

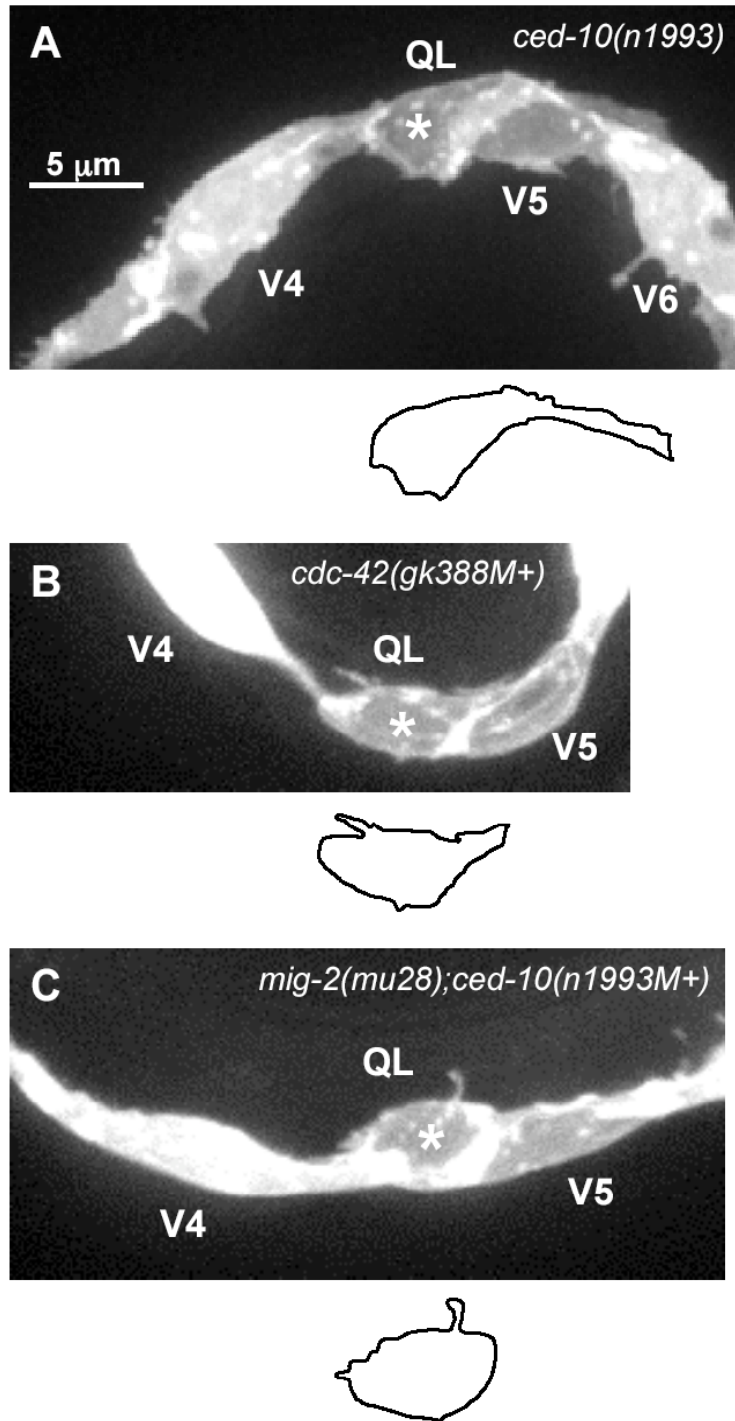
Figure 4.2



**Figure 4.2.** Polarizations of the Q neuroblasts at 1-1.5h after hatching. (A-F) Quantitation of the direction and extent of protrusions during the polarization stage of the Q neuroblasts at 1-1.5h after hatching. The graphs are organized as described in Fig. 4.1E. The asterisks in (D) represent statistically significant differences as compared to the *ced-10(n1993)* and *mig-2(mu28)* single mutants alone. For all cases,  $n \geq 25$ .

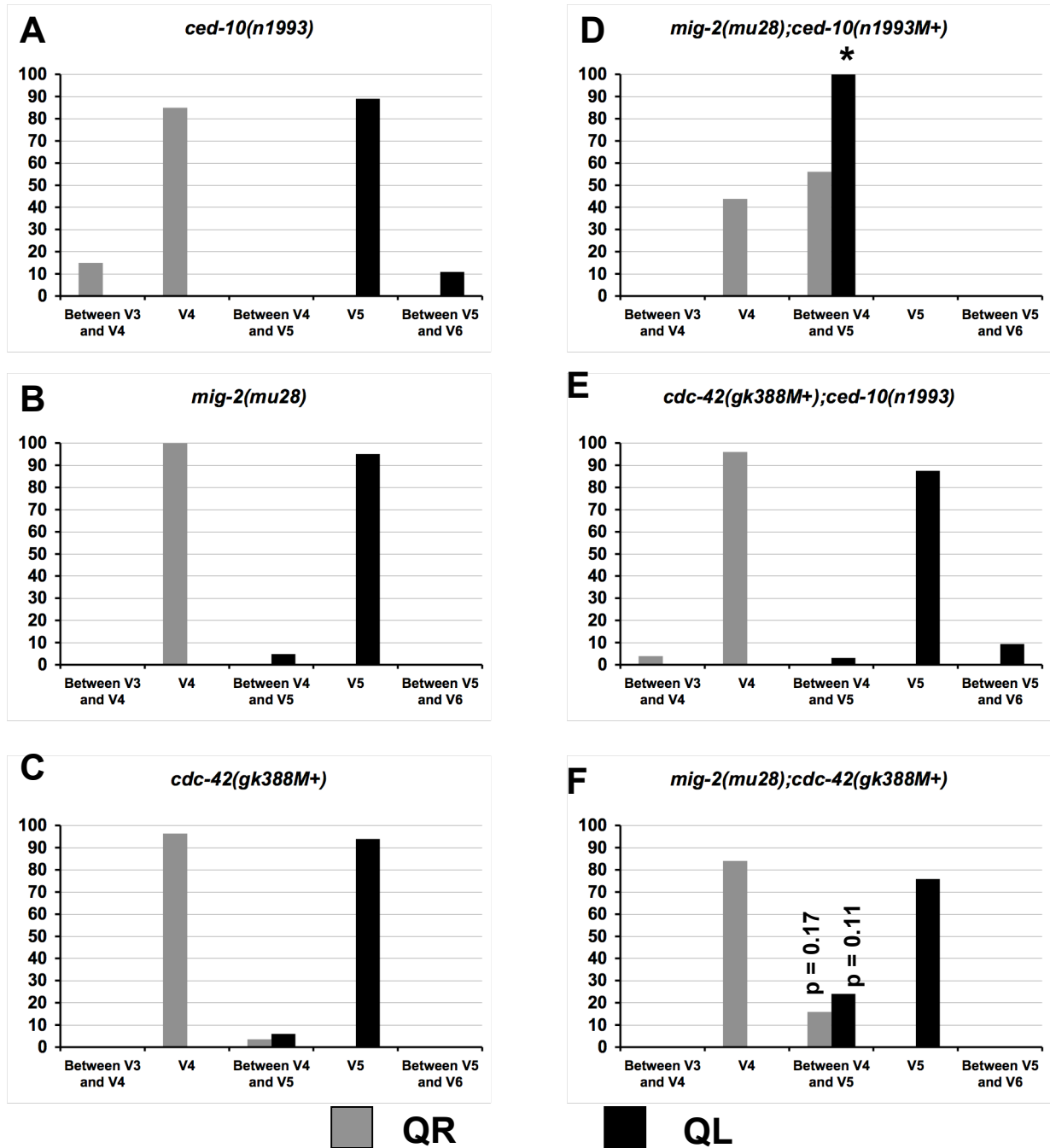


Figure 4.3



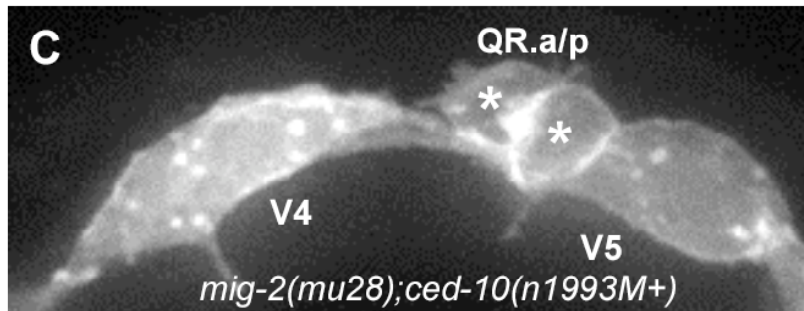
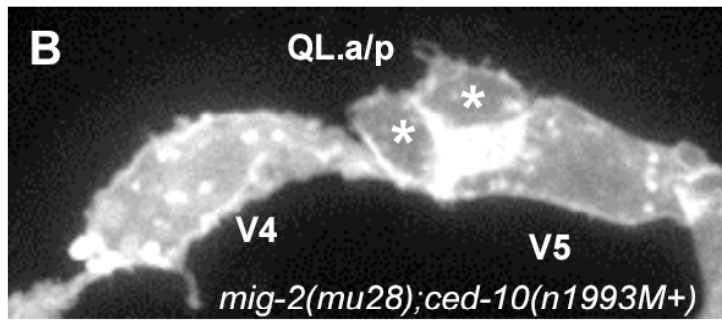
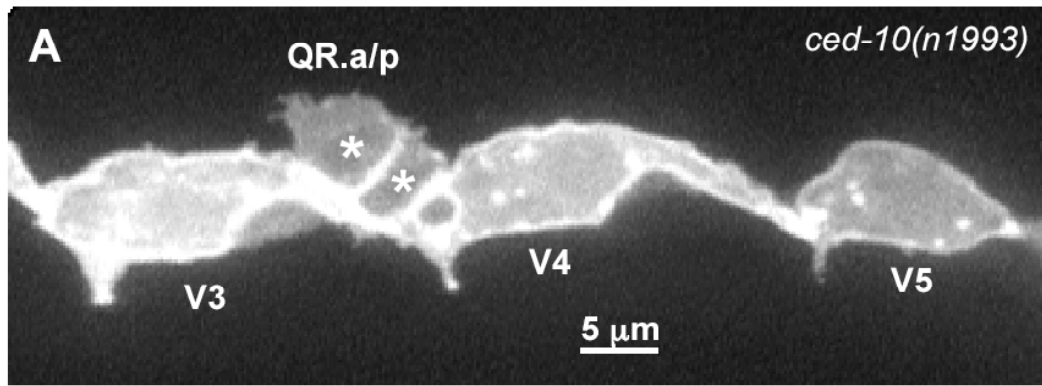
**Figure 4.3.** Failure of the Q neuroblasts to extend *wild type* protrusions. (A-C) Confocal fluorescent micrographs of Q neuroblasts in L1 larvae visualized with *scm::gfp::caax* expression at 1-1.5h after hatching. Asterisks mark the position of the Q neuroblasts. Tracings of the Q neuroblasts are located beneath each micrograph. The scale bar in (A) represents 5 $\mu$ m for (A-C). (A) A QL neuroblast in a *ced-10(n1993)* mutant extends protrusions posteriorly that are longer in size than in *wild type*, with the protrusion extending well onto the V6L seam cell. (B) A QL neuroblast in a *cdc-42(gk388M+)* mutant fails to send out robust protrusions posteriorly, though small protrusions extending in the proper posterior direction can be observed. (C) A QL neuroblast in a *mig-2(mu28);ced-10(n1993M+)* mutant fails to extend protrusions in either direction.

Figure 4.4



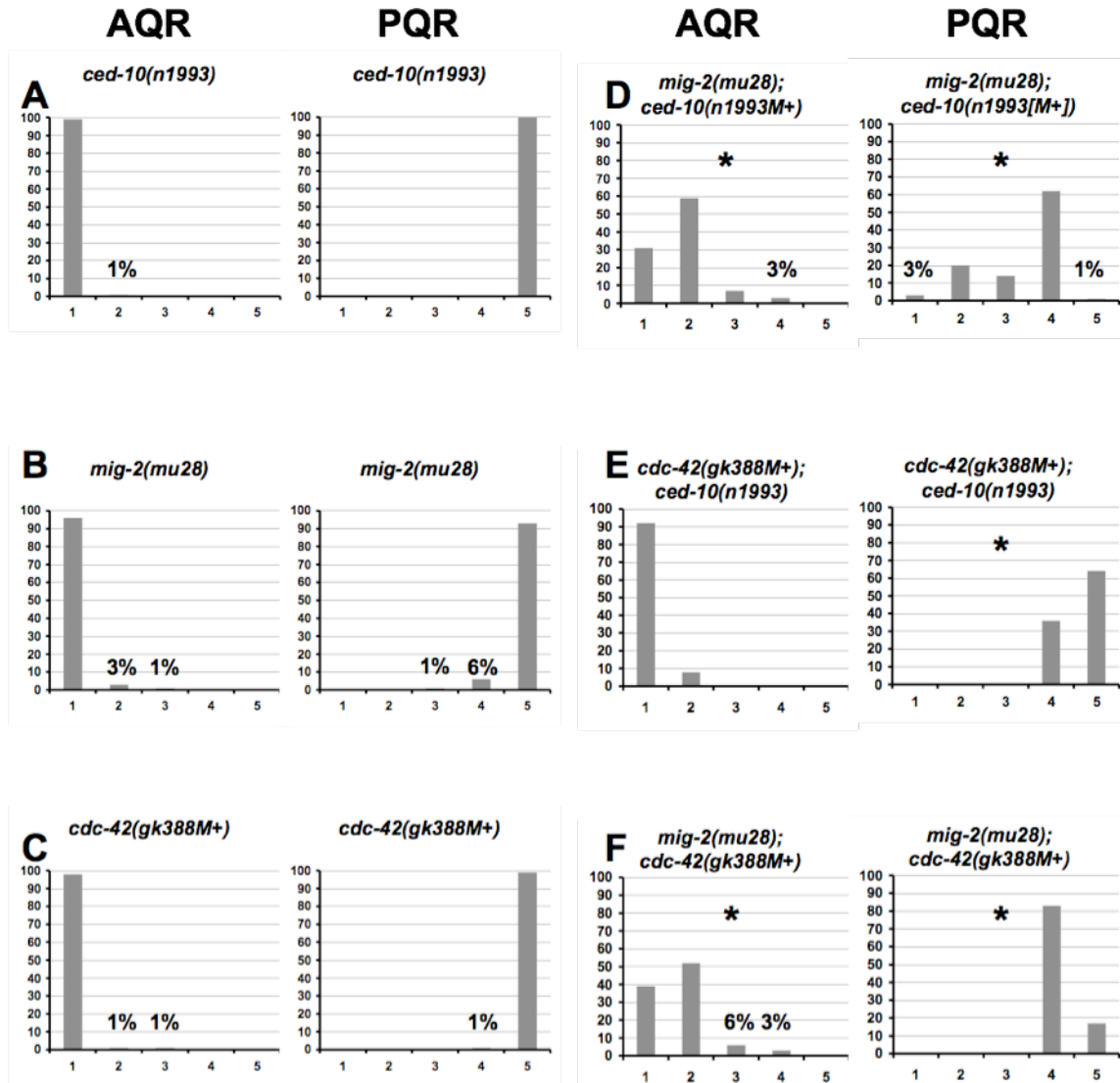
**Figure 4.4.** Migrations of the Q neuroblasts. (A-F) Quantitation of the location of the Q neuroblasts at division. The graphs are organized as described in Fig. 4.1F. The asterisk in (D) represents a statistically significant difference as compared to the *ced-10(n1993)* and *mig-2(mu28)* single mutants alone. (F) The p values for the Q neuroblasts that were located between the V4 and V5 seam cells upon division are indicated for both QR and QL. For all cases,  $n \geq 25$ .

Figure 4.5



**Figure 4.5.** Failure of the Q neuroblasts to migrate before dividing. (A-C) Confocal fluorescent micrographs of Q neuroblasts upon division in L1 larvae visualized with *scm::gfp::caax* expression. Asterisks mark the positions of the Q neuroblast descendants. Tracings of the Q neuroblast descendants are located beneath each micrograph. The scale bar in (A) represents 5 $\mu$ m for (A-C). (A) A QR neuroblast migrates past the normal stopping point over the V4R seam cell and divides between the V3R and V4R seam cells in *ced-10(n1993)* mutants. (B) A QL neuroblast fails to fully migrate before dividing, with the division occurring on the anterior edge of the V5L seam cell in *mig-2(mu28);ced-10(n1993M+)* mutants. (C) A QR neuroblast fails to migrate at all and divides at its birthplace between the V4R and V5R seam cells in *mig-2(mu28);ced-10(n1993M+)* mutants.

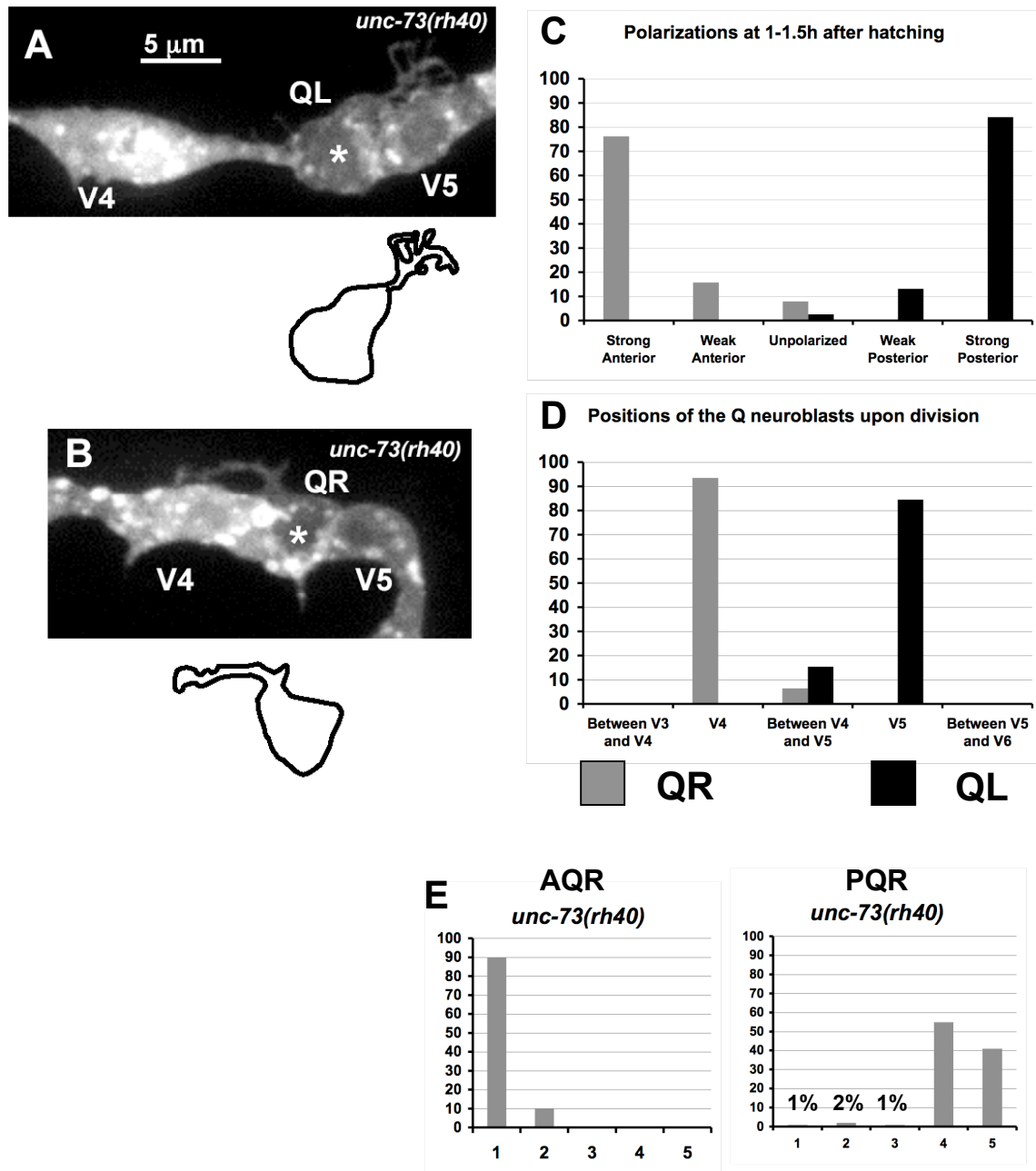
Figure 4.6



**Figure 4.6.** Final migratory positions of the Q neuroblast descendants, AQR and PQR. (A-F) Quantitation of the final migratory positions of the AQR and PQR neurons. The graphs are organized as described in Fig. 4.1H. The asterisks in (D-F) represent statistically significant differences for the double mutants as compared to the combination of the defects observed in the two single mutants than comprise the double mutant. For all cases, n = 100.

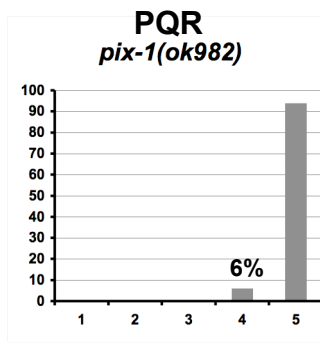
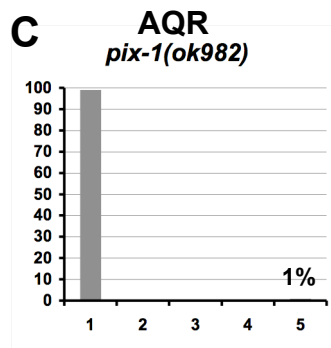
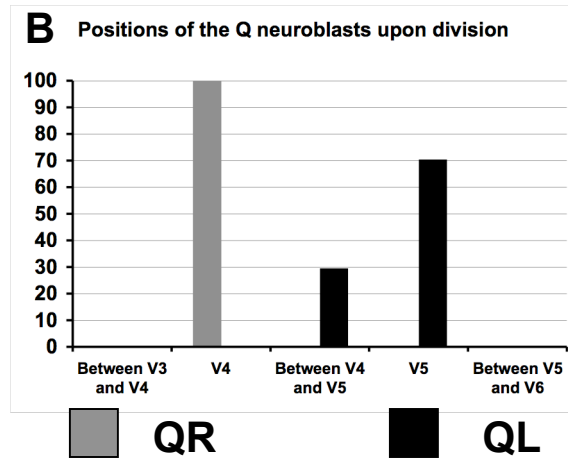
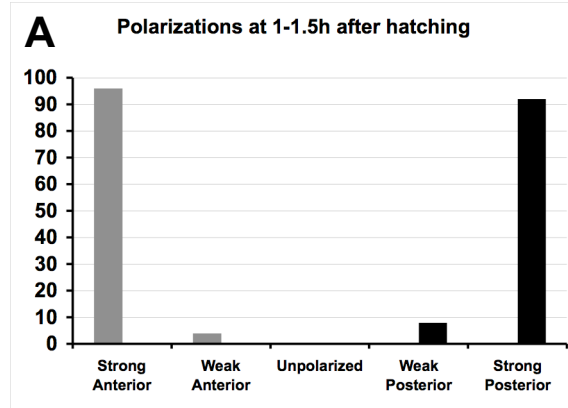


Figure 4.7



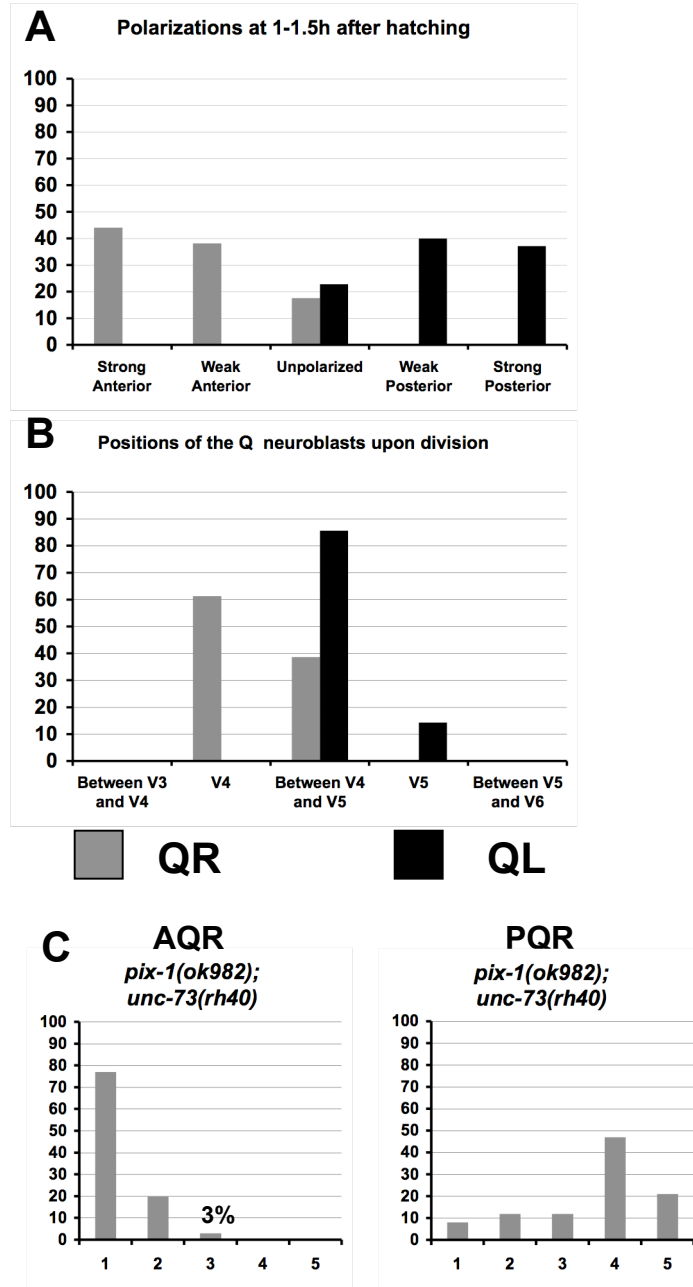
**Figure 4.7.** UNC-73/Trio is required for the proper polarizations and migrations of the Q neuroblasts and migrations of the Q cell descendants. (A,B) Confocal fluorescent micrographs of Q neuroblasts in *unc-73(rh40)* mutants in L1 larvae visualized with *scm::gfp::caax* expression at 1-1.5h after hatching. Asterisks mark the position of the Q neuroblasts. Tracings of the Q neuroblasts are located beneath each micrograph. The scale bar in (A) represents 5 $\mu$ m for (A,B). (A) A QL neuroblast polarizes in the correct posterior direction, but the size of the protrusions is reduced in size, resembling filopodia rather than lamellipodia. (B) A QR neuroblast polarizes in the correct anterior direction, but the size of the protrusions is reduced in size, resembling filopodia rather than lamellipodia. (C) Quantitation of the direction and extent of protrusions during the polarization stage of the Q neuroblasts at 1-1.5h after hatching in *unc-73(rh40)* mutants. The graphs are organized as described in Fig. 4.1E. For Q neuroblast polarizations, n = 38. (D) Quantitation of the location of the Q neuroblasts at division with respect to the adjacent seam cells in *unc-73(rh40)* mutants. The graphs are organized as described in Fig. 4.1F. For Q neuroblast migrations, n  $\geq$  31. (E) Quantitation of the final migratory positions of the AQR and PQR neurons in *unc-73(rh40)* mutants. The graphs are organized as described in Fig. 4.1H. For AQR and PQR migrations, n = 100.

Figure 4.8



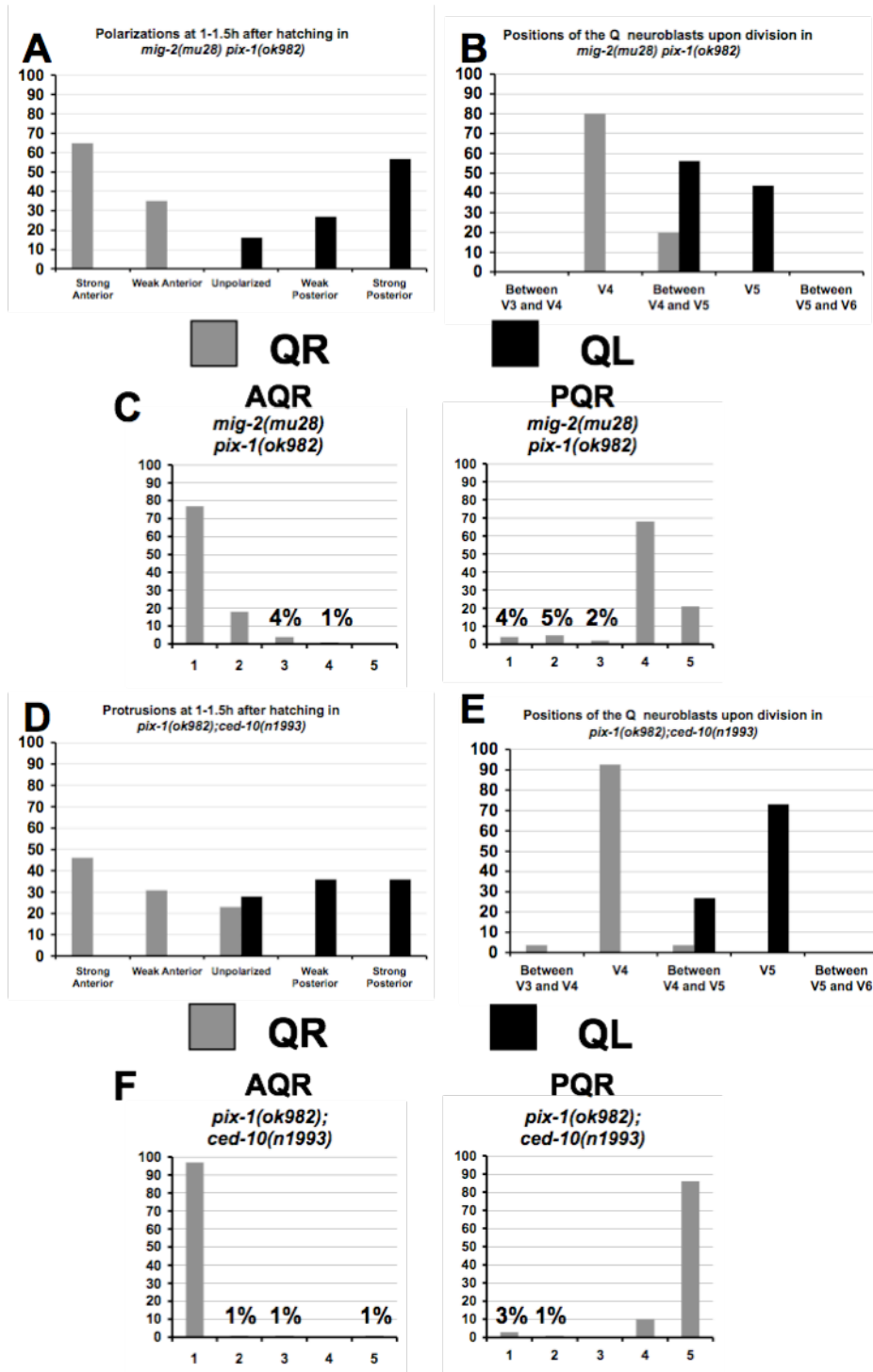
**Figure 4.8.** PIX-1/ $\beta$ PIX is required for the proper migrations of the QL neuroblast and the Q neuroblast descendants. (A) Quantitation of the direction and extent of protrusions during the polarization stage of the Q neuroblasts at 1-1.5h after hatching in *pix-1(ok982)* mutants. The graphs are organized as described in Fig. 4.1E. For Q neuroblast polarizations, n = 25. (B) Quantitation of the location of the Q neuroblasts at division with respect to the adjacent seam cells in *pix-1(ok982)* mutants. The graphs are organized as described in Fig. 4.1F. For Q neuroblast migrations, n  $\geq$  25. (C) Quantitation of the final migratory positions of the AQR and PQR neurons in *pix-1(ok982)* mutants. The graphs are organized as described in Fig. 4.1H. For AQR and PQR migrations, n = 100.

Figure 4.9



**Figure 4.9.** Double mutants of *pix-1* and *unc-73* display a synergistic increase in defects in the polarization and migration of the Q neuroblasts and the migrations of the Q neuroblast descendants. (A) Quantitation of the direction and extent of protrusions during the polarization stage of the Q neuroblasts at 1-1.5h after hatching in *pix-1(ok982);unc-73(rh40)* mutants. The graphs are organized as described in Fig. 4.1E. For Q neuroblast polarizations,  $n \geq 34$ . (B) Quantitation of the location of the Q neuroblasts at division with respect to the adjacent seam cells in *pix-1(ok982);unc-73(rh40)* mutants. The graphs are organized as described in Fig. 4.1F. For Q neuroblast migrations,  $n \geq 28$ . (C) Quantitation of the final migratory positions of the AQR and PQR neurons in *pix-1(ok982);unc-73(rh40)* mutants. The graphs are organized as described in Fig. 4.1H. For AQR and PQR migrations,  $n = 100$ .

Figure 4.10



**Figure 4.10.** Double mutants of *pix-1* with *mig-2* exhibit a synergistic increase in defects in Q neuroblast protrusion extension and migration and Q neuroblast descendant migration, whereas *pix-1;ced-10* double mutants do not display a large increase in defects in the protrusions or migrations of the Q neuroblasts or the Q neuroblast descendants. (A and D) Quantitation of the direction and extent of protrusions during the polarization stage of the Q neuroblasts at 1-1.5h after hatching. The graphs are organized as described in Fig. 1E. For Q neuroblast polarizations,  $n \geq 25$ . (B and E) Quantitation of the location of the Q neuroblasts at division with respect to the adjacent seam cells. The graphs are organized as described in Fig. 1F. For Q neuroblast migrations,  $n \geq 26$ . (C and F) Quantitation of the final migratory positions of the AQR and PQR neurons. The graphs are organized as described in Fig. 1H. For AQR and PQR migrations,  $n = 100$ .



## References

- Aspenstrom, P., Lindberg, U., and Hall, A. (1996). Two GTPases, Cdc42 and Rac, bind directly to a protein implicated in the immunodeficiency disorder Wiskott-Aldrich syndrome. *Curr Biol* 6, 70-75.
- Baum, P.D., and Garriga, G. (1997). Neuronal migrations and axon fasciculation are disrupted in *ina-1* integrin mutants. *Neuron* 19, 51-62.
- Baumgartner, M., Sillman, A.L., Blackwood, E.M., Srivastava, J., Madson, N., Schilling, J.W., Wright, J.H., and Barber, D.L. (2006). The Nck-interacting kinase phosphorylates ERM proteins for formation of lamellipodium by growth factors. *Proceedings of the National Academy of Sciences of the United States of America* 103, 13391-13396.
- Becker, E., Huynh-Do, U., Holland, S., Pawson, T., Daniel, T.O., and Skolnik, E.Y. (2000). Nck-interacting Ste20 kinase couples Eph receptors to c-Jun N-terminal kinase and integrin activation. *Mol Cell Biol* 20, 1537-1545.
- Brenner, S. (1974). The genetics of *Caenorhabditis elegans*. *Genetics* 77, 71-94.
- Ch'ng, Q., Williams, L., Lie, Y.S., Sym, M., Whangbo, J., and Kenyon, C. (2003). Identification of genes that regulate a left-right asymmetric neuronal migration in *Caenorhabditis elegans*. *Genetics* 164, 1355-1367.
- Chalfie, M., and Sulston, J. (1981). Developmental genetics of the mechanosensory neurons of *Caenorhabditis elegans*. *Developmental biology* 82, 358-370.
- Chalfie, M., Thomson, J.N., and Sulston, J.E. (1983). Induction of neuronal branching in *Caenorhabditis elegans*. *Science* 221, 61-63.
- Chapman, J.O., Li, H., and Lundquist, E.A. (2008). The MIG-15 NIK kinase acts cell-autonomously in neuroblast polarization and migration in *C. elegans*. *Developmental biology* 324, 245-257.
- Collins, C.S., Hong, J., Sapinoso, L., Zhou, Y., Liu, Z., Micklash, K., Schultz, P.G., and Hampton, G.M. (2006). A small interfering RNA screen for modulators of tumor cell motility identifies MAP4K4 as a promigratory kinase. *Proceedings of the National Academy of Sciences of the United States of America* 103, 3775-3780.
- Cowing, D., and Kenyon, C. (1996). Correct Hox gene expression established independently of position in *Caenorhabditis elegans*. *Nature* 382, 353-356.
- Debant, A., Serra-Pages, C., Seipel, K., O'Brien, S., Tang, M., Park, S.H., and Streuli, M. (1996). The multidomain protein Trio binds the LAR transmembrane

tyrosine phosphatase, contains a protein kinase domain, and has separate rac-specific and rho-specific guanine nucleotide exchange factor domains. *Proceedings of the National Academy of Sciences of the United States of America* **93**, 5466-5471.

Eisenmann, D.M. (2005). Wnt signaling. *WormBook*, 1-17.

Eisenmann, D.M., and Kim, S.K. (2000). Protruding vulva mutants identify novel loci and Wnt signaling factors that function during *Caenorhabditis elegans* vulva development. *Genetics* **156**, 1097-1116.

Eisenmann, D.M., Maloof, J.N., Simske, J.S., Kenyon, C., and Kim, S.K. (1998). The beta-catenin homolog BAR-1 and LET-60 Ras coordinately regulate the Hox gene *lin-39* during *Caenorhabditis elegans* vulval development. *Development (Cambridge, England)* **125**, 3667-3680.

Forrester, W.C., Kim, C., and Garriga, G. (2004). The *Caenorhabditis elegans* Ror RTK CAM-1 inhibits EGL-20/Wnt signaling in cell migration. *Genetics* **168**, 1951-1962.

Fu, C.A., Shen, M., Huang, B.C., Lasaga, J., Payan, D.G., and Luo, Y. (1999). TNIK, a novel member of the germinal center kinase family that activates the c-Jun N-terminal kinase pathway and regulates the cytoskeleton. *J Biol Chem* **274**, 30729-30737.

Garrity PA, R.Y., Salecker I, McGlade J, Pawson T, Zipursky SL (1996). *Drosophila* photoreceptor axon guidance and targeting requires the dreadlocks SH2/SH3 adapter protein. *Cell* **85**, 639-650.

Gobel, V., Barrett, P.L., Hall, D.H., and Fleming, J.T. (2004). Lumen morphogenesis in *C. elegans* requires the membrane-cytoskeleton linker *erm-1*. *Dev Cell* **6**, 865-873.

Hall, A. (1998). Rho GTPases and the actin cytoskeleton. *Science* **279**, 509-514.

Hall, A. (2005). Rho GTPases and the control of cell behaviour. *Biochem Soc Trans* **33**, 891-895.

Harris, J., Honigberg, L., Robinson, N., and Kenyon, C. (1996). Neuronal cell migration in *C. elegans*: regulation of Hox gene expression and cell position. *Development* **122**, 3117-3131.

Heasman, S.J., and Ridley, A.J. (2008). Mammalian Rho GTPases: new insights into their functions from in vivo studies. *Nat Rev Mol Cell Biol* **9**, 690-701.

Hedgecock, E.M., Culotti, J.G., and Hall, D.H. (1990). The *unc-5*, *unc-6*, and *unc-40* genes guide circumferential migrations of pioneer axons and mesodermal cells on the epidermis in *C. elegans*. *Neuron* **4**, 61-85.

Herman, M. (2001). *C. elegans* POP-1/TCF functions in a canonical Wnt pathway that controls cell migration and in a noncanonical Wnt pathway that controls cell polarity. *Development (Cambridge, England)* 128, 581-590.

Herman, M.A. (2003). Wnt signaling in *C. elegans*. In *Wnt signaling in Development* (ed. M. Kühl), pp. 187-212. (Georgetown, TX, Landes Biosciences).

Herman, R.K. (1984). Analysis of genetic mosaics of the nematode *Caenorhabditis elegans*. *Genetics* 108, 165-180.

Herskowitz, I. (1995). MAP kinase pathways in yeast: for mating and more. *Cell* 80, 187-197.

Higgs, H.N., and Pollard, T.D. (2000). Activation by Cdc42 and PIP(2) of Wiskott-Aldrich syndrome protein (WASp) stimulates actin nucleation by Arp2/3 complex. *J Cell Biol* 150, 1311-1320.

Honigberg, L., and Kenyon, C. (2000). Establishment of left/right asymmetry in neuroblast migration by UNC-40/DCC, UNC-73/Trio and DPY-19 proteins in *C. elegans*. *Development (Cambridge, England)* 127, 4655-4668.

Houalla, T., Hien Vuong, D., Ruan, W., Suter, B., and Rao, Y. (2005). The Ste20-like kinase misshapen functions together with Bicaudal-D and dynein in driving nuclear migration in the developing drosophila eye. *Mechanisms of development* 122, 97-108.

Insall, R.H., and Machesky, L.M. (2009). Actin dynamics at the leading edge: from simple machinery to complex networks. *Dev Cell* 17, 310-322.

Keino-Masu, K., Masu, M., Hinck, L., Leonardo, E.D., Chan, S.S.-Y., Culotti, J.G., Tessier-Lavigne, M. (1996). *Deleted in Colorectal Cancer* (DCC) encodes a netrin receptor. *Cell* 87, 175-185.

Kenyon, C. (1986a). A gene involved in the development of the posterior body region of *C. elegans*. *Cell* 46, 477-487.

Kenyon, C. (1986b). A gene involved in the development of the posterior body region of *C. elegans*. *Cell* 46, 477-487.

Kolluri, R., Toliyas, K.F., Carpenter, C.L., Rosen, F.S., and Kirchhausen, T. (1996). Direct interaction of the Wiskott-Aldrich syndrome protein with the GTPase Cdc42. *Proceedings of the National Academy of Sciences of the United States of America* 93, 5615-5618.

Korswagen, H.C., Herman, M.A., and Clevers, H.C. (2000). Distinct beta-catenins mediate adhesion and signalling functions in *C. elegans*. *Nature* 406, 527-532.

- Kubiseski, T.J., Culotti, J., and Pawson, T. (2003). Functional analysis of the *Caenorhabditis elegans* UNC-73B PH domain demonstrates a role in activation of the Rac GTPase in vitro and axon guidance in vivo. *Mol Cell Biol* 23, 6823-6835.
- Lauffenburger DA, H.A. (1996). Cell migration: a physically-integrated molecular process. *Cell Feb 9;84*, 359-369.
- Lehmann, J.M., Riethmuller, G., and Johnson, J.P. (1990). Nck, a melanoma cDNA encoding a cytoplasmic protein consisting of the src homology units SH2 and SH3. *Nucleic Acids Res* 18, 1048.
- Liu, H., Su, Y.C., Becker, E., Treisman, J., and Skolnik, E.Y. (1999). A *Drosophila* TNF-receptor-associated factor (TRAF) binds the ste20 kinase Misshapen and activates Jun kinase. *Curr Biol* 9, 101-104.
- Lucanic, M., and Cheng, H.J. (2008). A RAC/CDC-42-independent GIT/PIX/PAK signaling pathway mediates cell migration in *C. elegans*. *PLoS Genet* 4, e1000269.
- Lundquist, E.A., Reddien, P.W., Hartweg, E., Horvitz, H.R., and Bargmann, C.I. (2001). Three *C. elegans* Rac proteins and several alternative Rac regulators control axon guidance, cell migration and apoptotic cell phagocytosis. *Development (Cambridge, England)* 128, 4475-4488.
- Machesky, L.M., and Insall, R.H. (1998). Scar1 and the related Wiskott-Aldrich syndrome protein, WASP, regulate the actin cytoskeleton through the Arp2/3 complex. *Curr Biol* 8, 1347-1356.
- Mackay, D.J., and Hall, A. (1998). Rho GTPases. *J Biol Chem* 273, 20685-20688.
- Maloof, J.N., Whangbo, J., Harris, J.M., Jongeward, G.D., and Kenyon, C. (1999). A Wnt signaling pathway controls hox gene expression and neuroblast migration in *C. elegans*. *Development (Cambridge, England)* 126, 37-49.
- Mello, C., and Fire, A. (1995). DNA transformation. *Methods Cell Biol* 48, 451-482.
- Mohamed, A., Boudreau, J., and Chin-Sand, I. (2007). The Adaptor Molecule NCK-1 is a Component of the VAB-1 Eph RTK Signaling Pathway. In International Worm Meeting (Kingston, ON, Canada, Queen's University).
- Natarajan, L., Witwer, N.E., and Eisenmann, D.M. (2001). The divergent *Caenorhabditis elegans* beta-catenin proteins BAR-1, WRM-1 and HMP-2 make distinct protein interactions but retain functional redundancy in vivo. *Genetics* 159, 159-172.

- Nobes, C.D., and Hall, A. (1995). Rho, rac and cdc42 GTPases regulate the assembly of multimolecular focal complexes associated with actin stress fibers, lamalliposia and filopodia. *Cell* *81*, 53-62.
- Ou, G., and Vale, R.D. (2009). Molecular signatures of cell migration in *C. elegans* Q neuroblasts. *J Cell Biol* *185*, 77-85.
- Paricio, N., Feiguin, F., Boutros, M., Eaton, S., and Mlodzik, M. (1999). The *Drosophila* STE20-like kinase misshapen is required downstream of the Frizzled receptor in planar polarity signaling. *Embo J* *18*, 4669-4678.
- Poinat, P., De Arcangelis, A., Sookhareea, S., Zhu, X., Hedgecock, E.M., Labouesse, M., and Georges-Labouesse, E. (2002). A conserved interaction between beta1 integrin/PAT-3 and Nck-interacting kinase/MIG-15 that mediates commissural axon navigation in *C. elegans*. *Curr Biol* *12*, 622-631.
- Pollard, T.D., and Borisy, G.G. (2003). Cellular motility driven by assembly and disassembly of actin filaments. *Cell* *112*, 453-465.
- Raftopoulou, M., and Hall, A. (2004). Cell migration: Rho GTPases lead the way. *Developmental biology* *265*, 23-32.
- Reddien, P.W., and Horvitz, H.R. (2000). CED-2/CrkII and CED-10/Rac control phagocytosis and cell migration in *Caenorhabditis elegans*. *Nat Cell Biol* *2*, 131-136.
- Ridley, A.J., Paterson, H.F., Johnston, C.L., Diekmann, D., Hall, A. (1992). The small GTP-binding protein rac regulated growth factor-induced membrane ruffling. *Cell* *70*, 401-410.
- Ridley, A.J., Schwartz, M.A., Burridge, K., Firtel, R.A., Ginsberg, M.H., Borisy, G., Parsons, J.T., and Horwitz, A.R. (2003). Cell migration: integrating signals from front to back. *Science* *302*, 1704-1709.
- Salser, S.J., and Kenyon, C. (1992). Activation of a *C. elegans* Antennapedia homologue in migrating cells controls their direction of migration. *Nature* *355*, 255-258.
- Sanz-Moreno, V., Gadea, G., Ahn, J., Paterson, H., Marra, P., Pinner, S., Sahai, E., and Marshall, C.J. (2008). Rac activation and inactivation control plasticity of tumor cell movement. *Cell* *135*, 510-523.
- Sato, N., Yonemura, S., Obinata, T., and Tsukita, S. (1991). Radixin, a barbed end-capping actin-modulating protein, is concentrated at the cleavage furrow during cytokinesis. *J Cell Biol* *113*, 321-330.
- Sawa, H., Lobel, L., and Horvitz, H.R. (1996). The *Caenorhabditis elegans* gene *lin-17*, which is required for certain asymmetric cell divisions, encodes a putative

seven-transmembrane protein similar to the *Drosophila* frizzled protein. *Genes Dev* 10, 2189-2197.

Schmidt, K.L., Marcus-Gueret, N., Adeleye, A., Webber, J., Baillie, D., and Stringham, E.G. (2009). The cell migration molecule UNC-53/NAV2 is linked to the ARP2/3 complex by ABI-1. *Development (Cambridge, England)* 136, 563-574.

Shakir, M.A., Gill, J.S., and Lundquist, E.A. (2006). Interactions of UNC-34 Enabled with Rac GTPases and the NIK kinase MIG-15 in *Caenorhabditis elegans* axon pathfinding and neuronal migration. *Genetics* 172, 893-913.

Steven, R., Kubiseski, T.J., Zheng, H., Kulkarni, S., Mancillas, J., Ruiz Morales, A., Hogue, C.W.V., Pawson, T., and Culotti, J. (1998). UNC-73 activates the Rac GTPase and is required for cell and growth cone migrations in *C. elegans*. *Cell* 92, 785-795.

Su, Y.C., Han, J., Xu, S., Cobb, M., and Skolnik, E.Y. (1997). NIK is a new Ste20-related kinase that binds NCK and MEKK1 and activates the SAPK/JNK cascade via a conserved regulatory domain. *Embo J* 16, 1279-1290.

Su, Y.C., Maurel-Zaffran, C., Treisman, J.E., and Skolnik, E.Y. (2000). The Ste20 kinase misshapen regulates both photoreceptor axon targeting and dorsal closure, acting downstream of distinct signals. *Mol Cell Biol* 20, 4736-4744.

Su, Y.C., Treisman, J.E., and Skolnik, E.Y. (1998). The *Drosophila* Ste20-related kinase misshapen is required for embryonic dorsal closure and acts through a JNK MAPK module on an evolutionarily conserved signaling pathway. *Genes Dev* 12, 2371-2380.

Sulston, J. (1988). Cell lineage. In *The nematode Caenorhabditis elegans*, W.B. Wood, ed. (Cold Spring Harbor, New York, Cold Spring Harbor Laboratory), pp. 123-155.

Sulston, J., and Hodgkin, J. (1988). Methods. In *The Nematode Caenorhabditis elegans*, W.B. Wood, ed. (Cold Spring Harbor, New York, Cold Spring Harbor Laboratory Press), pp. 587-606.

Sulston, J.E., and Horvitz, H.R. (1977). Post-embryonic cell lineages of the nematode, *Caenorhabditis elegans*. *Developmental biology* 56, 110-156.

Sulston, J.E., Schierenberg, E., White, J.G., and Thomson, J.N. (1983). The embryonic cell lineage of the nematode *Caenorhabditis elegans*. *Dev Biol* 100, 64-119.

Sym, M., Robinson, N., and Kenyon, C. (1999). MIG-13 positions migrating cells along the anteroposterior body axis of *C. elegans*. *Cell* 98, 25-36.

Terns, R.M., Kroll-Conner, P., Zhu, J., Chung, S., and Rothman, J.H. (1997). A deficiency screen for zygotic loci required for establishment and patterning of the epidermis in *Caenorhabditis elegans*. *Genetics* 146, 185-206.

Tsukita, S., and Yonemura, S. (1997). ERM proteins: head-to-tail regulation of actin-plasma membrane interaction. *Trends Biochem Sci* 22, 53-58.

Van Furden, D., Johnson, K., Segbert, C., and Bossinger, O. (2004). The *C. elegans* ezrin-radixin-moesin protein ERM-1 is necessary for apical junction remodelling and tubulogenesis in the intestine. *Developmental biology* 272, 262-276.

Walston, T., Guo, C., Proenca, R., Wu, M., Herman, M., Hardin, J., and Hedgecock, E. (2006). mig-5/Dsh controls cell fate determination and cell migration in *C. elegans*. *Developmental biology* 298, 485-497.

Welch, M.D. (1999). The world according to Arp: regulation of actin nucleation by the Arp2/3 complex. *Trends Cell Biol* 9, 423-427.

Welch, M.D., and Mullins, R.D. (2002). Cellular control of actin nucleation. *Annu Rev Cell Dev Biol* 18, 247-288.

Whangbo, J., and Kenyon, C. (1999). A Wnt signaling system that specifies two patterns of cell migration in *C. elegans*. *Mol Cell* 4, 851-858.

White, J.G., Southgate, E., Thomson, J.N., and Brenner, S. (1986). The structure of the nervous system of the nematode *Caenorhabditis elegans*. *Philos Trans R Soc Lond* 314, 1-340.

Williams, L. (2002). A genetic analysis of the left-right asymmetric polarizations and migrations of the Q neuroblasts in *C. elegans*. Ph.D. thesis. University of California-San Francisco.

Wright, J.H., Wang, X., Manning, G., LaMere, B.J., Le, P., Zhu, S., Khatry, D., Flanagan, P.M., Buckley, S.D., Whyte, D.B., *et al.* (2003). The STE20 kinase HGK is broadly expressed in human tumor cells and can modulate cellular transformation, invasion, and adhesion. *Mol Cell Biol* 23, 2068-2082.

Wu, Y.C., Cheng, T.W., Lee, M.C., and Weng, N.Y. (2002). Distinct rac activation pathways control *Caenorhabditis elegans* cell migration and axon outgrowth. *Developmental biology* 250, 145-155.

Xue, Y., Wang, X., Li, Z., Gotoh, N., Chapman, D., and Skolnik, E.Y. (2001). Mesodermal patterning defect in mice lacking the Ste20 NCK interacting kinase (NIK). *Development* 128, 1559-1572.

Yochem, J., and Herman, R.K. (2005). Genetic mosaics. *WormBook*, 1-6.

Yu, S., Avery, L., Baude, E., and Garbers, D.L. (1997). Guanylyl cyclase expression in specific sensory neurons: a new family of chemosensory receptors. *Proceedings of the National Academy of Sciences of the United States of America* *94*, 3384-3387.

Zinovyeva, A.Y., Yamamoto, Y., Sawa, H., and Forrester, W.C. (2008). Complex Network of Wnt Signaling Regulates Neuronal Migrations During *Caenorhabditis elegans* Development. *Genetics* *179*, 1357-1371.